P. Starič, E. Margan

Wideband Amplifiers

Part 2:

Inductive Peaking Circuits

Complex solutions always have one simple explanation!
(Lunsford's Rule of scientific endeavor)

The Renaissance of Inductance

In Part 2 of Wideband Amplifiers we discuss various forms of inductive peaking circuits.

The topic of inductive peaking actually started with Oliver Heaviside's "Telegrapher's Equation" back in 1890s, in which for the first time an inductance was used to compensate a dominantly capacitive line to extend the bandwidth. The development flourished with radio, TV and radar circuits and reached a peak in oscilloscopes in 1970s.

With the widespread use of modern high speed low power operational amplifiers and digital electronics, the inductance virtually disappeared in signal transmission path, remaining mostly in power supply filtering and later in switching power supplies. By all too many contemporary electronics engineers, the inductance is being considered more as a nuisance, rather than a useful circuit component.

However, the available frequency spectrum is fixed and the bandwidth requirements are continuously rising, especially with modern wireless telecommunications. In our opinion the inductance just waits to be rediscovered by new generations of electronics circuit designers. So we believe that the inclusion of this subject in the book is fully justified.

Contents:

List of Figures:

List of Tables:

(blank page)

2.0 Introduction

In the early days of wideband amplifiers 'suitable coils' were added to the load (consisting of resistors and stray capacitances) in order to extend the bandwidth, causing in most cases a resonance peak in the frequency response. Hence the term *inductive peaking*. Even though later designers of wideband amplifiers were more careful in doing their best to achieve as flat a frequency response as possible, the word 'peaking' remained in use and it is still used today.

In some respect the British engineer *S. Butterworth* might be considered the first to introduce coils in the (then) anode circuits of electronic tubes to construct an amplifier with a maximally flat frequency (low pass) response. In his work **On the Theory of Filter Amplifiers**, published as early as October 1930 [Ref. 2.1], besides introducing the pole placement which was later named after him, he also mentioned: *"The writer has constructed filter units in which the resistances and inductances are wound round a cylinder of length 3in and diameter 1.25 in, whilst the necessary condensers are contained within the core of the cylinder"*. However, it is hard to tell exactly the year when these 'necessary condensers' were omitted to leave only the stray and inter-electrode capacitances of the electronic tubes to form, together with the properly dimensioned coils and load resistances, a **wideband amplifier** with maximally flat frequency response. This was probably done some time in the mid 1930s, when the first electronic voltmeters, oscilloscopes, and television amplifiers were constructed.

The need for wideband and pulse amplifiers was emphasized with the introduction of radar during the Second World War. A book of historical value, *G. E. Valley & H. Wallman*, **Vacuum Tube Amplifiers** [Ref. 2.2] was written right after the war and published in 1948. Apart from details about other types of amplifiers, the most important knowledge about wideband amplifiers, gained during the war in the Radiation Laboratory at Massachusetts Institute of Technology, was made public. In this work the amplifier step response calculation also received the necessary attention.

After the war people who worked in the Radiation Laboratory spread over USA and UK, and many of them started working at firms where oscilloscopes were produced. Many articles were written about wideband amplifiers with inductive peaking, but books which would thoroughly discuss wideband amplifiers were almost non-existent. The reason was probably because the emphasis has shifted from the frequency domain to the time domain, where a gap-free mathematical discussion was considered difficult. Nevertheless, here and there a book on this subject appeared, and one of the most significant was published in 1957 in Prague: *J. Bednařík & J. Daněk*, **Obrazové zesilovače pro televisí a měřicí techniku**, (Video Amplifiers for Television and Measuring Techniques) [Ref. 2.3]. There the authors attempted to present a thorough discussion of all inductive peaking circuits known at that time and also of high frequency resonant amplifiers. Computers were a rare commodity in those days, with restricted access, and equally rare was the programming knowledge; this prevented the authors from executing some important calculations, which were too elaborate to be done by pencil and paper.

An important change in wideband amplifier design, using inductive peaking, was introduced by *E.L. Ginzton*, *W.R. Hewlett*, *J.H. Jasberg*, and *J.D. Noe* in their revolutionary article **Distributed Amplification**, [Ref. 2.4]. This was an amplifier with electronic tubes connected in parallel, where the grid and anode interconnections were made of lumped sections of a delay line. In this way the bandwidth of the amplifier was extended beyond

the limits imposed by the mutual conductance (g_m) divided by stray capacitance (C_{in}) of electronic tubes. For reasons which we will discuss in Part 3, this type of amplification has a rather limited application if transistors are used instead of electronic tubes. The necessary delay in a distributed amplifier was realized using the so-called 'm-derived' T-coils, which did not have a constant input impedance. **The correct T-coil circuit** was developed in 1964 by *C.R. Battjes* [Ref. 2.17] and was used for inductive peaking of wideband amplifiers. Compared with a simple series peaking circuit, a T-coil circuit improves the bandwidth and rise time exactly twofold. For many years the T-coil peaking circuits were considered a trade secret, so the first complete mathematical derivations were published by a pupil of C.R. Battjes only in the 1980s [Ref. 2.5, 2.6, 2.41] and in 1995 by C. R. Battjes himself [Ref. 2.18]. **Transistor inter-stage coupling with T-coils** represented a special problem, which was solved by *R.I. Ross* in late 1960s. This too was considered a proprietary matter and appeared in print some ten to twenty years later [Ref. 2.7, 2.8, 2.9]. Owing to the superb performance of the T-coil circuit we shall discuss it very thoroughly. The transistor inter-stage T-coil coupling will be derived in Part 3.

Here in Part 2, we shall first explain the basic idea of inductive peaking, followed by the discussion of the peaking circuits with poles only: series peaking two-pole, series peaking three-pole, T-coil two-pole, T-coil three-pole, and L+T four-pole circuits. This will be followed by peaking circuits with poles and zeros: shunt peaking two-pole and one-zero circuit, shunt peaking three-pole and two-zero circuit, and shunt–series peaking circuit. For each of the circuits discussed we shall calculate and plot the frequency, phase, envelope delay, and the step response. The emphasis will be on T-coil circuits, owing to their superb performance. All the necessary calculations will be explained as we proceed and, whenever practical, the complete derivations will be given. The exception is the step response of the series peaking circuit with one complex conjugate pole pair, which was already derived and explained in Part 1. Since the complete calculation for the step-responses of four-pole L+T circuits and shunt–series peaking circuits is rather complicated, only the final formulae will be given. Those readers who want to have the derivations for these circuits as well, will be able to do so themselves by learning and applying the principles derived in Part 1 and 2 (some assistance can also be found in Appendix 2.1, 2.2 and 2.3 on the disk).

To the beginners we strongly recommend the study of Sec. 2.2 and 2.3: the circuit examples are simple enough to allow the analysis to be easily followed and learned; the same methods can then be applied to more sophisticated circuits in other sections, in which some of the most basic details are omitted and some equations imported from those two sections.

At the end of Part 2 we shall draw two diagrams, showing the Butterworth (MFA) frequency responses and the Bessel (MFED) step responses, to offer an easy comparison of performance. Finally, in Appendix 2.4 (disk) we give a summary table containing the essential design parameters and equations for all the circuits discussed.

2.1 The Principle of Inductive Peaking

A simple common base transistor amplifier is shown in Fig. 2.1.1. A current step source i_s is connected to the emitter; the time scale has its origin $t = 0$ at the current step transition time and is normalized to the system time constant, RC. The collector is loaded by a resistor R; in addition there is the collector–base capacitance C_{cb}, along with the unavoidable stray capacitance C_s and the load capacitance C_L in parallel. Their sum is denoted by C.

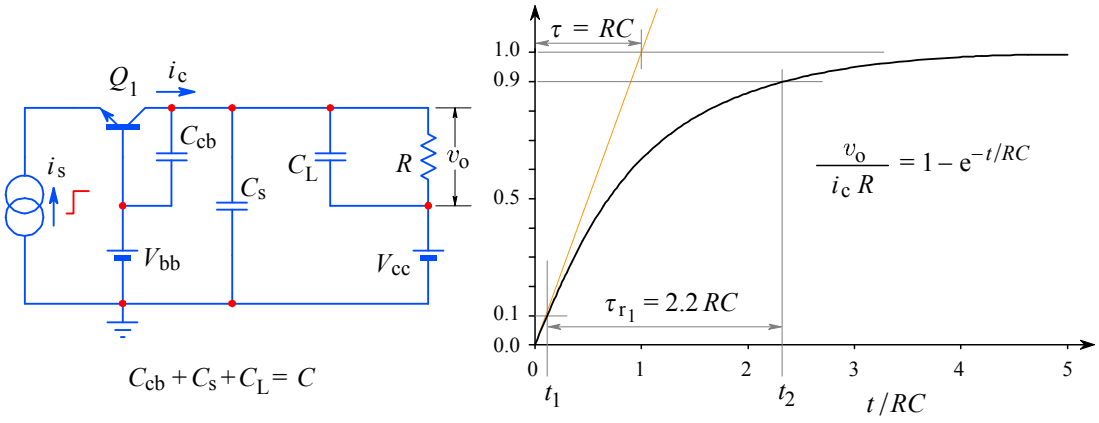

Fig. 2.1.1: A common base amplifier with RC load: the basic circuit and its step response.

Because of these capacitances, the output voltage v_o does not jump suddenly to the value $i_c R$, where i_c is the collector current. Instead this voltage rises exponentially according to the formula (see Part 1, Eq. 1.7.15):

$$v_o = i_c R\left(1 - e^{-t/RC}\right) \tag{2.1.1}$$

The time elapsed between 10 % and 90 % of the final output voltage value ($i_c R$), we call the *rise time*, τ_{r_1} (the index '1' indicates that it is the rise time of a single-pole circuit). We calculate it by inserting the 10 % and 90 % levels into the Eq. 2.1.1:

$$0.1\, i_c R = i_c R\left(1 - e^{-t_1/RC}\right) \quad \Rightarrow \quad t_1 = RC \ln 0.9 \tag{2.1.2}$$

Similarly for t_2:

$$0.9\, i_c R = i_c R\left(1 - e^{-t_2/RC}\right) \quad \Rightarrow \quad t_2 = RC \ln 0.1 \tag{2.1.3}$$

The rise time is the difference between these two instants:

$$\tau_{r_1} = t_2 - t_1 = RC \ln 0.9 - RC \ln 0.1 = RC \ln \frac{0.9}{0.1} = \boxed{2.197\, RC} \approx 2.2\, RC \tag{2.1.4}$$

The value 2.197 *RC* is the reference against which we shall compare the rise time of all other circuits in the following sections of the book.

Since in wideband amplifiers we strive to make the output voltage a replica of the input voltage (except for the amplitude), we want to reduce the rise time of the amplifier as much as possible. As the output voltage rises more current flows through R and less current remains to charge C. Obviously, we would achieve a shorter rise time if we could disconnect R in some way until C is charged to the desired level. To do so let us introduce a switch S between the capacitor C and the load resistor R. This switch is open at time $t = 0$, when the current step starts, but closes at time $t = RC$, as in Fig. 2.1.2. In this way we force all the available current to the capacitor, so it charges linearly to the voltage $i_c R$. When the capacitor has reached this voltage, the switch S is closed, routing all the current to the loading resistor R.

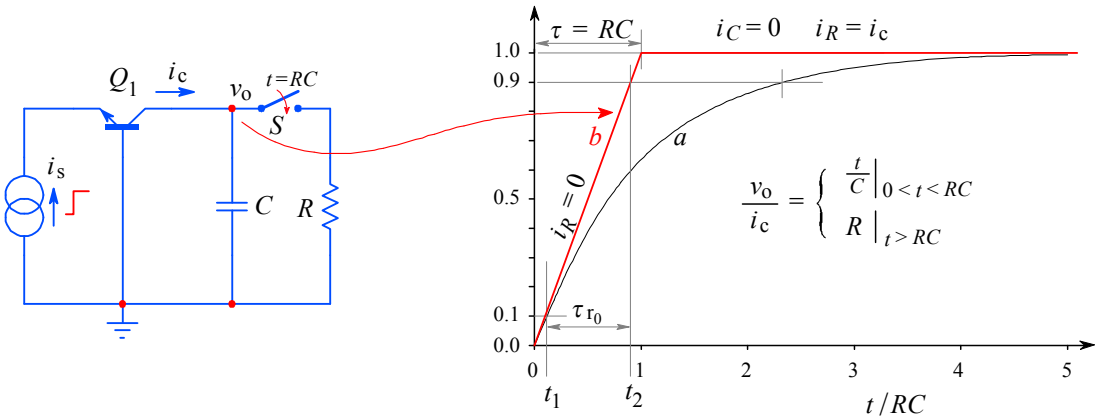

Fig. 2.1.2: A hypothetical ideal rise time circuit. The switch disconnects R from the circuit, so that all of i_c is available to charge C; but after a time $t = RC$ the switch is closed and all i_c flows through R. The resulting output voltage is shown in ***b***, compared with the exponential response in ***a***.

By comparing Fig. 2.1.1 with Fig. 2.1.2, we note a substantial decrease in rise time τ_{r_0}, which we calculate from the output voltage:

$$v_o = \frac{1}{C}\int_0^{\tau} i_c\, dt = \frac{i_c}{C}\, t\Big|_{t=0}^{t=\tau} = i_c\, R \tag{2.1.5}$$

where $\tau = RC$. Since the charging of the capacitor is linear, as shown in Fig. 2.1.2, the rise time is simply:

$$\tau_{r_0} = 0.9\, RC - 0.1\, RC = 0.8\, RC \tag{2.1.6}$$

In comparison with Fig. 2.1.1, where there was no switch, the improvement factor of the rise time is:

$$\eta_r = \frac{\tau_{r_1}}{\tau_{r_0}} = \frac{2.20\, RC}{0.8\, RC} = 2.75 \tag{2.1.7}$$

It is evident that the **rise time** (Eq. 2.1.6) **is independent of the actual value of the current i_c, but the maximum voltage $i_c R$** (Eq. 2.1.5) **is not**. On the other hand, the smaller the resistor R the smaller is the rise time. Clearly the introduction of the switch S would mean a great improvement. By using a more powerful transistor and a lower value resistor R we could (at least in principle) decrease the rise time at a will (provided that C remains unchanged). Unfortunately, it is impossible to make a low on-resistance switch,

functioning as in Fig. 2.1.2, which would also suitably follow the signal and automatically open and close in nanoseconds or even in microseconds. So it remains only a nice idea.

But instead of a switch we can insert an appropriate inductance L between the capacitor C and resistor R and so **partially** achieve the effect of the switch, as shown in Fig. 2.1.3. Since the current through an inductor can not change instantaneously, more current will be charging C, at least initially. The configuration of the RLC network allows us to take the output voltage either from the resistor R or from the capacitor C. In the first case we have a *series peaking network*, whilst in the second case we speak of a *shunt peaking network*. Both types of peaking networks are used in wideband amplifiers.

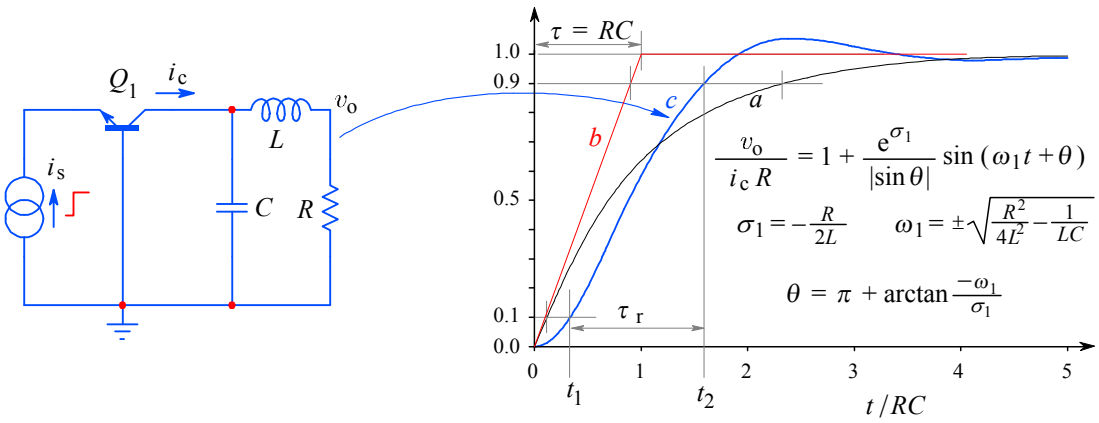

Fig. 2.1.3: A common base amplifier with the series peaking circuit. The output voltage v_o (curve *c*) is compared with the exponential response (*a*, $L = 0$) and the response using the ideal switch (*b*). If we were to take the output voltage from the capacitor C, we would have a shunt peaking circuit (see Sec. 2.7). We have already seen the complete derivation of the procedure for calculating the step response in Part 1, Sec. 1.14. However, the response optimization in accordance with different design criteria is shown in Sec. 2.2 for the series peaking circuit and in Sec. 2.7 for the shunt peaking circuit.

Fig. 2.1.3 is the simplest series peaking circuit. Later, when we discuss T-coil circuits, we shall not just achieve rise time improvements similar to that in Eq. 2.1.7, but in cases in which it is possible (usually it is) to split C into two parts, we shall obtain a substantially greater improvement.

(blank page)

2.2 Two pole series peaking circuit

Besides the series peaking circuit, in this section we shall discuss all the significant mathematical methods which are needed to calculate the frequency, phase and time delay response, the upper half power frequency and the rise time. In addition, we shall derive the most important design parameters of the series peaking circuit, which we will use in the other sections of the book also.

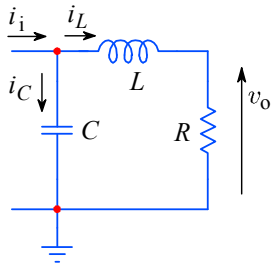

Fig. 2.2.1: A two-pole series peaking circuit.

In Fig. 2.2.1 we have repeated the collector loading circuit of Fig. 2.1.3. Since the inductive peaking circuits are used mostly as collector load circuits, from here on we shall omit the transistor symbol; instead we shall show the input current I_i (formerly I_c) flowing into the network, with the common ground as its drain. At first we shall discuss the behavior of the network in the frequency domain, assuming that I_i is the RMS value of the sinusoidally changing input current i_i. This current is split into two parts: the current through the capacitance I_C, and the current through the inductance I_L. Thus we have:

$$I_i = I_C + I_L = V_i\, j\omega C + \frac{V_i}{j\omega L + R} = V_i \left(j\omega C + \frac{1}{j\omega L + R} \right) \tag{2.2.1}$$

where the input voltage V_i is the product of the driving current I_i and the input impedance Z_i (represented by the expression in parentheses). The output voltage is:

$$V_o = I_L\, R = V_i \frac{R}{j\omega L + R} \tag{2.2.2}$$

From these equations we obtain the transfer function:

$$\frac{V_o}{I_i} = \frac{V_i \dfrac{R}{j\omega L + R}}{V_i \left(j\omega C + \dfrac{1}{j\omega L + R} \right)} = \frac{R}{j\omega C\,(j\omega L + R) + 1}$$

$$= \frac{R}{-\omega^2 LC + Rj\omega C + 1} \tag{2.2.3}$$

Let us set $I_i = 1\,V/R$ and $L = mR^2C$, where m is a dimensionless parameter; also let us substitute $j\omega$ with s. With these substitutions the output voltage $V_o = F(s)$ becomes:

$$F(s) = \frac{1}{s^2\, mR^2C^2 + sRC + 1} = \frac{1}{mR^2C^2} \cdot \frac{1}{s^2 + \dfrac{s}{mRC} + \dfrac{1}{mR^2C^2}} \tag{2.2.4}$$

The denominator roots, which for an efficient peaking must be complex conjugates, as in Fig. 2.2.2, are the poles of $F(s)$:

$$s_{1,2} = \sigma_1 \pm j\omega_1 = -\frac{1}{2mRC} \pm j\sqrt{\frac{1}{mR^2C^2} - \frac{1}{4m^2R^2C^2}} \tag{2.2.5}$$

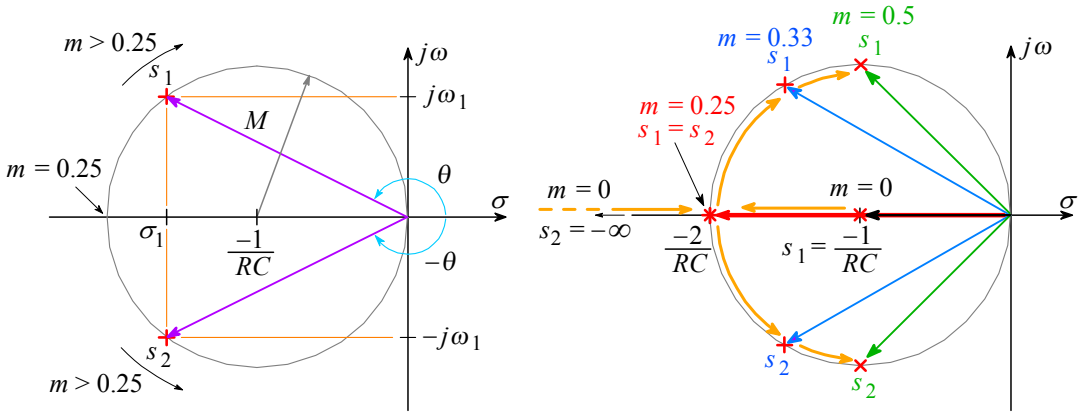

Fig. 2.2.2: The poles s_1 and s_2 in the complex plane. If the parameter $m = 0$, the poles are $s_1 = -1/RC$ and $s_2 = -\infty$. by increasing m, they travel along the real axis towards each other and meet at $s_1 = s_2 = -2/RC$ (for $m = 0.25$). Increasing m further, the poles split into a complex conjugate pair traveling along the circle, the radius of which is $r = 1/RC$ and its center at $\sigma = -r$. The figure on the right shows the four characteristic layouts, which are explained in detail in the text.

With these poles we may write Eq. 2.2.4 also in the following form:

$$F(s) = \frac{1}{mR^2C^2} \cdot \frac{1}{(s - s_1)(s - s_2)} \tag{2.2.6}$$

At DC ($s = 0$) Eq. 2.2.6 shrinks to:

$$F(0) = \frac{1}{mR^2C^2} \cdot \frac{1}{s_1 s_2} \tag{2.2.7}$$

By dividing Eq. 2.2.6 by Eq. 2.2.7, we obtain the **amplitude normalized** transfer function:

$$F(s) = \frac{s_1 s_2}{(s - s_1)(s - s_2)} \tag{2.2.8}$$

We shall need this expression for the calculation of the step response. But for the frequency response $F(j\omega)$ we replace both poles by their components from Eq. 2.2.5 and group the imaginary parts to obtain:

$$F(j\omega) = \frac{\sigma_1^2 + \omega_1^2}{[-\sigma_1 + j(\omega - \omega_1)]\,[-\sigma_1 + j(\omega + \omega_1)]} \tag{2.2.9}$$

We are often interested in the magnitude, $|F(\omega)|$, which we obtain by multiplying $F(j\omega)$ by its own complex conjugate and then taking the root:

$$|F(\omega)| = \sqrt{F(j\omega) \cdot F^*(j\omega)} = \frac{\sigma_1^2 + \omega_1^2}{\sqrt{[\sigma_1^2 + (\omega - \omega_1)^2]\,[\sigma_1^2 + (\omega + \omega_1)^2]}} \tag{2.2.10}$$

The next step is the calculation of the parameter m. Its value depends on the type of poles we want to have, which in turn depend on the intended application of the amplifier. In general, for sine wave signal amplification we prefer the Butterworth poles, whilst for

pulse amplification we prefer the Bessel poles. If high bandwidth is not of primary importance, we can use a 'critically damped' system for a zero overshoot step response. Other types of poles are optimized for use in filters, where our primary goal is to selectively amplify only a part of the spectrum. Poles are discussed in Part 4 (derived from some chosen optimization criteria) and Part 6 (computer algorithms).

2.2.1 Butterworth Poles for Maximally Flat Amplitude Response (MFA)

We shall calculate the actual values of the poles as well as the parameter m, by using Eq. 2.2.5 where we factor out $1/2mRC$. If the square root of Eq. 2.2.11 is imaginary, which is true for $m > 0.25$, we can also factor out the imaginary unit:

$$s_{1,2} = \frac{1}{2mRC}\left(-1 \pm \sqrt{1-4m}\right) = \frac{1}{2mRC}\left(-1 \pm j\sqrt{4m-1}\right) \qquad (2.2.11)$$

We now compare this relation with the normalized 2nd-order Butterworth poles (the reader can find them in Part 4, Table 4.3.1, or by running the BUTTAP computer routine given in Part 6). The values obtained are $\sigma_{1t} = -0.7071$ and $\omega_{1t} = \pm 0.7071$.

Note: From now on we will append the index 't' to the poles taken from the tables or calculated by a suitable computer program; these values are normalized to the frequency of 1 *radian per second*.

Since both the real and imaginary axis of the Laplace plane have the dimension of frequency, the pole dimension is *radians per second* [rad/s]; however, it has become almost a custom not to write the dimensions.

The sign is also seldom written; instead, most authors leave it to the reader to keep in mind that the poles of unconditionally stable systems always have the real part negative and the imaginary part is either zero or both positive and negative, forming a complex conjugate pair.

To make it easier for the reader, we shall always have the symbols σ and ω signed as required by the mathematical operation to be performed, whilst the numerical values within the symbols will always be negative for σ and positive for ω. For example, we shall express a complex conjugated pole pair $(s_1, s_2) = (s_1, s_1^*)$ as:

$$s_1 = \sigma_1 + j\,\omega_1 = -0.7071 + j\,0.7071$$
$$s_2 = \sigma_2 + j\,\omega_2 = -0.7071 - j\,0.7071$$

$$\Rightarrow \quad s_2 = \sigma_1 - j\,\omega_1 = s_1^*$$

A real pole will be given as:

$$s_3 = \sigma_3 = -1.000$$

Each σ_i and ω_i will bear the index of the pole s_i (and not their table order number). We shall use the odd index for complex conjugate pair components (with the appropriate $+/-$ sign for the imaginary part).

In order to have the same response, the poles of Eq. 2.2.11 must be proportional to those from the tables, so the ratio of their imaginary to the real part must be the same:

$$\frac{\Im\{s_{1t}\}}{\Re\{s_{1t}\}} = \frac{\Im\{s_1\}}{\Re\{s_1\}} \;\Rightarrow\; \frac{\omega_{1t}}{\sigma_{1t}} = \frac{\omega_1}{\sigma_1} \;\Rightarrow\; \frac{0.7071}{-0.7071} = \frac{\sqrt{4m-1}}{-1} = -1 \qquad (2.2.12)$$

and the same is true for s_2 (except the sign). From the square root of Eq. 2.2.12 it follows that the value of m which satisfies our requirement for the Butterworth poles must be:

$$m = 0.5 \qquad (2.2.13)$$

Thus the inductance is:

$$L = mR^2C = 0.5\,R^2C \qquad (2.2.14)$$

Finally, by inserting the value of m back into Eq. 2.2.11 the poles of our system are:

$$s_{1,2} = \sigma_1 \pm j\omega_1 = \frac{1}{RC}\left(-1 \pm j\right) \qquad (2.2.15)$$

The value $1/RC = \omega_h$ is equal to the upper half power frequency of the non-peaking amplifier of Fig. 2.1.1 (at this frequency, since power is proportional to voltage squared, the voltage gain drops to $1/\sqrt{2} = 0.7071$). If we put $1/RC = 1$ (or $R = 1\,\Omega$ and $C = 1\,\mathrm{F}$, or $R = 500\,\mathrm{k}\Omega$ and $C = 2\,\mu\mathrm{F}$, or any other similar combination, provided that it can be driven by the signal source), we obtain the normalized (denoted by the index 'n') poles:

$$s_{1n,2n} = \sigma_{1n} \pm j\omega_{1n} = -1 \pm j \qquad (2.2.16)$$

If we use normalized poles, we must also normalize the frequency: $j\omega/\omega_h$ instead of $j\omega$.

Note: It is important not to confuse our system with normalized poles (Eq. 2.2.16) with the system having normalized Butterworth poles taken from the table (s_{1t}, $s_{2t} = -0.707 \pm j\,0.707$). Although both are Butterworth-type and both are normalized, they differ in bandwidth:

$$\sqrt{s_{1t}s_{2t}} = 1 \qquad \text{whilst} \qquad \sqrt{s_{1n}s_{2n}} = \sqrt{2} \qquad (2.2.17)$$

This will become evident soon in Sec. 2.2.4, where we shall calculate and plot the magnitude (absolute value) of the frequency response.

2.2.2 Bessel Poles for Maximally Flat Envelope Delay (MFED) Response

From Table 4.4.3 in Part 4 (or by using the BESTAP routine in Part 6), the poles for the 2nd-order Bessel system are $\sigma_{1t} = -1.7544$ and $\omega_{1t} = \pm 1.5000$. Then, as for the Butterworth case above, the ratio of their imaginary to real component is:

$$\frac{\Im\{s_1\}}{\Re\{s_1\}} = \frac{\omega_{1t}}{\sigma_{1t}} \quad\Rightarrow\quad \frac{\sqrt{4m-1}}{-1} = \frac{1.5000}{-1.7544} \qquad (2.2.18)$$

Solving for m gives:

$$m = \frac{1}{3} \qquad (2.2.19)$$

So the inductance is:

$$L = 0.3\dot{3}\;R^2C \qquad (2.2.20)$$

and the poles are:

$$s_{1,2} = \frac{1}{RC}\left(-1.5 \pm j\,0.866\right) \qquad (2.2.21)$$

2.2.3 Critical Damping (CD)

In this case both poles are real and equal, so the imaginary part in Eq. 2.2.11 (the square root) must be zero:

$$4m - 1 = 0 \qquad \Rightarrow \qquad m = 0.25 \tag{2.2.22}$$

from which the inductance is:

$$L = 0.25\, R^2 C \tag{2.2.23}$$

resulting in a double real pole:

$$s_{1,2} = -\frac{2}{RC} \tag{2.2.24}$$

In general the parameter m may be calculated with the aid of Fig. 2.2.2, where both poles and the angle θ are shown. If the poles are expressed by Eq. 2.2.11:

$$\tan\theta = \frac{\Im\{s_1\}}{\Re\{s_1\}} = \frac{\omega_1}{\sigma_1} = \frac{\sqrt{4m-1}}{-1} \tag{2.2.25}$$

and from this we obtain:

$$\boxed{m = \frac{1 + \tan^2\theta}{4}} \tag{2.2.26}$$

which is also equal to $1/4\cos^2\theta$, as can be found in some literature. We prefer Eq. 2.2.26 .

Now we have all the data needed for further calculations of the frequency, phase, time delay, and step responses.

2.2.4 Frequency Response Magnitude

We have already written the magnitude in Eq. 2.2.10. Here we will use the normalized frequency ω/ω_h:

$$\boxed{\left|F(\omega)\right| = \frac{\sigma_{1n}^2 + \omega_{1n}^2}{\sqrt{\left[\sigma_{1n}^2 + \left(\frac{\omega}{\omega_h} + \omega_{1n}\right)^2\right]\left[\sigma_{1n}^2 + \left(\frac{\omega}{\omega_h} - \omega_{1n}\right)^2\right]}}} \tag{2.2.27}$$

This is a normalized equation, in magnitude as $\left|F(\omega)\right| = 1$ for $\omega = 0$, and in frequency to the upper half power frequency ω_h of the non-peaking system.

Inserting the pole types of MFA, MFED, and CD, and the frequency in the range $0.1 < (\omega/\omega_h) < 10$, we obtain the diagrams in Fig. 2.2.3 .

2.2.5 Upper Half Power Frequency

An important amplifier parameter is its upper half power frequency, which we shall name ω_H for the peaking amplifier (in contrast to ω_h in the non-peaking case). This is the frequency at which the output voltage V_o drops to $V_{ODC}/\sqrt{2}$, where V_{ODC} is the output voltage at DC ($\omega = 0$), or, if normalized, to $1\,V/\sqrt{2}$. Since the power is proportional to

the square of the voltage, the normalized output power $P_o = (1\,\mathrm{V})^2/2$, which is one half of the output power at DC. We can calculate the upper half power frequency from Eq. 2.2.27, by inserting $\omega = \omega_H$; the result must be $1/\sqrt{2}$:

$$\left|F(\omega_H)\right| = \frac{\sigma_1^2 + \omega_1^2}{\sqrt{\left[\sigma_1^2 + (\omega_H + \omega_1)^2\right]\left[\sigma_1^2 + (\omega_H - \omega_1)^2\right]}} = \frac{1}{\sqrt{2}} \qquad (2.2.28)$$

We shall use the term *upper half power frequency* intentionally, rather than the term *upper −3 dB frequency*, which is commonly found in the literature. Whilst it has become a custom to express the amplifier gain in dB, the dB scale (the log of the output to input power ratio) implies that the driving circuit, which supplies the current I_i to the input, has the same internal resistance as the loading resistor R. This is not the case in most of the circuits which we shall discuss.

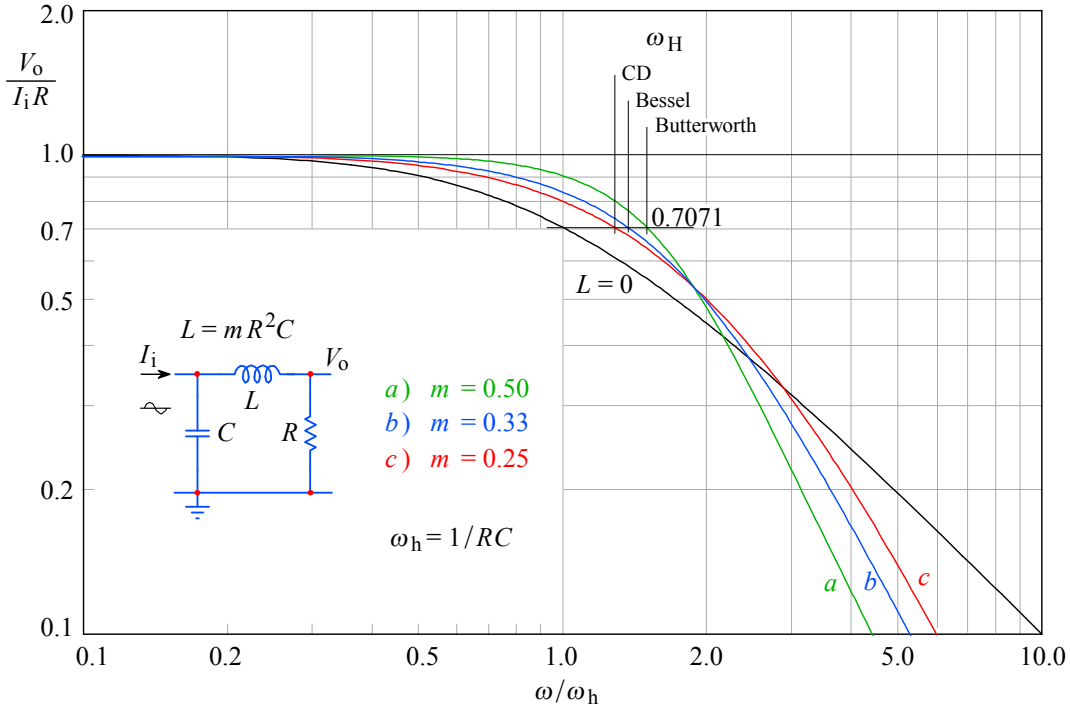

Fig. 2.2.3: Frequency response magnitude of the two-pole series peaking circuit for some characteristic values of m: ***a)*** $m = 0.5$ is the maximally flat amplitude (MFA) response; ***b)*** $m = 0.33$ is the maximally flat envelope delay (MFED) response; ***c)*** $m = 0.25$ is the critical damping (CD) case; the non-peaking case ($m = 0 \Rightarrow L = 0$) is the reference. The bandwidth of all peaking responses is improved compared to the non-peaking bandwidth ω_h at $V_o/I_i R = 0.7071$.

For a series peaking circuit the calculation of ω_H is relatively easy. The calculation becomes progressively more difficult for more sophisticated networks, where more poles and sometimes even zeros are introduced. In such cases it is better to use a computer and in Part 6 we have presented the development of routines which the reader can use to calculate the various response functions.

If we solve Eq. 2.2.28 for ω_H/ω_h we can define [Ref. 2.2, 2.4]:

$$\boxed{\eta_b = \frac{\omega_H}{\omega_h}} \qquad (2.2.29)$$

The value η_b is the cut off frequency improvement factor, defined as the ratio of the system upper half power frequency against that of the non-peaking amplifier (and, since the lower half power frequency of a wideband amplifier is generally very low, usually it is flat down to DC, we may call η_b also the *bandwidth improvement factor*). In Table 2.2.1 at the end of this section the bandwidth improvement factors and other data for different values of the parameter m are given.

2.2.6 Phase Response

We calculate the phase angle φ of the output voltage V_o referred to the input current I_i by finding the phase shift $\varphi_k(\omega)$ of each pole $s_k = \sigma_k \pm j\,\omega_k$ and then sum them:

$$\varphi(\omega) = \sum_{k=1}^{n} \varphi_k(\omega) = \sum_{k=1}^{n} \arctan \frac{\omega \mp \omega_k}{\sigma_k} \tag{2.2.30}$$

In Eq. 2.2.30 we have the ratio of the imaginary part to the real part of the pole, so the pole values may be either exact or normalized. For normalized values we must also normalize the frequency variable as ω/ω_h. Our frequency response function (Eq. 2.2.8) has two complex conjugated poles, therefore the phase response is:

$$\varphi(\omega) = \arctan \frac{\dfrac{\omega}{\omega_h} - \omega_{1n}}{\sigma_{1n}} + \arctan \frac{\dfrac{\omega}{\omega_h} + \omega_{1n}}{\sigma_{1n}} \tag{2.2.31}$$

In Fig. 2.2.4 the phase plots corresponding to the same values of m as in Fig. 2.2.3 are shown:

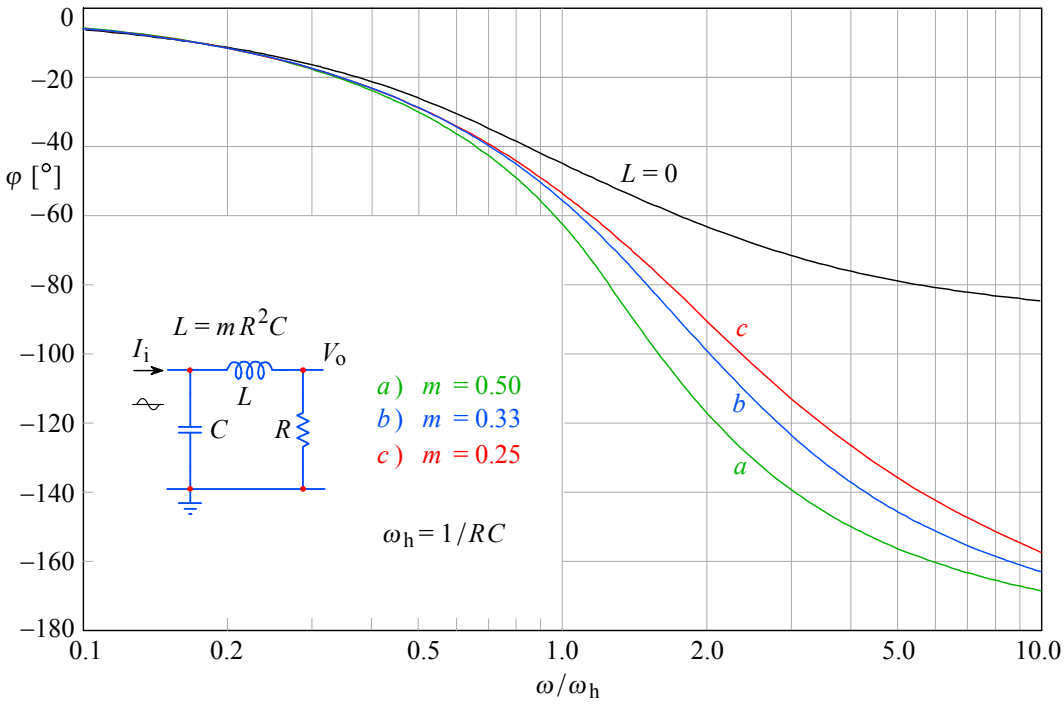

Fig. 2.2.4: Phase response of the series peaking circuit for ***a)*** MFA, ***b)*** MFED and ***c)*** CD case, compared with the non-peaking response ($L = 0$). The phase angle scale was converted from radians to degrees by multiplying it by $180/\pi$. For $\omega \to \infty$ the non-peaking (single-pole) response has its asymptote at 90°, whilst the second-order peaking systems have their asymptote at 180°.

2.2.7 Phase Delay and Envelope Delay

For each pole the *phase delay* (or the *phase advance* for each zero) is:

$$\tau_\varphi = \frac{\varphi}{\omega} \tag{2.2.32}$$

If ω is the positive angular frequency with which the input signal phasor rotates, then the angle φ by which the output signal phasor lags the input is defined in the direction opposite to ω, meaning that, for a phase-delay, φ will be negative, as in Fig. 2.2.4; consequently τ_φ will also be negative. Note that τ_φ has the dimension of time.

Now, τ_φ is obviously frequency dependent, so in order to evaluate the time domain performance of a wideband amplifier on a fair basis we are much more interested in the 'specific' phase delay, known as the *envelope delay* (also *group delay*), which is a frequency derivative of the phase angle as the function of frequency:

$$\tau_e = \frac{d\varphi(\omega)}{d\omega} \tag{2.2.33}$$

Here, too, a negative result means a delay and a positive result an advance against the input signal. In Fig. 2.2.5 a tentative explanation of the difference between the phase delay and the envelope delay is displayed both in time domain and as a phasor diagram.

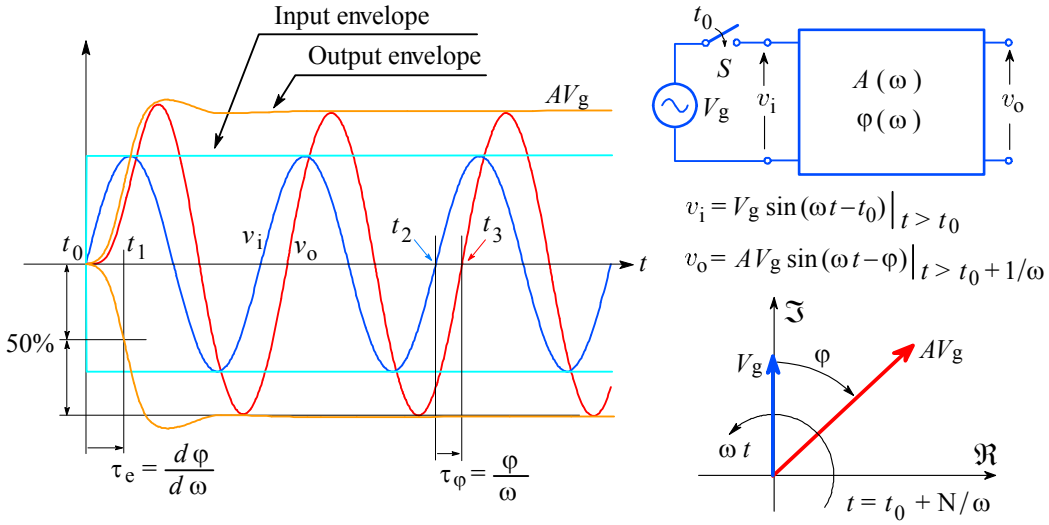

Fig. 2.2.5: Phase delay and envelope delay definitions. The switch S is closed at the instant t_0, applying a sinusoidal voltage with amplitude V_g to the input of the amplifier having a frequency dependent amplitude response $A(\omega)$ and its associated phase response $\varphi(\omega)$. The input signal envelope is a unit step. The output envelope lags the input by $\tau_e = d\varphi/d\omega$, measured from t_0 to t_1, where t_1 is the instant at which the output envelope reaches 50% of its final value. A number of periods later (N/ω), the phase delay can be measured as the time between the input and output zero crossing, indicated by t_2 and t_3, and is expressed as $\tau_\varphi = \varphi/\omega$. Note the phase lag being defined in the opposite direction of the rotation ωt in the corresponding phasor diagram.

In the phase advance case, when zeros dominate over poles, the name suggests that the output voltage will change before input, which is impossible, of course. To see what actually happens we apply a sinewave to two simple RC networks, low pass and high pass, as shown in Fig. 2.2.6. Compare the phase advance case, v_{oHP}, with the phase delay case, v_{oLP}. The input signal frequency is equal to the network cutoff, $1/RC$.

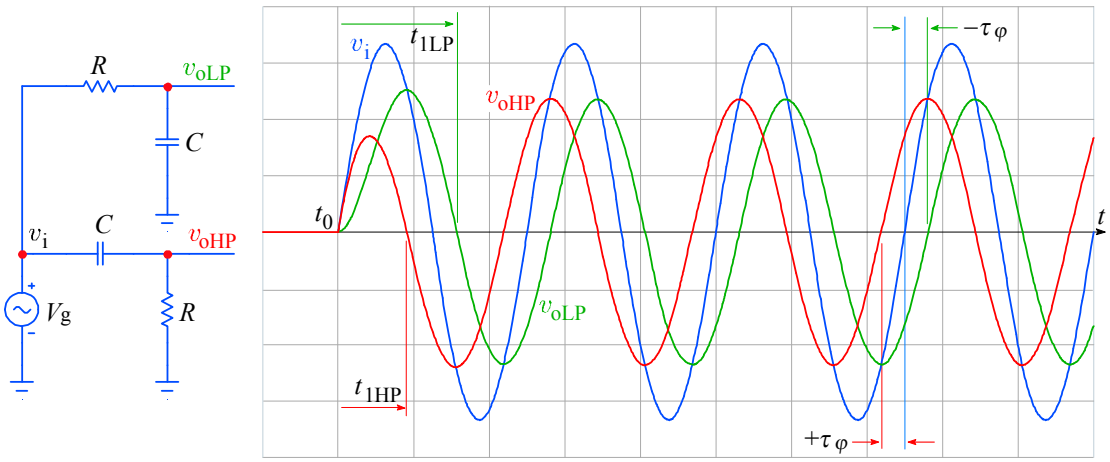

Fig. 2.2.6: Phase delay and phase advance. It is evident that both output signals undergo a phase modulation during the first half period. The time from t_0 to the first 'zero crossing' of the output is shorter for v_{oHP} (t_{1HP}) and longer for v_{oLP} (t_{1LP}). However, both envelopes lag the input envelope. On the other hand, the phase, measured after a number of periods, exhibits an advance of $+\tau_\varphi$ for the high pass network and a delay of $-\tau_\varphi$ for the low pass network.

Returning to the envelope delay for the series peaking circuit, in accordance with Eq. 2.2.33 we must differentiate Eq. 2.2.30. For each pole we have:

$$\frac{d\varphi}{d\omega} = \frac{d}{d\omega}\left[\arctan\frac{\omega \mp \omega_i}{\sigma_i}\right] = \frac{\sigma_i}{\sigma_i^2 + (\omega \mp \omega_i)^2} \tag{2.2.34}$$

and, as for the phase delay, the total envelope delay is the sum of the contributions of each pole (and zero, if any). Again, if we use normalized poles and the normalized frequency, we obtain the normalized envelope delay, $\tau_e\,\omega_h$, resulting in a unit delay at DC.

For the 2-pole case we have:

$$\tau_e\,\omega_h = \frac{\sigma_{1n}}{\sigma_{1n}^2 + \left(\dfrac{\omega}{\omega_h} - \omega_{1n}\right)^2} + \frac{\sigma_{1n}}{\sigma_{1n}^2 + \left(\dfrac{\omega}{\omega_h} + \omega_{1n}\right)^2} \tag{2.2.35}$$

The plots for the same values of m as before, in accordance with Eq. 2.2.35, are shown in Fig. 2.2.7.

For pulse amplification the importance of achieving a flat envelope delay cannot be overstated. A flat delay means that all the important frequencies will reach the output with unaltered phase, preserving the shape of the input signal as much as possible for the given bandwidth, thus resulting in minimal overshoot of the step response (see the next section). Also, a flat delay means that, since it is a phase derivative, the phase must be a linear function of frequency up to the cutoff. This is why Bessel systems are often being referred to as 'linear phase' systems. This property can not be seen in the log scale used here, but if plotted against a linearly scaled frequency it would be seen. We leave it to the curious reader to try it by himself.

In contrast the Butterworth system shows a pronounced delay near the cut off frequency. Conceivably, this will reveal the system resonance upon the step excitation.

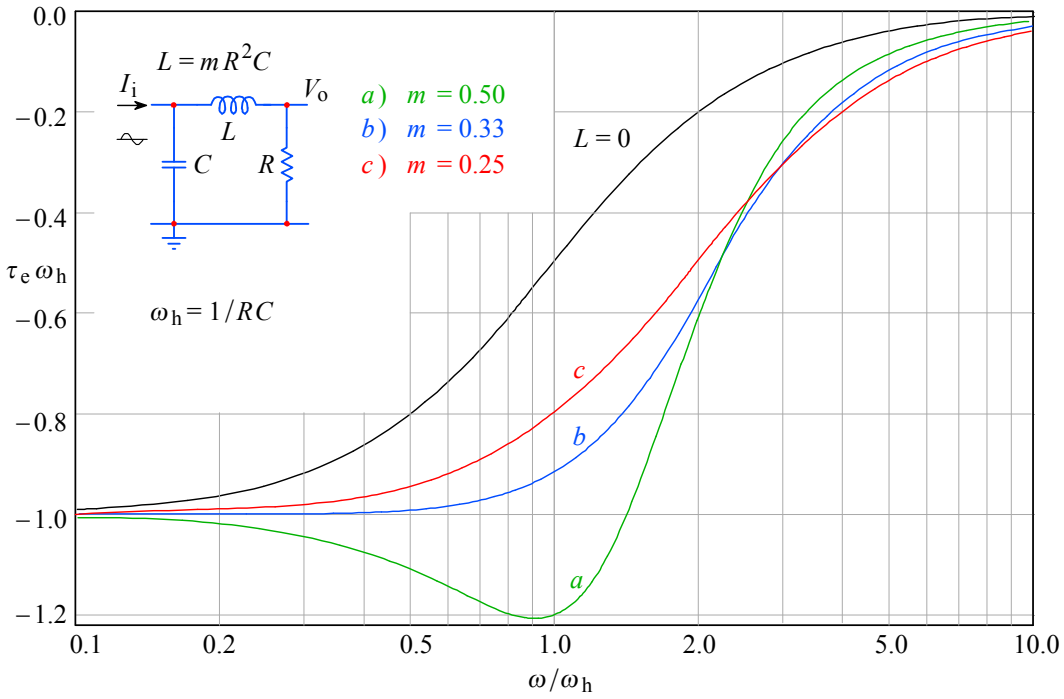

Fig. 2.2.7: Envelope delay of the series peaking circuit for the same characteristic values of m as before: ***a)*** MFA, ***b)*** MFED, ***c)*** CD. Note the MFED plot being flat up to nearly $0.5\,\omega_h$.

2.2.8 Step Response

We have already derived the formula for the step response in Part 1, Eq. 1.14.29:

$$g(t) = 1 + \frac{1}{|\sin\theta|}\, e^{\sigma_1 t} \sin(\omega_1 t + \theta) \tag{2.2.36}$$

where θ is the pole angle in radians, $\theta = \arctan(\omega_1/\sigma_1) + \pi$ (read the following Note!).

Note: We are often forced to calculate some of the circuit parameters from the trigonometric relations between the real and imaginary components of the pole. The Cartesian coordinates of the pole s_1 in the Laplace plane are σ_1 on the real axis and ω_1 on the imaginary axis. In polar coordinates the pole is expressed as $Me^{j\theta}$, where M is the modulus (the distance of the pole from the origin of the complex plane):

$$M = \sqrt{(\sigma_1 + j\omega_1)(\sigma_1 - j\omega_1)} = \sqrt{\sigma_1^2 + \omega_1^2}$$

and its argument (angle) θ, defined so that:

$$\tan\theta = \frac{\Im\{s_1\}}{\Re\{s_1\}} = \frac{\omega_1}{\sigma_1}$$

Now, a mathematically correct definition of the positive-valued angle is counter-clockwise from the positive real axis; so if σ_1 is negative, θ will be greater than $\pi/2$. However, the *tangent* function is defined within the range of $\mp\pi/2$ and then repeats for values between $\pi \pm k\,\pi/2$. Therefore, by taking the *arctangent*, $\theta = \arctan(\omega_1/\sigma_1)$, we loose the information about which half of the complex plane the pole actually lies in and consequently a sign can be wrong. This is bad, because the left (negative) side of the real axis is associated with energy dissipative, that is, resistive circuit action, while the right (positive) side is associated with energy generative action (this is why

unconditionally stable circuits have the poles always in the left half of the complex plane), so it is undesirable to mix up the two cases.

To keep our analytical expressions simple we will keep tracking the pole layout and correct the sign and value of the arctan( ) by adding π radians to the angle θ wherever necessary. But in order to avoid any confusion our computer algorithm should use a different form of equation (see Part 6).

See Appendix 2.3 (on the disk) for more details.

To use the normalized values of poles in Eq. 2.2.36 we must also enter the normalized time, t/T, where T is the system time constant, $T = RC$. Thus we obtain:

a) for Butterworth poles (MFA):

$$g_a(t) = 1 + \sqrt{2}\ \mathrm{e}^{-t/T} \sin\left(t/T + 0.785 + \pi\right) \tag{2.2.37}$$

b) for Bessel poles (MFED):

$$g_b(t) = 1 + 2\,\mathrm{e}^{-1.5\,t/T} \sin\left(0.866\,t/T + 0.5236 + \pi\right) \tag{2.2.38}$$

c) for Critical damping (CD) we have a double real pole at s_1, so Eq. 2.2.36 is not valid here, because it was derived for simple poles. To calculate the step response for the function with a double pole, we start with Eq. 2.2.8, insert the same (real!) value $(s_1 = s_2)$ and multiply it by the unit step operator $1/s$. The resulting equation:

$$\boxed{G(s) = \frac{s_1^2}{s\,(s - s_1)^2}} \tag{2.2.39}$$

has the time domain function:

$$g(t) = \mathcal{L}^{-1}\{G(s)\} = \sum \mathrm{res}\,\frac{s_1^2\,\mathrm{e}^{st}}{s\,(s - s_1)^2} \tag{2.2.40}$$

There are two residues, res_0 and res_1; $s = 0$ is a simple pole, so for res_0 we have:

$$\mathrm{res}_0 = \lim_{s \to 0} s\left[\frac{s_1^2\,\mathrm{e}^{st}}{s\,(s - s_1)^2}\right] = 1$$

But s_1 is a double pole, so for res_1 we must use Eq. 1.11.12 in Part 1, which for $n = 2$ results in:

$$\mathrm{res}_1 = \lim_{s \to s_1} \frac{d}{ds}\left[(s - s_1)^2\,\frac{s_1^2\,\mathrm{e}^{st}}{s\,(s - s_1)^2}\right] = \mathrm{e}^{s_1 t}\,(s_1 t - 1)$$

The sum of the residues is then:

$$\boxed{g(t) = 1 + \mathrm{e}^{\sigma_1 t}\,(\sigma_1 t - 1)} \tag{2.2.41}$$

Eq. 2.2.39 has a double **real** pole $s_1 = \sigma_1 = -2/RC$ or, normalized, $\sigma_{1n} = -2$. We insert this in the Eq. 2.2.41 to obtain the CD step response plot (curve c, $m = 0.25$):

$$g_c(t) = 1 - \mathrm{e}^{-2t/T}\,(1 + 2t/T) \tag{2.2.42}$$

The step-response plots of all three cases are shown in Fig. 2.2.8. Also shown is the non-peaking response as the reference ($L = 0$). The MFA overshoot is $\delta = 4.3\,\%$, whilst for the MFED case it is 10 times smaller!

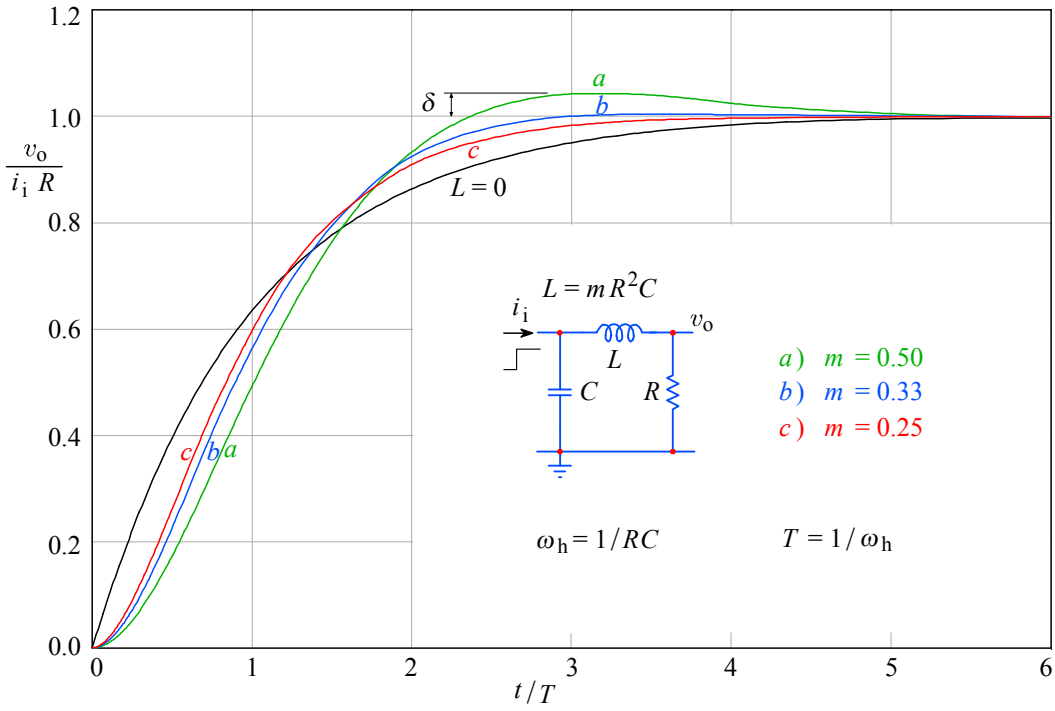

Fig. 2.2.8: Step response of the series peaking circuit for the four characteristic values of m: ***a)*** MFA; ***b)*** MFED; ***c)*** CD. The case $m = 0$ ($L = 0$) is the reference. The MFA overshoot is $\delta = 4.3\,\%$, whilst for MFED it is only $\delta = 0.43\,\%$.

2.2.9 Rise Time

The most important parameter, by which the time domain performance of a wideband amplifier is evaluated, is the rise time. As we have already seen in Fig. 2.1.1, this is the difference between the instants at which the step response crosses the 90 % and 10 % levels of the final value. For the non-peaking amplifier, we have labeled this time as τ_{r_1} and we have already calculated it by Eq. 2.1.4, obtaining the value $\approx 2.20\,RC$. The risetime of a peaking amplifier is labeled τ_R.

To calculate τ_R we use Eq. 2.1.4. For more complex circuits, the step response function can be rather complicated, consequently the analytical calculation becomes difficult, and in such cases it is better to use a computer (see Part 6). The rise time improvement against a non-peaking amplifier is:

$$\eta_r = \frac{\tau_{r_1}}{\tau_R} \tag{2.2.43}$$

The values for the bandwidth improvement η_b and for the rise time improvement η_r are similar, but in general **they are not equal**. In practice we more often use η_b, the calculation of which is easier. If the step response overshoot is not too large ($\delta < 2\,\%$) we can **approximate** the rise time by starting from the formula for the cut off frequency:

$$\omega_h = 2\pi f_h = \frac{1}{RC} \qquad \text{and furthermore} \qquad f_h = \frac{1}{2\pi RC}$$

where ω_h is the upper half power frequency in [rad/s], whilst f_h is the upper half-power frequency in Hz. We have already calculated the non-peaking risetime τ_{r_1} by Eq. 2.1.4 and found it to be $\approx 2.20\,RC$. From this we obtain $\tau_{r_1} f_h = 2.20/2\pi \approx 0.35$, and this relation we meet very frequently in practice:

$$\boxed{\tau_{r_1} \approx \frac{0.35}{f_h}} \tag{2.2.44}$$

By replacing f_h with f_H in this equation, we obtain (an estimate of) the rise time of the **peaking** amplifier. However, Eq. 2.2.44 is exact only for the single-pole amplifier, where the load is the parallel RC network. For all other cases, Eq. 2.2.44 **can be used as an approximation only if the overshoot $\delta < 2\,\%$**. The overshoot of a Butterworth two-pole network amounts to 4.3 % and it becomes larger with each additional pole(-pair), thus calculating the rise time by Eq. 2.2.43 will result in an excessive error. Even greater error will result for networks with Chebyshev and Cauer (elliptic) system poles. In such cases we must compute the actual system step response and find the risetime from it. For Bessel poles, the error is tolerable since the ω_h-normalized Bessel frequency response closely follows the first-order response up to ω_h. Nevertheless, by using a computer to obtain the rise time from the step response will yield a more accurate result.

2.2.10 Input Impedance

We shall use the series peaking network also as an addition to T-coil peaking. This is possible since the T-coil network has a constant input impedance (the T-coil is discussed in Sec. 2.4, 2.5 and 2.6). Therefore it is useful to know the input impedance of the series peaking network. From Fig. 2.2.1 it is evident that the input impedance is a capacitor C in parallel with the serially connected L and R:

$$Z_i = \frac{1}{j\omega C + 1/(j\omega L + R)} = \frac{j\omega L + R}{1 - \omega^2 LC + j\omega RC} \tag{2.2.45}$$

It would be inconvenient to continue with this expression. To simplify we substitute $L = mR^2C$ and $\omega_h = 1/RC$, obtaining:

$$Z_i = R\,\frac{1 + m\left(\dfrac{j\omega}{\omega_h}\right)}{1 - m\left(\dfrac{\omega}{\omega_h}\right)^2 + \dfrac{j\omega}{\omega_h}} \tag{2.2.46}$$

By making the denominator real and carrying out some further rearrangement we obtain:

$$Z_i = R\,\frac{1 + \left(\dfrac{j\omega}{\omega_h}\right)\left[(m-1) - m^2\left(\dfrac{\omega}{\omega_h}\right)^2\right]}{1 + (1-2m)\left(\dfrac{\omega}{\omega_h}\right)^2 + m^2\left(\dfrac{\omega}{\omega_h}\right)^4} \tag{2.2.47}$$

and the phase angle is:

$$\varphi = \arctan\frac{\Im\{Z_i\}}{\Re\{Z_i\}} = \arctan\left\{\left(\frac{\omega}{\omega_h}\right)\left[(m-1) - m^2\left(\frac{\omega}{\omega_h}\right)^2\right]\right\} \tag{2.2.48}$$

The normalized impedance modulus is:

$$\frac{|Z_\mathrm{i}|}{R} = \sqrt{\Re\left\{\frac{Z_\mathrm{i}}{R}\right\}^2 + \Im\left\{\frac{Z_\mathrm{i}}{R}\right\}^2}$$

$$= \frac{\sqrt{1+\left(\frac{\omega}{\omega_\mathrm{h}}\right)^2\left[(m-1)-m^2\left(\frac{\omega}{\omega_\mathrm{h}}\right)^2\right]^2}}{1+(1-2\,m)\left(\frac{\omega}{\omega_\mathrm{h}}\right)^2+m^2\left(\frac{\omega}{\omega_\mathrm{h}}\right)^4} \qquad (2.2.49)$$

In Fig. 2.2.9 the plots of Eq. 2.2.49 and Eq. 2.2.48 for the same values of m as before are shown:

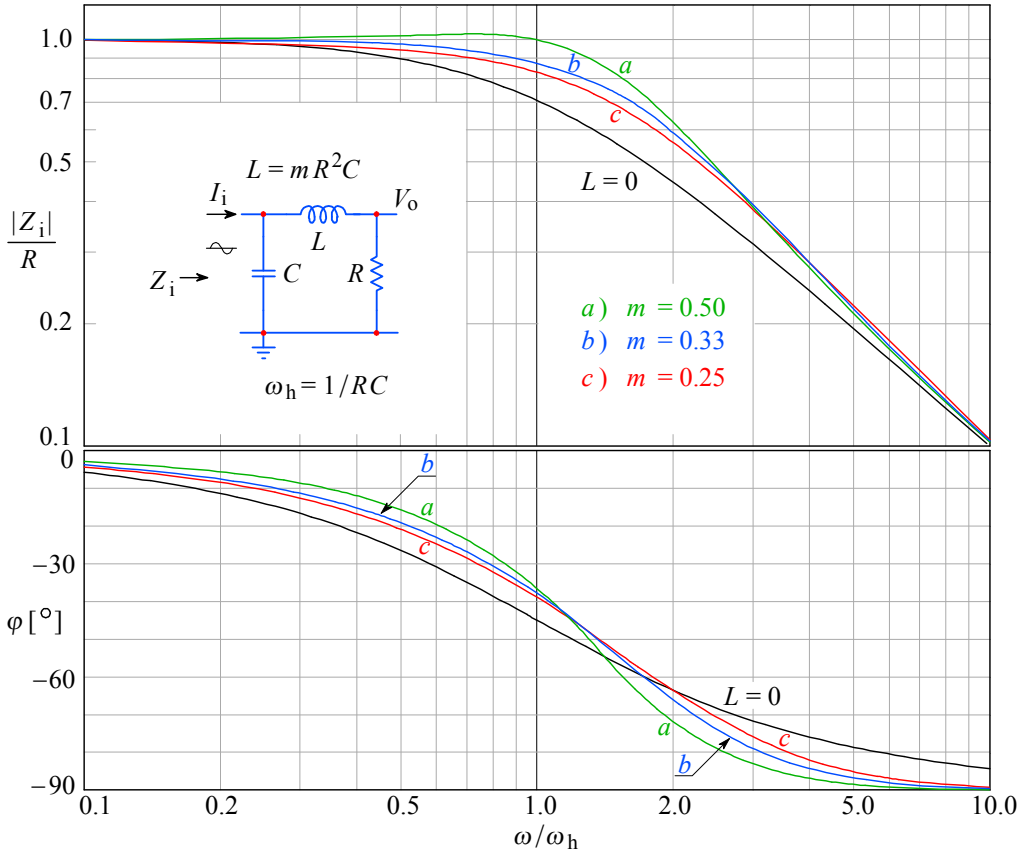

Fig. 2.2.9: Input impedance modulus (normalized) and the associated phase angle of the series peaking circuit for the characteristic values of m. Note that for high frequencies the input impedance approaches that of the capacitance. ***a)*** MFA; ***b)*** MFED; ***c)*** CD.

Table 2.2.1 shows the design parameters of the two-pole series peaking circuit:

Table 2.2.1

response	m	η_b	η_r	δ [%]
MFA	0.50	1.41	1.45	4.30
MFED	0.33	1.36	1.39	0.43
CD	0.25	1.28	1.31	0.00

Table 2.2.1: 2nd-order series peaking circuit parameters summarized: m is the inductance proportionality factor; η_b is the bandwidth improvement; η_r is the risetime improvement; and δ is the step response overshoot.

2.3 Three Pole Series Peaking Circuit

In a practical amplifier we cannot have a pure two-pole series-peaking circuit. The output of the amplifier is always connected to something, be it the next amplifying stage or, say, a cathode ray tube. Any device connected to the output will have at least some capacitance. Therefore the series peaking circuit shown in Fig. 2.3.1 is what we generally encounter in practice. Here we have three independent reactive elements (two capacitors and one inductor), so the circuit has three poles. In order to extract the greatest possible bandwidth from this circuit, the value of the input capacitor C_i, which is in parallel to the loading resistor R, must always be smaller than the loading capacitance C. Since the network is reciprocal, which means we may exchange the input and the output, the condition $C_\mathrm{i} < C$ can always be met. As we will see later, the ratio C/C_i depends on the pole pattern selected and it can not be chosen at random.

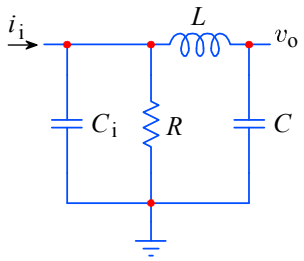

Fig. 2.3.1: The three-pole series peaking circuit.

We shall calculate the network transfer function from the input admittance:

$$Y_\mathrm{i} = j\omega C_\mathrm{i} + \frac{1}{R} + \frac{1}{j\omega L + \dfrac{1}{j\omega C}} \tag{2.3.1}$$

The input impedance is then:

$$Z_\mathrm{i} = \frac{1}{Y_\mathrm{i}} = \frac{R(1-\omega^2 LC)}{(1+j\omega\, C_\mathrm{i} R)(1-\omega^2 LC) + j\omega\, CR} \tag{2.3.2}$$

The input voltage is:

$$V_\mathrm{i} = I_\mathrm{i}\, Z_\mathrm{i} \tag{2.3.3}$$

and the output voltage is:

$$V_\mathrm{o} = a\, V_\mathrm{i} = a\, I_\mathrm{i}\, Z_\mathrm{i} \tag{2.3.4}$$

where a is the voltage attenuation caused by the elements L and C:

$$a = \frac{\dfrac{1}{j\omega C}}{\dfrac{1}{j\omega C} + j\omega L} = \frac{1}{1-\omega^2 LC} \tag{2.3.5}$$

If we insert Eq. 2.3.2 and Eq. 2.3.5 into Eq. 2.3.4, we obtain:

$$V_\mathrm{o} = I_\mathrm{i}\, \frac{R}{1 + j\omega R(C + C_\mathrm{i}) - \omega^2 LC - j\omega^3 C_\mathrm{i} CLR} \tag{2.3.6}$$

Since $I_i R$ is the voltage at zero frequency, we can obtain the amplitude-normalized transfer function by dividing Eq. 2.3.6 by $I_i R$:

$$F(\omega) = \frac{1}{1 + j\omega R(C + C_i) - \omega^2 LC - j\omega^3 C_i CRL} \tag{2.3.7}$$

Let us now make the following three substitutions:

$$L = m\,R^2(C + C_i) \qquad n = \frac{C}{C + C_i} \qquad \omega_h = \frac{1}{R(C + C_i)} \tag{2.3.8}$$

where ω_h is the upper half power frequency of the non-peaking case ($L = 0$). With these substitutions we obtain the function which is normalized both in amplitude and in frequency (to the non-peaking system cut off):

$$F(\omega) = \frac{1}{1 + j\,\frac{\omega}{\omega_h} - m\,n\left(\frac{\omega}{\omega_h}\right)^2 - j\,m\,n\,(1-n)\left(\frac{\omega}{\omega_h}\right)^3} \tag{2.3.9}$$

Since the denominator is a 3rd-order polynomial we have three poles, one of which must be real and the remaining two should be complex conjugated (readers less experienced in mathematics can find the general solutions for polynomials of 1st-, 2nd-, 3rd-and 4th-order in Appendix 2.1). Here we shall show how to calculate the required parameters in an easier way. The magnitude is:

$$\left|F(\omega)\right| = \frac{1}{\sqrt{\left(\Re\{F(\omega)\}\right)^2 + \left(\Im\{F(\omega)\}\right)^2}} \tag{2.3.10}$$

By rearranging the real and imaginary parts in Eq. 2.3.9 and inserting them into Eq. 2.3.10, we obtain:

$$\left|F(\omega)\right| = \frac{1}{\sqrt{\left[1 - m\,n\left(\frac{\omega}{\omega_h}\right)^2\right]^2 + \left[\frac{\omega}{\omega_h} - m\,n\,(1-n)\left(\frac{\omega}{\omega_h}\right)^3\right]^2}} \tag{2.3.11}$$

The squaring of both expressions under the root gives:

$$\left|F(\chi)\right| = \frac{1}{\sqrt{1 + (1 - 2\,m\,n)\chi^2 + m\,n\,[m\,n - 2(1-n)]\chi^4 + m^2\,n^2(1-n)^2\chi^6}} \tag{2.3.12}$$

where we have used $\chi = \omega/\omega_h$ in order to be able to write the equation on a single line.

2.3.1 Butterworth Poles (MFA)

The magnitude of the normalized frequency response for a three-pole Butterworth function is:

$$\left|F(\omega)\right| = \frac{1}{\sqrt{1 + \left(\frac{\omega}{\omega_h}\right)^6}} \tag{2.3.13}$$

By comparing Eq. 2.3.13 with Eq. 2.3.12 we realize that the factors at $(\omega/\omega_h)^2$ and at $(\omega/\omega_h)^4$ in Eq. 2.3.12 must be zero if we want the function to correspond to Butterworth poles:

$$1 - 2\,m\,n = 0 \qquad \text{and} \qquad m\,n - 2(1-n) = 0$$

$$\Rightarrow \qquad m = 2/3 \qquad \text{and} \qquad n = 3/4 \tag{2.3.14}$$

With these data we can calculate the actual values of Butterworth poles and the upper half power frequency. By inserting m and n into Eq. 2.3.12 and, considering that now the coefficients at $(\omega/\omega_h)^2$ and at $(\omega/\omega_h)^4$ are zero, we obtain the frequency response; its plot is shown in Fig. 2.3.2 as curve *a*.

To calculate the poles we insert the values for m and n into Eq. 2.3.9 and by inserting s instead of $j\omega/\omega_h$, the denominator of Eq. 2.3.9 gets the form:

$$\mathcal{D} = 0.125\,s^3 + 0.5\,s^2 + s + 1 \tag{2.3.15}$$

To obtain the canonical form we divide this equation by 0.125. Then to find the roots we equate it to zero:

$$s^3 + 4\,s^2 + 8\,s + 8 = 0 \tag{2.3.16}$$

The roots of this function are the normalized poles of the function $F(s)$:

$$s_{1n}\,,\,s_{2n} = \sigma_{1n} \pm j\,\omega_{1n} = -1 \pm j\,\sqrt{3}$$

$$s_{3n} = \sigma_{3n} = -2 \tag{2.3.17}$$

The values are the normalized to ω_h, considering that $\omega_h = 1/R(C_i + C) = 1$.

All Butterworth poles lie on a circle with a radius equal to the system upper half-power frequency; the real pole s_{3n} also lies on the same circle. Now remember that the poles in tables are normalized to $\omega_h = 1$ rad/s, so their radius is equal to 1. This means that (for Butterworth poles only!) s_{3n}/s_{3t} is already the bandwidth improvement ratio, $\omega_H/\omega_h = \eta_b$, and in our case it is equal to 2 (we would obtain the same value from the factor at $(\omega/\omega_h)^6$ of Eq.2.3.12, $1/\sqrt[6]{m^2n^2(1-n)^2} = 2$).

2.3.2. Bessel Poles (MFED)

The 'classical' way of calculating the parameters m and n for Bessel poles is first to derive the formula for the envelope delay, $\tau_e = d\varphi/d\omega$. This is a rational function of ω. By equating the two coefficients in the numerator with the corresponding two in the denominator polynomial we obtain two equations from which both parameters may be calculated. However, this is a lengthy and error-prone procedure. A more direct and easier way is as follows: in the literature [e.g. Ref. 2.10, 2.11], or with an appropriate computer program (as in Part 6, BESTAP), we look for the Bessel 3rd-order polynomial:

$$B_3(s) = s^3 + 6\,s^2 + 15\,s + 15 \tag{2.3.18}$$

The canonical form of the denominator of Eq. 2.3.9, with s instead of $j\omega/\omega_h$, is:

$$\mathcal{D} = s^3 + \frac{s^2}{1-n} + \frac{s}{m\,n\,(1-n)} + \frac{1}{m\,n\,(1-n)} \tag{2.3.19}$$

The functions in Eq. 2.3.18 and Eq. 2.3.19 must be the same. This is only possible if the corresponding coefficients are equal. Thus we may write the following two equations:

$$\frac{1}{1-n} = 6 \qquad \text{and} \qquad \frac{1}{m\,n\,(1-n)} = 15 \tag{2.3.20}$$

This gives the following values for the parameters:

$$m = 0.480 \qquad \text{and} \qquad n = 0.833 \tag{2.3.21}$$

The roots of Eq. 2.3.18 (or Eq. 2.3.19, with the above values for m and n) are the Bessel poles of the function $F(s)$:

$$\begin{aligned} s_{1n,2n} &= \sigma_{1n} \pm j\,\omega_{1n} = -1.8389 \pm j\,1.7544 \\ s_{3n} &= \sigma_{3n} = -2.3222 \end{aligned} \tag{2.3.22}$$

Note that the same values are obtained from the pole tables (or by running the BESTAP, Part 6 routine); in general, for Bessel poles normalized to a unit delay, $s_{kn} = s_{kt}$.

With these poles the frequency response, according to Eq. 2.3.11, results in the curve *b* in Fig. 2.3.2. The Bessel poles are derived from the condition that the transfer function has a unit envelope delay at the origin, so there is no simple way of relating it to the upper half power frequency ω_H. We need to calculate $|F(\omega)|$ numerically for a range, say, $1 < \omega/\omega_h < 3$, using either Eq. 2.3.11 or the FREQW algorithm in Part 6, and find ω_H from it. The bandwidth improvement factor for Bessel poles is given in Table 2.3.1 at the end of this section.

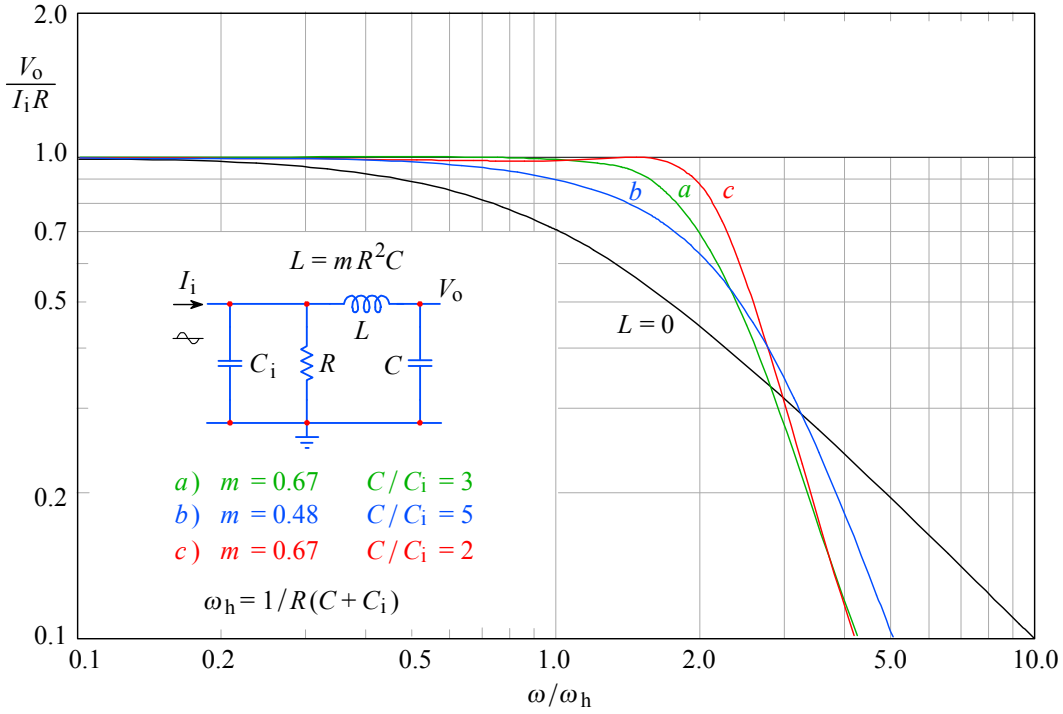

Fig. 2.3.2: Frequency response of the third-order series peaking circuit for different values of m. The correct setting for the required pole pattern is achieved by the input to output capacitance ratio, C/C_i. Fair circuit performance comparison is met by normalization to the total capacitance $C + C_i$. Here we have: ***a)*** MFA; ***b)*** MFED; ***c)*** SPEC, and the non-peaking ($L = 0$) case as a reference. Although being of highest bandwidth, the SPEC case is non-optimal, owing to the slight but notable dip in the range $0.5 < \omega/\omega_h < 1.2$.

2.3.3 Special Case (SPEC)

In practice it is sometimes difficult to achieve the capacitance ratio C/C_i required for Butterworth or for Bessel poles. Let us see what the frequency response would be if we take the capacitance ratio $C/C_\mathrm{i} = 2$, which we shall call a *special case* (SPEC). This makes both parameters equal, $m = n = 0.667$, and the canonical form of the denominator in Eq. 2.3.9, where $(j\omega/\omega_\mathrm{h}) = s$, is then:

$$\mathcal{D} = s^3 + 3\,s^2 + 6.7255\,s + 6.7255 = 0 \tag{2.3.23}$$

Its roots are the required poles:

$$\begin{aligned} s_{1\mathrm{n},2\mathrm{n}} &= \sigma_{1\mathrm{n}} \pm j\,\omega_{1\mathrm{n}} = -0.7500 \pm j\,1.9848 \\ s_{3\mathrm{n}} &= \sigma_{3\mathrm{n}} = -1.5000 \end{aligned} \tag{2.3.24}$$

The corresponding frequency response is the curve *c* in Fig. 2.3.2. This gives a bandwidth improvement $\eta_\mathrm{b} = 2.28$, which sounds very fine if there were not a small dip in the range $0.5 < (\omega/\omega_\mathrm{h}) < 1.2$. So we regrettably realize that the ratio C/C_i can not be chosen at random. The aberrations are even greater for the envelope delay and the step response, as we shall see later.

2.3.4 Phase Response

For the calculation of phase response we can use Eq. 2.2.31, but we must also add the influence of the real pole $\sigma_{3\mathrm{n}}$:

$$\varphi = \arctan\frac{\dfrac{\omega}{\omega_\mathrm{h}} - \omega_{1\mathrm{n}}}{\sigma_{1\mathrm{n}}} + \arctan\frac{\dfrac{\omega}{\omega_\mathrm{h}} + \omega_{1\mathrm{n}}}{\sigma_{1\mathrm{n}}} + \arctan\frac{\dfrac{\omega}{\omega_\mathrm{h}}}{\sigma_{3\mathrm{n}}} \tag{2.3.25}$$

In Fig. 2.3.3 we have plotted the phase response for different values of parameters m and n. Instead of the parameter n, the ratio C/C_i is given.

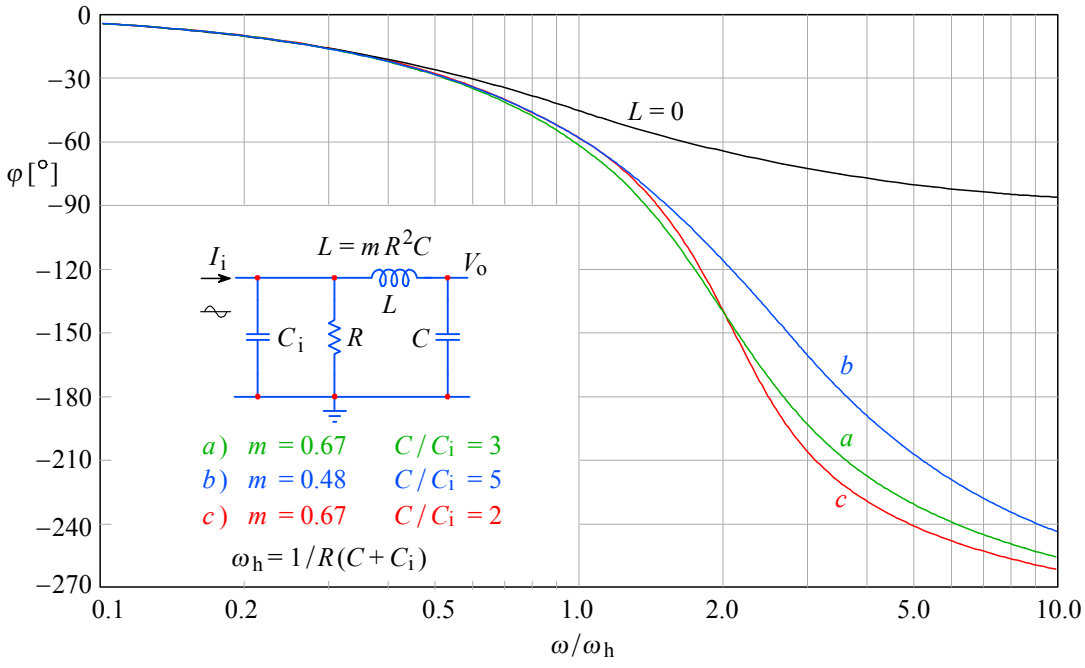

Fig. 2.3.3: Phase response of the third-order series peaking circuit for different values of m: ***a)*** MFA; ***b)*** MFED; ***c)*** SPEC; the non-peaking ($L = 0$) case is the reference.

2.3.5. Envelope-delay

We apply Eq. 2.2.35 to which we add the influence of the real pole σ_{3n}:

$$\tau_e\omega_h = \frac{\sigma_{1n}}{\sigma_{1n}^2 + \left(\frac{\omega}{\omega_h} + \omega_{1n}\right)^2} + \frac{\sigma_{1n}}{\sigma_{1n}^2 + \left(\frac{\omega}{\omega_h} - \omega_{1n}\right)^2} + \frac{\sigma_{3n}}{\sigma_{3n}^2 + \left(\frac{\omega}{\omega_h}\right)^2} \tag{2.3.26}$$

In Fig. 2.3.4 the corresponding plots for different values of parameters m and n are shown; instead of n the ratio C/C_i is given.

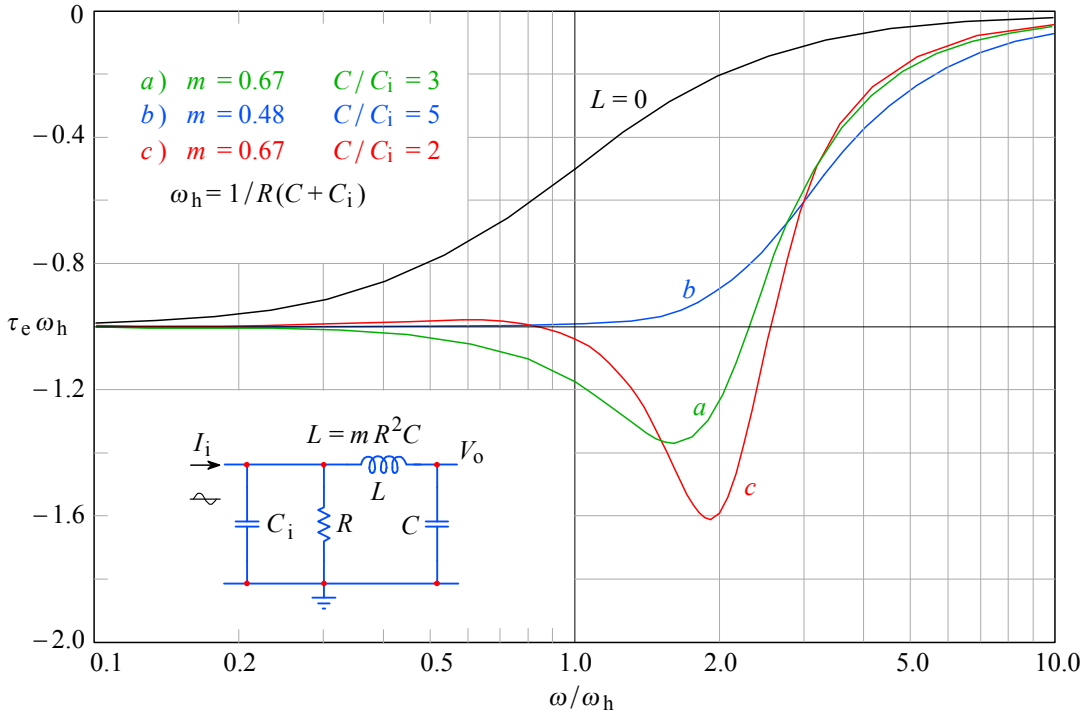

Fig. 2.3.4: Envelope delay of the third-order series peaking circuit for some characteristic values of m: ***a)*** MFA; ***b)*** MFED; ***c)*** SPEC; the non-peaking ($L = 0$) case is the reference. Note the MFED flatness extending beyond ω_h.

2.3.6 Step Response

The calculation is done in a way similar to the case of a two-pole series peaking circuit. Our starting point is Eq. 2.3.9, where we consider that we have two complex conjugate poles s_1 and s_2, and a real pole s_3. The resulting equation must be transformed into a similar form as Eq. 2.2.8. We need a normalized form of equation, so we must multiply the numerator by $-s_1 s_2 s_3$ (see Appendix 2.2). So we obtain a general form:

$$F(s) = \frac{-s_1\,s_2\,s_3}{(s - s_1)(s - s_2)(s - s_3)} \tag{2.3.27}$$

Since we apply a unit step to the network input, the above expression must be multiplied by $1/s$ to obtain a new, fourth-order function:

$$G(s) = \frac{-s_1\,s_2\,s_3}{s\,(s - s_1)(s - s_2)(s - s_3)} \tag{2.3.28}$$

The sum of the residues of $G(s)$ is the step response:

$$g(t) = \mathcal{L}^{-1}\{G(s)\} = \sum_{i=0}^{3} \text{res}_i\,\{G(s)\} \tag{2.3.29}$$

Since the calculation of a three-pole network step response is lengthy, we give here only the final result. The curious reader can find the full derivation in Appendix 2.3.

$$g(t) = 1 - \frac{\sigma_3}{\omega_1 C}\sqrt{A^2 + \omega_1^2 B^2}\;\mathrm{e}^{\sigma_1 t}\sin(\omega_1 t + \beta) - \frac{\sigma_1^2 + \omega_1^2}{C}\,\mathrm{e}^{\sigma_3 t} \tag{2.3.30}$$

where:

$$\begin{aligned} A &= \sigma_1(\sigma_1 - \sigma_3) - \omega_1^2 & B &= 2\,\sigma_1 - \sigma_3 \\ C &= (\sigma_1 - \sigma_3)^2 + \omega_1^2 & \beta &= \arctan(-\omega_1 B/A) + \pi \end{aligned} \tag{2.3.31}$$

Note that we have written β for the initial phase angle of the resonance function, instead of the usual θ, in order to emphasize the difference between the response phase and the angle of the complex conjugated pole pair (in two-pole circuits they have the same value). We enter the normalized poles from Eq. 2.3.17, 2.3.22, and 2.3.24, and the normalized time $t/R(C_\mathrm{i} + C) = t/T$, obtaining the step responses (plotted in Fig. 2.3.5):

a) For Butterworth poles, where $m = 0.667$ and $n = 0.750$ ($\beta = \pi$ rad):

$$g_a(t) = 1 + 1.155\,\mathrm{e}^{-t/T}\sin(1.732\,t/T + \pi) - \mathrm{e}^{-2\,t/T} \tag{2.3.32}$$

b) For Bessel poles, where $m = 0.480$ and $n = 0.833$ ($\beta = 2.5970$ rad):

$$g_b(t) = 1 + 1.839\,\mathrm{e}^{-1.839\,t/T}\sin(1.754\,t/T + 2.597) - 1.951\,\mathrm{e}^{-2.322\,t/T} \tag{2.3.33}$$

c) For our Special Case, where $m = n = 0.667$ ($\beta = \pi$ rad):

$$g_c(t) = 1 + 0.756\,\mathrm{e}^{-0.75\,t/T}\sin(1.985\,t/T + \pi) - \mathrm{e}^{-1.5\,t/T} \tag{2.3.34}$$

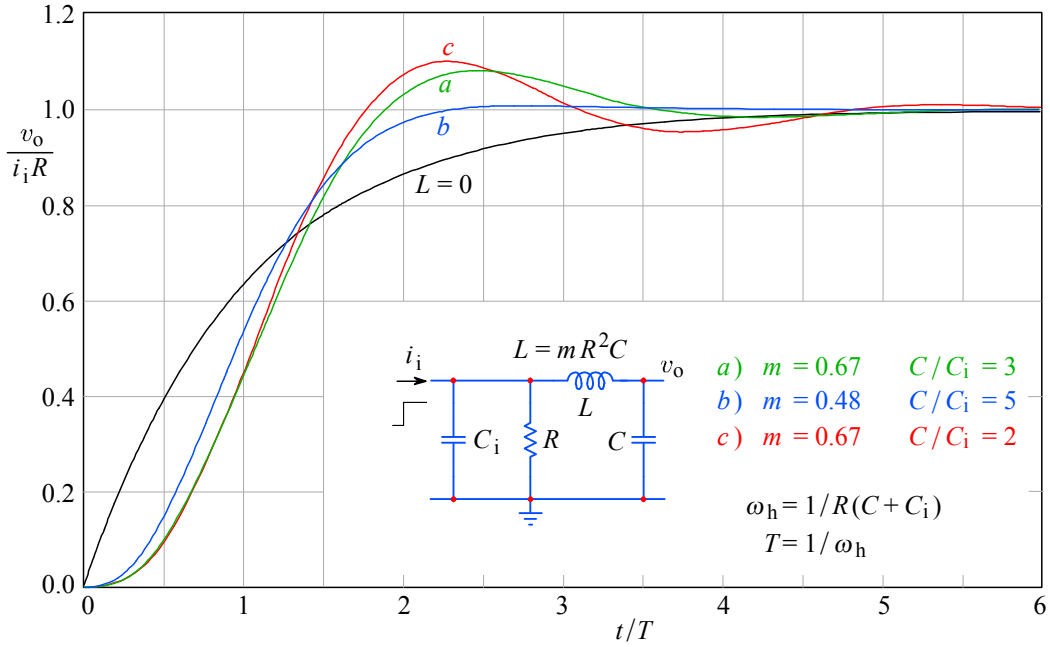

Fig. 2.3.5: Step response of the third-order series peaking circuit for some characteristic values of m: ***a)*** MFA; ***b)*** MFED; ***c)*** SPEC; the non-peaking ($L = 0$) case is the reference. The overshoot of both MFA and SPEC case is too large to be suitable for pulse amplification.

The pole patterns for the three response types discussed are shown in Fig. 2.3.6. Note the three different second-order curves fitting each pole pattern: a (large) horizontal ellipse for MFED, a circle for MFA, and a vertical ellipse for the SPEC case.

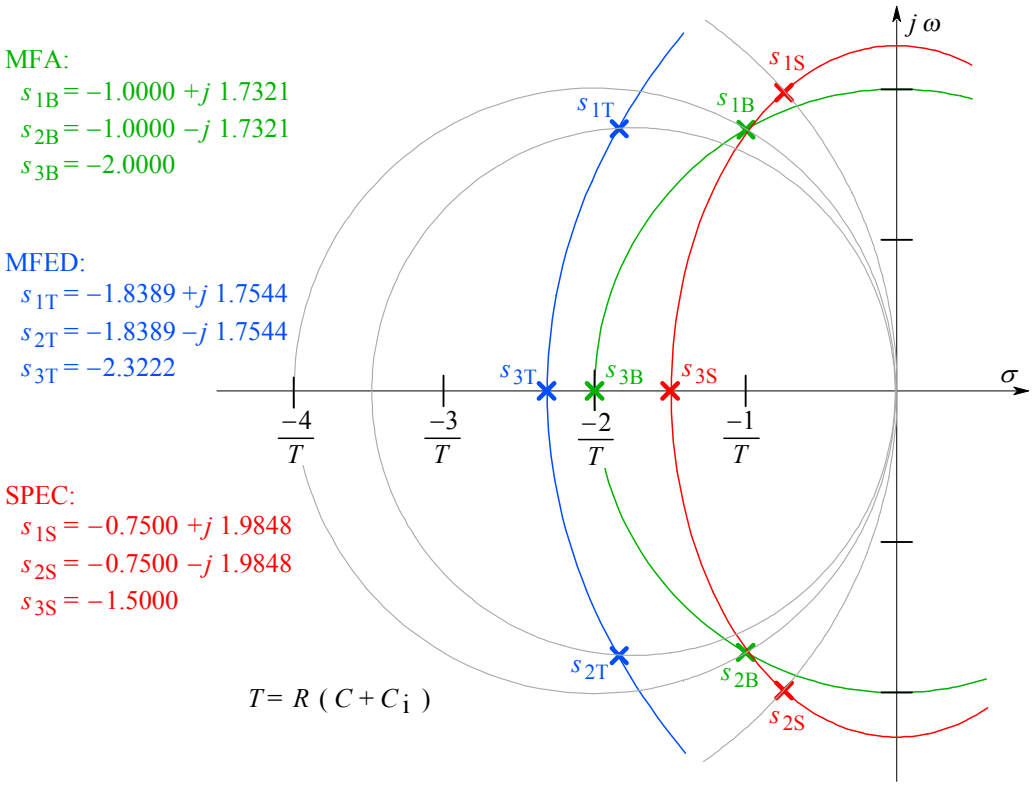

Fig. 2.3.6: Pole patterns of the 3-pole series peaking circuit for the MFA, the MFED, and the SPEC case. The curves on which the poles lie are: a circle with the center at the origin for MFA; an ellipse with both foci on the real axis (the nearer at the origin) for the MFED; and an ellipse with both foci on the imaginary axis for the SPEC case (which is effectively a Chebyshev-type pole pattern). Also shown are the characteristic circles of each complex conjugate pole pair.

Table 2.3.1 resumes the parameters for the three versions of the 3-pole series peaking circuit. Note the high overshoot values for the MFA and the SPEC case, both unacceptable for a pulse amplifier.

Table 2.3.1

response	m	n	η_b	η_r	δ %
a) MFA	0.667	0.750	2.00	1.92	8.1
b) MFED	0.480	0.833	1.75	1.77	0.7
c) SPEC	0.667	0.667	2.28	2.09	10.2

Table 2.3.1: Third-order series peaking circuit parameters.

Table 2.3.1 is based on equal $R(C + C_i)$. From a practical point of view, given the value of the load resistance R, the realizability of the desired response is governed by the ratio C/C_i. If the driving point capacitance C_i is small enough we keep the loading capacitance C as it is and increase C_i as required. Otherwise, we increase C. Since the bandwidth is a function of the sum $C + C_i$, it is clear that an MFED system will be more difficult to realize ($C/C_i = 5$) than an MFA system ($C/C_i = 3$); also its actual bandwidth will be even lower than what can be expected from η_b alone.

2.4 Two-Pole T-coil[1] Peaking Circuit

The circuit schematic of a two-pole T-coil peaking network is shown in Fig. 2.4.1*a*. The main component of this circuit is the center tapped coil L, which is bridged by the capacitance C_b, consisting (ideally) of the coil's self-capacitance [Ref. 2.4, 2.17-2.21]. Since the coils in the equivalent network in Fig. 2.4.1*b* form a letter 'T', we call it a T-coil network. The magnetic coupling factor k between both halves of the coil L and the bridging capacitance C_b must be in a certain relation, dependent on the network poles layout. In addition the relation $R = \sqrt{L/C}$ must hold in order to obtain a constant input impedance $Z_i = R$ at any frequency [Ref. 2.18, 2.21]. This is true if the elements of the network do not have any losses. Owing to losses in a practical circuit, the input impedance may be considered to be constant only up to a certain frequency, which, with a careful design, can be high enough for the application of the T-coil circuit in a wideband amplifier.

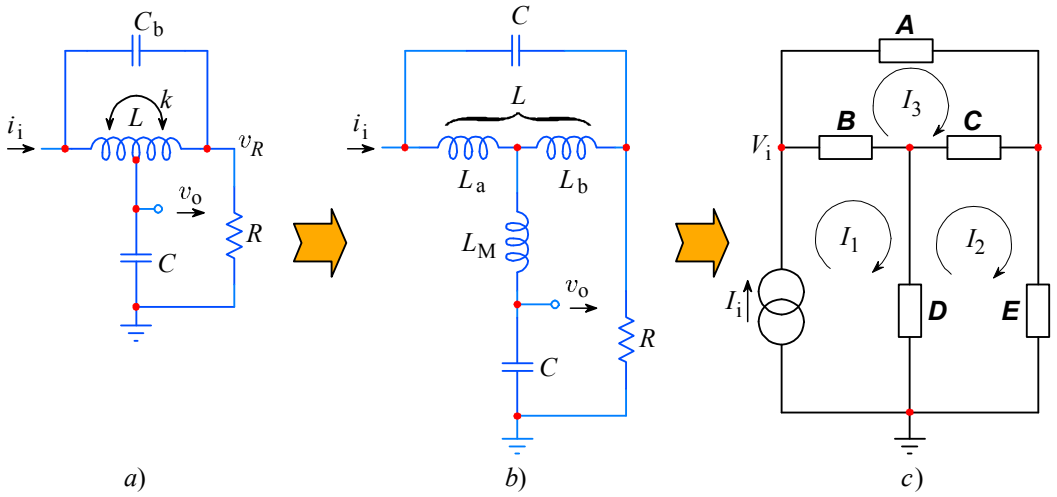

Fig. 2.4.1: ***a)*** The basic T-coil circuit: the voltage output is taken from the center tap node of the inductance L and its two parts are magnetically coupled by the factor $0 < k < 1$; ***b)*** an equivalent circuit, with no magnetic coupling between the coils — it has been replaced by the mutual inductance L_M; ***c)*** a simplified generalized impedance circuit, excited by the current generator I_i, showing the current loops.

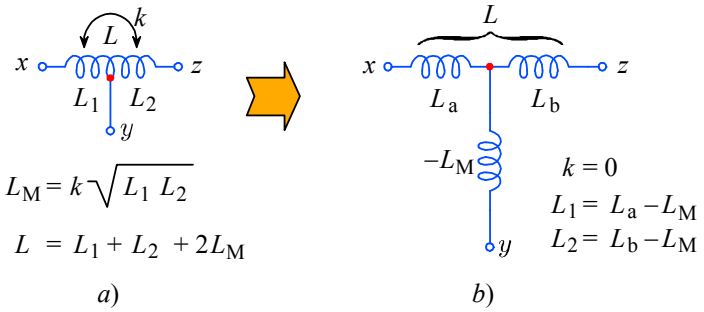

Fig. 2.4.2: Modeling the coupling factor: ***a)*** The T-coil coupling factor k between the two halves L_1 and L_2 of the total inductance L can be represented by ***b)*** an equivalent circuit, having two separate (non-coupled) inductances, in which the magnetic coupling is modeled by the mutual inductance L_M (negative in value), so that $L_1 = L_a - L_M$ and $L_2 = L_b - L_M$.

[1] Networks with tapped coils have been used already in 1948 [Ref. 2.4] and 1954 [Ref. 2.16], but since the bridging capacitance C_b has not been accounted for, the networks described did not have a constant input impedance, as do have the T-coil networks discussed in this and the following three sections.

If the output is taken from the loading resistor R, the network in Fig. 2.4.1*a* behaves as an all pass network. **However, for peaking purposes we take the output voltage from the capacitor *C* and in this application the circuit is a low pass filter.**

The equivalent network in Fig. 2.4.1*b* needs to be explained. We will do this with the aid of Fig. 2.4.2. The original network has a center tapped coil whose inductance L can be calculated by the same general equation for two coupled coils, [Ref. 2.18, 2.28]:

$$L = L_1 + L_2 + 2\,L_\mathrm{M} \tag{2.4.1}$$

where L_1 and L_2 are the inductances of the respective coil parts (which, in general, need not to be equal) and L_M is their mutual inductance. L_M is taken twice, since the magnetic induction from L_1 to L_2 is equal to the induction from L_2 to L_1 and both contribute to the total. If k is the factor of magnetic coupling between L_1 and L_2 the mutual inductance is:

$$L_\mathrm{M} = k\,\sqrt{L_1 L_2} \tag{2.4.2}$$

In the equivalent circuit, with no coupling between the coils, we have:

$$L_\mathrm{a} = L_1 + L_\mathrm{M} \qquad\qquad L_\mathrm{b} = L_2 + L_\mathrm{M} \tag{2.4.3}$$

Then L_1 and L_2 are:

$$L_1 = L_\mathrm{a} - L_\mathrm{M} \qquad\qquad L_2 = L_\mathrm{b} - L_\mathrm{M} \tag{2.4.4}$$

Note the negative sign of L_M, which is a consequence of magnetic coupling; owing to this the driving impedance at the center tap as seen by C is lower than without the coupling. In the symmetrical case, when $L_1 = L_2$, we can calculate the value of L_1 and L_2 from the required coupling k and total inductance L:

$$L_1 = L_2 = \frac{L}{2\,(1+k)} \tag{2.4.5}$$

Thus we have proved that the circuits in Fig. 2.4.1*a* and 2.4.1*b* are equivalent, even though no coupling exists between the coils in the circuit of Fig. 2.4.1*b*.

The corresponding generalized impedance model of the T-coil circuit is shown in Fig. 2.4.1*c*, where the input voltage V_i is equal to the product of the input current and the circuit impedance, $I_\mathrm{i} Z_\mathrm{i}$. The input current splits into I_1 and I_2. The current I_3 flows in the remaining loop. The impedances in the branches are:

$$\begin{aligned} \boldsymbol{A} &= 1/s\,C_\mathrm{b} \\ \boldsymbol{B} &= s\,L_\mathrm{a} \\ \boldsymbol{C} &= s\,L_\mathrm{b} \\ \boldsymbol{D} &= -\,s\,L_\mathrm{M} + 1/s\,C \\ \boldsymbol{E} &= R \end{aligned} \tag{2.4.6}$$

We have written s instead of $j\omega$. With these substitutions the calculation will be much easier. Frankly, from here on, the whole calculation could be done by a suitable computer program, but then some important intermediate results, which we want to explain in detail, would not be shown. So we will do a hand calculation and only at the very end, where the difficulties will increase, shall we use a computer.

We form a system of equations in accordance with the current loops in Fig. 2.4.1*c*:

$$\begin{aligned} V_\mathrm{i} &= I_1(\boldsymbol{B}+\boldsymbol{D}) - I_2\,\boldsymbol{D} - I_3\,\boldsymbol{B} \\ 0 &= -I_1\,\boldsymbol{D} + I_2\,(\boldsymbol{C}+\boldsymbol{D}+\boldsymbol{E}) - I_3\,\boldsymbol{C} \\ 0 &= -I_1\,\boldsymbol{B} - I_2\,\boldsymbol{C} + I_3\,(\boldsymbol{A}+\boldsymbol{B}+\boldsymbol{C}) \end{aligned} \tag{2.4.7}$$

The determinant of the coefficients is:

$$\Delta = \begin{vmatrix} \boldsymbol{B}+\boldsymbol{D} & -\boldsymbol{D} & -\boldsymbol{B} \\ -\boldsymbol{D} & \boldsymbol{C}+\boldsymbol{D}+\boldsymbol{E} & -\boldsymbol{C} \\ -\boldsymbol{B} & -\boldsymbol{C} & \boldsymbol{A}+\boldsymbol{B}+\boldsymbol{C} \end{vmatrix} \tag{2.4.8}$$

with the solution:

$$\begin{aligned} \Delta = {} & (\boldsymbol{B}+\boldsymbol{D})\,[(\boldsymbol{C}+\boldsymbol{D}+\boldsymbol{E})(\boldsymbol{A}+\boldsymbol{B}+\boldsymbol{C}) - \boldsymbol{C}^2] \\ & + \boldsymbol{D}\,[-\boldsymbol{D}(\boldsymbol{A}+\boldsymbol{B}+\boldsymbol{C}) - \boldsymbol{BC}] - \boldsymbol{B}\,[\boldsymbol{DC} + \boldsymbol{B}(\boldsymbol{C}+\boldsymbol{D}+\boldsymbol{E})] \end{aligned} \tag{2.4.9}$$

After multiplication some terms will cancel. Thus the solution is simplified to:

$$\Delta = \boldsymbol{BCA} + \boldsymbol{BDA} + \boldsymbol{BEA} + \boldsymbol{BEC} + \boldsymbol{DCA} + \boldsymbol{DEA} + \boldsymbol{DEB} + \boldsymbol{DEC} \tag{2.4.10}$$

For further calculation we shall need both cofactors Δ_{11} and Δ_{12}. The cofactor for I_1 is:

$$\begin{aligned} \Delta_{11} &= \begin{vmatrix} V_\mathrm{i} & -\boldsymbol{D} & -\boldsymbol{B} \\ 0 & \boldsymbol{C}+\boldsymbol{D}+\boldsymbol{E} & -\boldsymbol{C} \\ 0 & -\boldsymbol{C} & \boldsymbol{A}+\boldsymbol{B}+\boldsymbol{C} \end{vmatrix} \\ &= V_\mathrm{i}\,(\boldsymbol{CA} + \boldsymbol{CB} + \boldsymbol{DA} + \boldsymbol{DB} + \boldsymbol{DC} + \boldsymbol{EA} + \boldsymbol{EB} + \boldsymbol{EC}) \end{aligned} \tag{2.4.11}$$

and in a similar way the cofactor for I_2:

$$\begin{aligned} \Delta_{12} &= \begin{vmatrix} \boldsymbol{B}+\boldsymbol{D} & V_\mathrm{i} & -\boldsymbol{D} \\ -\boldsymbol{D} & 0 & -\boldsymbol{C} \\ -\boldsymbol{B} & 0 & \boldsymbol{A}+\boldsymbol{B}+\boldsymbol{C} \end{vmatrix} \\ &= V_\mathrm{i}\,(\boldsymbol{DA} + \boldsymbol{DB} + \boldsymbol{DC} + \boldsymbol{BC}) \end{aligned} \tag{2.4.12}$$

Let us first find the input admittance, which we would like to be equal to $1/R = 1/\boldsymbol{E}$.

$$\begin{aligned} Y &= \frac{I_1}{V_\mathrm{i}} = \frac{\Delta_{11}}{V_\mathrm{i}\Delta} \\ &= \frac{\boldsymbol{CA} + \boldsymbol{CB} + \boldsymbol{DA} + \boldsymbol{DB} + \boldsymbol{DC} + \boldsymbol{EA} + \boldsymbol{EB} + \boldsymbol{EC}}{\boldsymbol{BCA} + \boldsymbol{BDA} + \boldsymbol{BEA} + \boldsymbol{BEC} + \boldsymbol{DCA} + \boldsymbol{DEA} + \boldsymbol{DEB} + \boldsymbol{DEC}} = \frac{1}{\boldsymbol{E}} \end{aligned} \tag{2.4.13}$$

After eliminating the fractions and canceling some terms, we obtain the expression:

$$\boldsymbol{BCA} + \boldsymbol{BDA} + \boldsymbol{BEA} + \boldsymbol{DCA} - \boldsymbol{ECA} - \boldsymbol{E}^2\boldsymbol{A} - \boldsymbol{E}^2\boldsymbol{B} - \boldsymbol{E}^2\boldsymbol{C} = 0 \tag{2.4.14}$$

Now we put in the values from Eq. 2.4.6, considering that $L_\mathrm{a} = L_\mathrm{b}$, perform all the multiplications, and arrange the terms with the decreasing powers of s. We obtain:

$$s\left[\left(\frac{L_\mathrm{a}^2}{C_\mathrm{b}}-\frac{L\,L_\mathrm{M}}{C_\mathrm{b}}\right)-R^2L\right]+\frac{1}{s}\left(\frac{L}{C\,C_\mathrm{b}}-\frac{R^2}{C_\mathrm{b}}\right)=0 \tag{2.4.15}$$

or, in a general form:

$$s\,\boldsymbol{K}_1+s^{-1}\boldsymbol{K}_2=0 \tag{2.4.16}$$

This expression tells us that the input admittance can indeed be made equal to $1/R$, as we wanted in Eq. 2.4.13. For a constant input admittance circuit, Eq. 2.4.16 must be valid for any s [Ref. 2.21]. This is possible only if both $\boldsymbol{K}_1$ and $\boldsymbol{K}_2$ are zero (*Ross' method*):

$$\boldsymbol{K}_1=\frac{L_\mathrm{a}^2}{C_\mathrm{b}}-\frac{L\,L_\mathrm{M}}{C_\mathrm{b}}-R^2L=0 \tag{2.4.17}$$

$$\boldsymbol{K}_2=\frac{L}{C\,C_\mathrm{b}}-\frac{R^2}{C_\mathrm{b}}=0 \tag{2.4.18}$$

From this we obtain the following two relations:

$$\begin{aligned} L&=R^2C\\ L_\mathrm{M}&=\frac{L}{4}-R^2C_\mathrm{b}=R^2\left(\frac{C}{4}-C_\mathrm{b}\right)\end{aligned} \tag{2.4.19}$$

For the symmetrical case, with the tap at the center of the coil, $L_\mathrm{a}=L_\mathrm{b}=L/2$. Since only two parameters, C and R, are known initially, we must obtain another, independent equation in order to calculate the parameters L_M and C_b. For this we can use the transimpedance equation, V_o/I_1 ($I_\mathrm{i}=I_1$, see Fig. 2.4.2.*b*). From Fig. 2.4.1*c* it is evident that the current difference I_1-I_2 flows through branch D. This difference current, multiplied by the impedance $1/sC$, is equal to the output voltage V_o. The transimpedance is then:

$$\frac{V_\mathrm{o}}{I_1}=\frac{1}{s\,C}\cdot\frac{I_1-I_2}{I_1} \tag{2.4.20}$$

The currents are calculated by Cramer's rule:

$$I_1=\frac{\Delta_{11}}{\Delta}\qquad\text{and}\qquad I_2=\frac{\Delta_{12}}{\Delta} \tag{2.4.21}$$

and if we put these expressions into Eq. 2.4.20 we obtain:

$$\frac{V_\mathrm{o}}{I_1}=\frac{1}{s\,C}\cdot\frac{\Delta_{11}-\Delta_{12}}{\Delta_{11}} \tag{2.4.22}$$

Again we make use of the common expressions in Eq. 2.4.6. The difference of both cofactors is:

$$\Delta_{11}-\Delta_{12}=V_\mathrm{i}\,(\boldsymbol{CA}+\boldsymbol{EA}+\boldsymbol{EB}+\boldsymbol{EC}) \tag{2.4.23}$$

With these expressions, the transimpedance is:

$$\frac{V_o}{I_1} = \frac{1}{s\,C} \cdot \frac{\boldsymbol{CA + EA + EB + EC}}{\boldsymbol{CA + CB + DA + DB + DC + EA + EB + EC}} \tag{2.4.24}$$

The voltage V_i is a factor of both the numerator and the denominator, so it cancels out. Now we replace the common expressions with those from Eq. 2.4.6, express L_M with Eq. 2.4.19, perform the indicated multiplication, make the long division of the polynomials, and the result is a relatively simple expression:

$$F(s) = \frac{V_o}{I_1} = \frac{R}{s^2 R^2 C\,C_b + sRC/2 + 1} \tag{2.4.25}$$

Although the author of this idea, Bob Ross, calculated it 'by hand' [Ref. 2.21], we will not follow his example because this calculation is a formidable work. With modern computer programs (such as *Mathematica* [Ref. 2.34] or similar [Ref. 2.35, 2.38, 2.39, 2.40]), the calculation takes less time than is needed to type in the data.

For those designers who want to construct a distributed amplifier using electronic tubes or FETs (**but not transistors**, as we will see in Part 3!), where the resistor R is replaced by another T-coil circuit and so forth (forming a lumped delay line), it is important to know the transimpedance from the input I_1 to the voltage V_R. The result is:

$$\frac{V_R}{I_1} = R\,\frac{s^2 R^2 C\,C_b - sRC/2 + 1}{s^2 R^2 C\,C_b + sRC/2 + 1} \tag{2.4.26}$$

Besides the two poles on the left side of the s-plane, s_{1p} and s_{2p}, this equation also has two symmetrically placed zeros on the right side of the s-plane, s_{1z} and s_{2z}, as shown in Fig. 2.4.3. Since Eq. 2.4.26 has equal powers of s both in the numerator and the denominator it is an all pass response. We shall return to this when we shall calculate the step response.

The poles are the roots of the denominator of Eq. 2.4.25. The canonical form is:

$$s^2 + s\,\frac{1}{2RC_b} + \frac{1}{R^2 C\,C_b} = 0 \tag{2.4.27}$$

In general the roots are complex conjugates:

$$s_{1,2} = \sigma_1 \pm j\,\omega_1 = -\frac{1}{4RC_b} \pm \sqrt{\frac{1}{(4RC_b)^2} - \frac{1}{R^2 C\,C_b}} \tag{2.4.28}$$

By factoring out $1/4RC_b$ we obtain a more convenient expression:

$$s_{1,2} = -\frac{1}{4RC_b}\left(1 \pm \sqrt{1 - \frac{16\,C_b}{C}}\right) \tag{2.4.29}$$

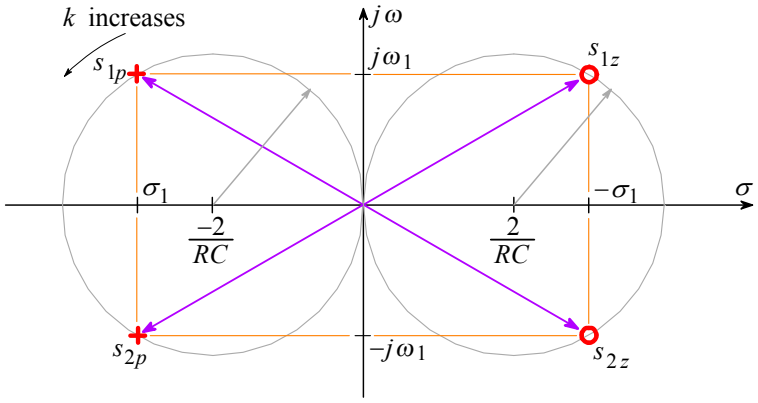

Fig. 2.4.3: The poles (s_{1p} and s_{2p}) and zeros (s_{1z} and s_{2z}) of the all pass transimpedance function corresponding to Eq. 2.4.26 and Fig. 2.4.1*a*. By changing the bridge capacitance C_b and the mutual inductance L_M (by the coupling factor k) according to Eq. 2.4.19, both poles and both zeros travel along the circles shown.

An efficient inductive peaking circuit must have complex poles. By taking the imaginary unit out of the square root, the terms within it exchange signs. Then the pole angle θ can be calculated from the ratio of its imaginary to the real component, as we have done before. From Fig. 2.2.4:

$$\tan\theta = \frac{\Im\{s_1\}}{\Re\{s_1\}} = \frac{\sqrt{\dfrac{16\,C_\mathrm{b}}{C} - 1}}{-1} \tag{2.4.30}$$

This gives a general result:

$$\boxed{C_\mathrm{b} = C\,\frac{1+\tan^2\theta}{16}} \tag{2.4.31}$$

The Bessel pole placement is show in Fig. 2.4.4. The characteristic angle θ is measured from the positive real axis.

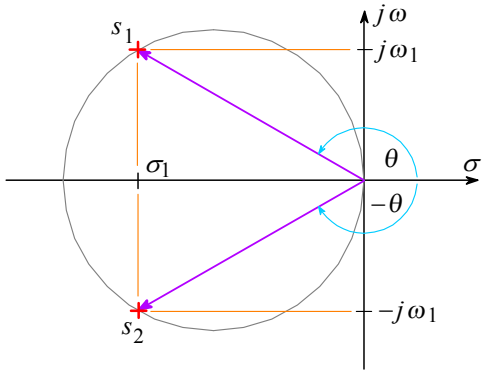

Fig. 2.4.4: The layout of complex conjugate poles s_1 and s_2 of a second-order Bessel transfer function. In this case, the angle is $\theta = 150°$.

By using the pole angle, which we have calculated previously, and Eq. 2.4.31, the corresponding bridging capacitance can be found:

For Bessel poles:

$$\theta = 150° \qquad \tan^2\theta = 1/3 \qquad C_\mathrm{b} = C/12 \tag{2.4.32}$$

For Butterworth poles:

$$\theta = 135° \qquad \tan^2\theta = 1 \qquad C_\mathrm{b} = C/8 \tag{2.4.33}$$

The corresponding mutual inductance is, according to Eq. 2.4.19:

for Bessel poles:

$$L_M = \frac{R^2\,C}{6} \tag{2.4.34}$$

and for Butterworth poles:

$$L_M = \frac{R^2\,C}{8} \tag{2.4.35}$$

The general expression for the coupling factor is [Ref. 2.21, 2.28, 2.33]:

$$k = \frac{L_M}{\sqrt{L_1\,L_2}} = \frac{L_M}{\sqrt{(L_a - L_M)(L_b - L_M)}} \tag{2.4.36}$$

By considering that $L_a = L_b = L/2 = R^2\,C/2$ we obtain:

$$k = \frac{L_M}{\frac{L}{2} - L_M} = \frac{R^2\left(\frac{C}{4} - C_b\right)}{\frac{R^2C}{2} - R^2\left(\frac{C}{4} - C_b\right)} = \frac{\frac{C}{4} - C_b}{\frac{C}{4} + C_b} \tag{2.4.37}$$

If C_b is expressed by Eq. 2.4.31, we may derive a very interesting expression for the coupling factor k:

$$\boxed{k = \frac{3 - \tan^2\theta}{5 + \tan^2\theta}} \tag{2.4.38}$$

Since $\theta = 150°$ for the Bessel pole pair and 135° for the Butterworth pole pair, the corresponding coupling factor is:

for Bessel poles:

$$k = 0.5 \tag{2.4.39}$$

for Butterworth poles:

$$k = 0.3\dot{3} \tag{2.4.40}$$

Let us calculate the parameters k, L_M and C_b for two additional cases. If we want to avoid any overshoot, then both poles must be real and equal. In this case $\theta = 180°$ and the damping of the circuit is critical (CD). The expression under the root of Eq. 2.4.29 must be zero and we obtain:

$$C_b = \frac{C}{16} \qquad L_M = \frac{3\,R^2C}{16} \qquad k = 0.6 \tag{2.4.41}$$

We are also interested in the circuit values for the limiting case in which the coupling factor k and consequently the mutual inductance L_M are zero. Here we calculate C_b from Eq. 2.4.31:

$$C_b = \frac{C}{4}\bigg|_{\substack{k=0\\L_M=0}} \tag{2.4.42}$$

The next task is to calculate the poles for all four cases. We will show only the calculation for Bessel poles; the other calculations are equal.

For the starting expression we use the denominator of Eq. 2.4.25 in the canonical form, which we equate to zero:

$$s^2 + s\,\frac{1}{2RC_\mathrm{b}} + \frac{1}{R^2CC_\mathrm{b}} = 0 \tag{2.4.43}$$

Now we insert $C_\mathrm{b} = C/12$, which corresponds to Bessel poles; the result is:

$$s^2 + s\,\frac{6}{RC} + \frac{12}{R^2C^2} = 0 \tag{2.4.44}$$

By factoring out $1/RC$ the roots (poles of Eq. 2.4.25) are:

$$s_{1,2} = \sigma_1 \pm j\,\omega_1 = \frac{1}{RC}\,(\,-3 \pm j\,\sqrt{3}\,) \tag{2.4.45}$$

In a similar way we calculate the Butterworth poles, where $C_\mathrm{b} = C/8$:

$$s_{1,2} = \sigma_1 \pm j\,\omega_1 = \frac{1}{RC}\,(\,-2 \pm j\,2\,) \tag{2.4.46}$$

For critical damping (CD) the imaginary part of the poles is zero, so $C_\mathrm{b} = C/16$, as found before. The poles are:

$$s_{1,2} = \sigma_1 = -\,\frac{4}{RC} \tag{2.4.47}$$

In the no-coupling case ($k = 0$) the bridging capacitance $C_\mathrm{b} = C/4$, and the poles are:

$$s_{1,2} = \sigma_1 \pm j\,\omega_1 = \frac{1}{RC}\,(\,-1 \pm j\,\sqrt{3}\,) \tag{2.4.48}$$

For all four kinds of poles, the input impedance $Z_\mathrm{i} = R = \sqrt{L/C}$ and it is independent of frequency. Now we have all the necessary data to calculate the frequency, phase, time delay and the step response.

2.4.1 Frequency Response

We can use the amplitude- and frequency-normalized Eq. 2.2.27:

$$\left|F(\omega)\right| = \frac{\sigma_{1\mathrm{n}}^2 + \omega_{1\mathrm{n}}^2}{\sqrt{\left[\sigma_{1\mathrm{n}}^2 + \left(\frac{\omega}{\omega_\mathrm{h}} + \omega_{1\mathrm{n}}\right)^2\right]\left[\sigma_{1\mathrm{n}}^2 + \left(\frac{\omega}{\omega_\mathrm{h}} - \omega_{1\mathrm{n}}\right)^2\right]}}$$

By inserting the values for normalized poles, with $RC = 1$ and $\omega_\mathrm{h} = 1/RC$, we can plot the response for each of the four types of poles, as shown in Fig. 2.4.5.

By comparing this diagram with the frequency-response plot for a simple series peaking circuit in Fig. 2.2.3, we realize that the upper cut off frequency ω_H of the T-coil circuit is exactly twice as much as it is for the two-pole series peaking circuit (by comparing, of course, the responses for the same kind of poles). I.e., for Butterworth poles we had $s_{1\mathrm{n},2\mathrm{n}} = 1 \pm j$ (Eq. 2.2.16) for the series peaking circuit, whilst here we have $s_{1\mathrm{n},2\mathrm{n}} = 2 \pm j\,2$. Thus the bandwidth improvement factor for a two pole T-coil circuit, compared with the single pole (RC) circuit is $\eta_\mathrm{b} = 2.83$ (the ratio of the absolute values of poles). Similarly, for other kinds of poles, the bandwidth improvement is greater too, as

reported in Table 2.4.1 at the end of this section. Owing to this property, it is worth considering the use of a T-coil circuit whenever possible. For the same reason we shall discuss T-coil circuits further in detail.

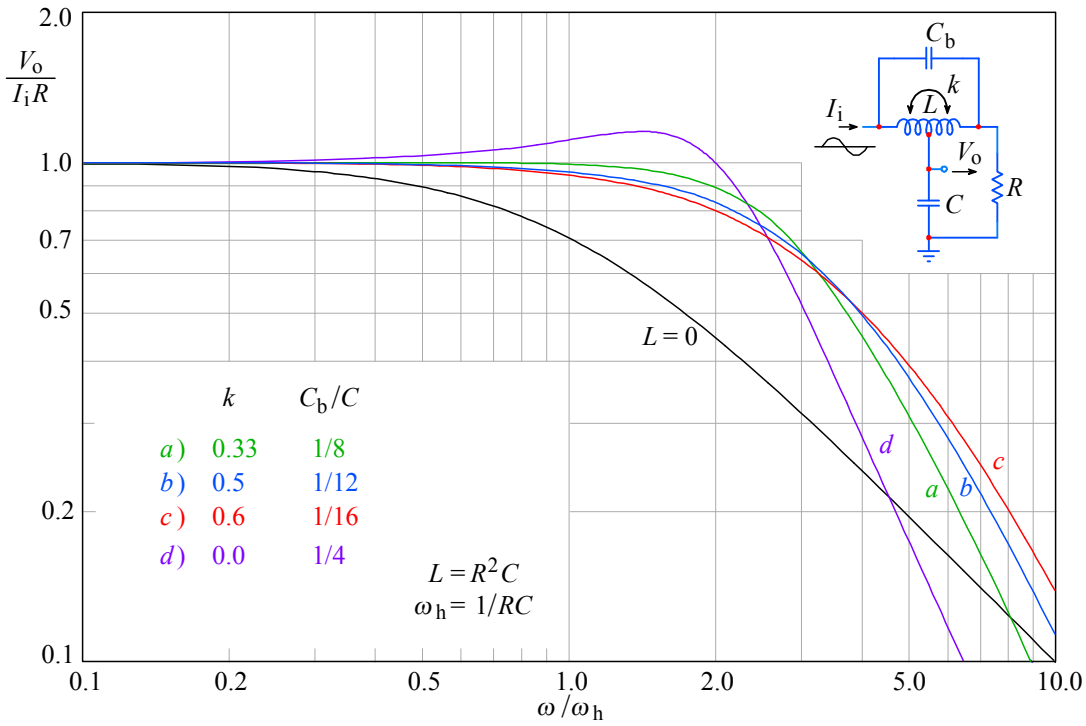

Fig. 2.4.5: The frequency response magnitude of the T-coil, taken from the coil center tap. The curve ***a)*** is the MFA (Butterworth) case, ***b)*** is the MFED (Bessel) case, ***c)*** is the critical damping (CD) case and ***d)*** is the no-coupling ($k = 0$) case. The non-peaking ($L = 0$) case is the reference. The bandwidth extension is notably larger, not only compared with the two-pole series peaking, but also to the three-pole series peaking circuit.

2.4.2 Phase Response

Here we use again the Eq. 2.2.31:

$$\varphi = \arctan \frac{\frac{\omega}{\omega_h} - \omega_{1n}}{\sigma_{1n}} + \arctan \frac{\frac{\omega}{\omega_h} + \omega_{1n}}{\sigma_{1n}}$$

and, by inserting the values for the normalized poles, as we did in the calculation of the frequency response, we obtain the plots shown in Fig. 2.4.6.

2.4.3 Envelope Delay

We use again Eq. 2.2.35:

$$\tau_e \omega_h = \frac{\sigma_{1n}}{\sigma_{1n}^2 + \left(\frac{\omega}{\omega_h} - \omega_{1n}\right)^2} + \frac{\sigma_{1n}}{\sigma_{1n}^2 + \left(\frac{\omega}{\omega_h} + \omega_{1n}\right)^2}$$

and, with the pole values as before, we get the Fig. 2.4.7 responses.

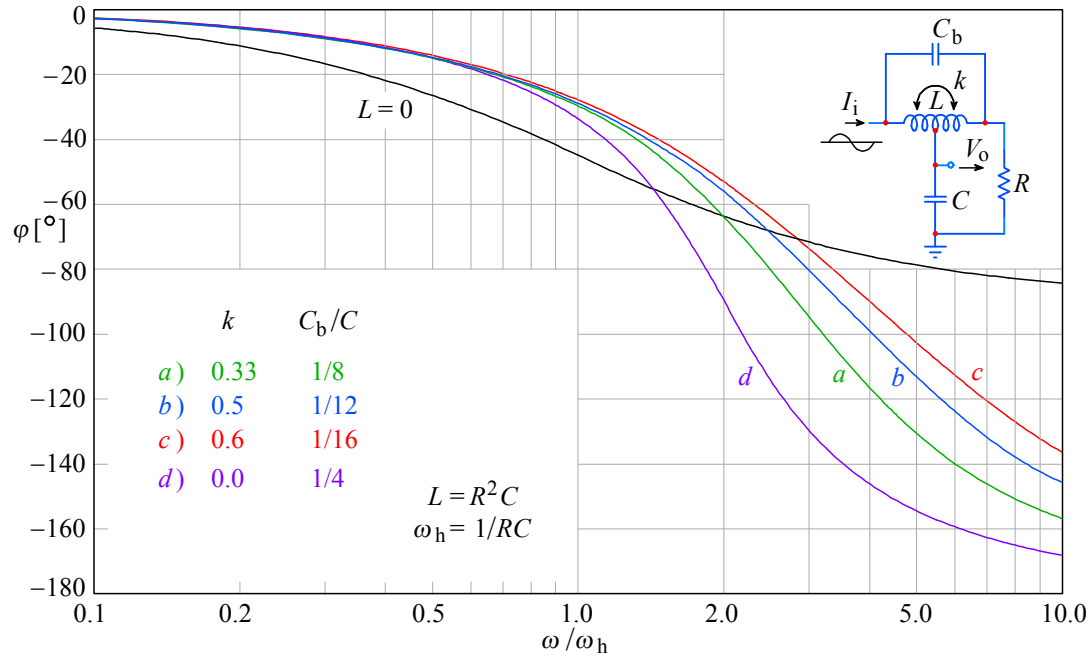

Fig. 2.4.6: The transfer function phase angle of the T-coil circuit, for the same values of coupling and capacitance ratio as for the frequency response magnitude. ***a)*** is MFA, ***b)*** is MFED, ***c)*** is CD and ***d)*** is the no-coupling case. The non-peaking ($L = 0$) case is the reference.

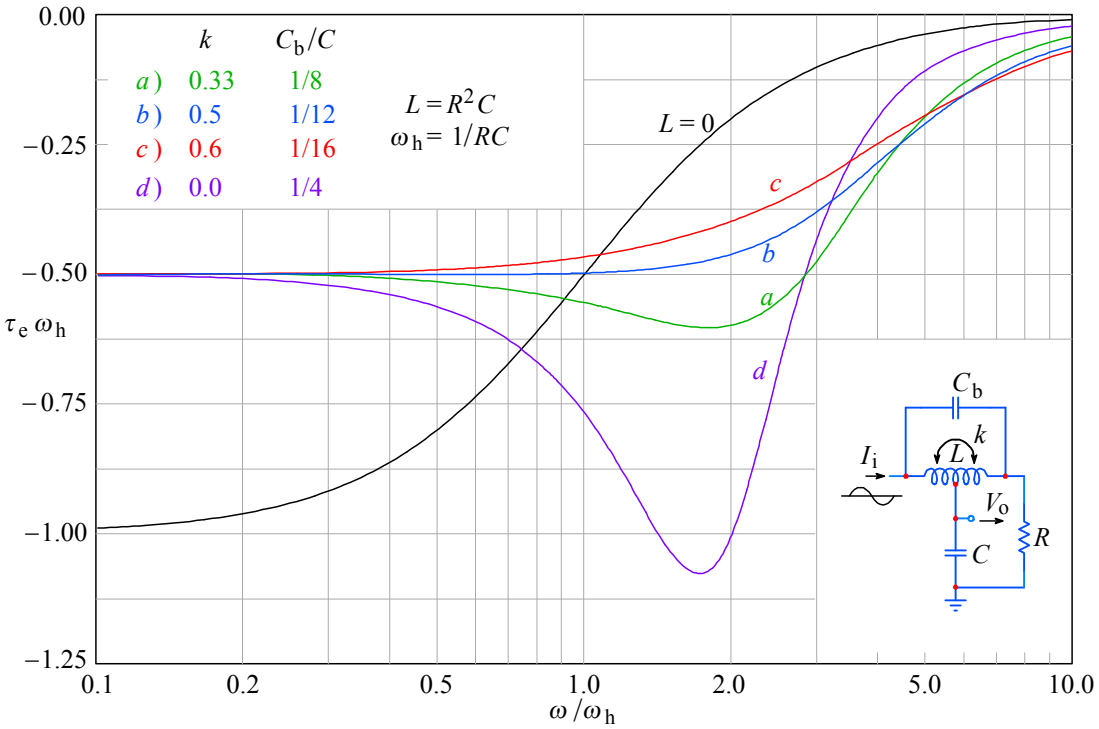

Fig. 2.4.7: The envelope delay of the T-coil: ***a)*** MFA, ***b)*** MFED, ***c)*** CD, ***d)*** $k = 0$. The T-coil circuit delay at low frequencies is exactly one half of that in the $L = 0$ case.

2.4.4 Step Response

We derive the step response from Eq. 2.4.25, as shown in Part 1, Eq. 1.14.29. We take Eq. 2.2.36 for complex poles (MFA, MFED, and the case $k = 0$) and Eq. 2.2.41 for double pole (the CD case). To make the expressions simpler we insert the numerical values of normalized poles and substitute $t/RC = t/T$:

a) for Butterworth poles (MFA), where $k = 0.3\dot{3}$ and $C_\mathrm{b} = C/8$:

$$g_a(t) = 1 + \sqrt{2}\,\mathrm{e}^{-2\,t/T}\,\sin\left(2\,t/T + 0.7854 + \pi\right) \tag{2.4.49}$$

b) for Bessel poles (MFED), where $k = 0.5$ and $C_\mathrm{b} = C/12$:

$$g_b(t) = 1 + 2\,\mathrm{e}^{-3\,t/T}\,\sin\left(\sqrt{3}\;t/T + 0.5236 + \pi\right) \tag{2.4.50}$$

c) for Critical Damping (CD), where $k = 0.6$ and $C_\mathrm{b} = C/16$:

$$g_c(t) = 1 - \mathrm{e}^{-4\,t/T}\,\left(1 + 4\,t/T\right) \tag{2.4.51}$$

d) for $k = 0$ and $C_\mathrm{b} = C/4$:

$$g_d(t) = 1 + \frac{2}{\sqrt{3}}\,\mathrm{e}^{-\,t/T}\,\sin\left(\sqrt{3}\;t/T + 1.0472 + \pi\right) \tag{2.4.52}$$

The plots corresponding to these four equations are shown in Fig. 2.4.8. Also shown are the corresponding four pole patterns.

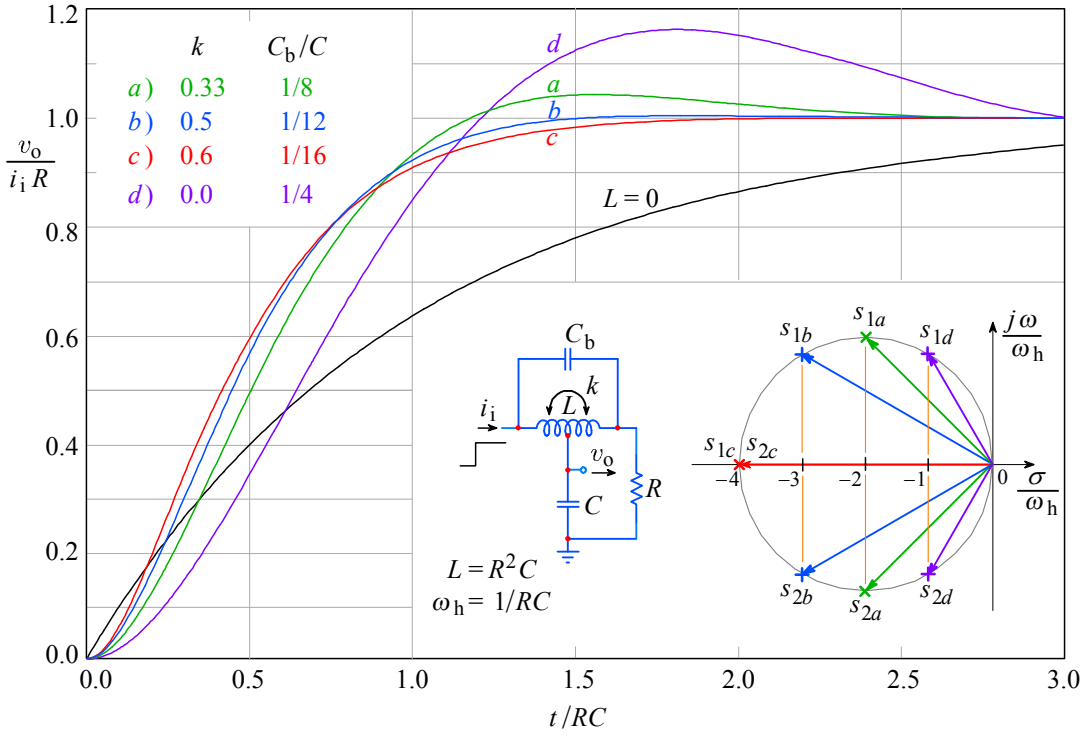

Fig. 2.4.8: The step response of the T-coil circuit. As before, ***a)*** is MFA, ***b)*** is MFED, ***c)*** is CD and ***d)*** is the case $k = 0$. The non-peaking case ($L = 0$) is the reference. The no-coupling case has excessive overshoot, 16.3 %, but MFA overshoot is also high, 4.3 %. Note the pole pattern of the four cases: the closer the poles are to the imaginary axis, the greater is the overshoot. The diameter of the circle on which the poles lie is $4/RC$.

2.4.5 Step Response from Input to v_R

For the application as a delay network, or if we want to design a distributed amplifier with either electronic tubes or FETs we need to know the transmission from the input to the load R, where we have the voltage v_R. For the calculation we use Eq. 2.4.26, which we normalize by making $RC = 1$. Here in addition to the two poles in the left half of the s-plane we also have two symmetrically placed zeros in the right half of the s-plane:

$$s_{1,2} = \sigma_1 \pm j\omega_1 \qquad s_{3,4} = -\sigma_1 \pm j\omega_1 \tag{2.4.53}$$

We shall write Eq. 2.4.26 in the form:

$$F(s) = \frac{s^2R^2CC_b - sRC/2 + 1}{s^2R^2CC_b + sRC/2 + 1} = \frac{(s - s_3)(s - s_4)}{(s - s_1)(s - s_2)} \tag{2.4.54}$$

By multiplication with $1/s$ we obtain the corresponding formula for the step response in the frequency domain:

$$G(s) = \frac{(s - s_3)(s - s_4)}{s\,(s - s_1)(s - s_2)} \tag{2.4.55}$$

and the corresponding time function:

$$g(t) = \mathcal{L}^{-1}\{G(s)\} = \sum \text{res}\,\frac{(s - s_3)(s - s_4)}{s\,(s - s_1)(s - s_2)}\,e^{st} \tag{2.4.56}$$

This operation is performed by contour integration, as explained in Part 1. The integration path must encircle all three poles; however, it is not necessary to encircle the zeros.

Since the function has the poles and zeros arranged symmetrically with respect to both axes we shall express all the components with σ_1 and ω_1, taking care of the polarity of each pole and zero, according to Eq. 2.4.53. We have three residues:

$$\text{res}_0 = \lim_{s\to 0} s\left[\frac{(s - s_3)\,(s - s_4)}{s\,(s - s_1)\,(s - s_2)}\,e^{st}\right] = \frac{s_3\,s_4}{s_1\,s_2} = \frac{\sigma_1^2 + \omega_1^2}{\sigma_1^2 + \omega_1^2} = 1$$

$$\text{res}_1 = \lim_{s\to s_1}(s - s_1)\left[\frac{(s - s_3)\,(s - s_4)}{s\,(s - s_1)\,(s - s_2)}\,e^{st}\right] = \frac{(s_1 - s_3)(s_1 - s_4)}{s_1(s_1 - s_2)}\,e^{s_1 t}$$

$$= \frac{[(\sigma_1 + j\omega_1) - (-\sigma_1 + j\omega_1)][(\sigma_1 + j\omega_1) - (-\sigma_1 - j\omega_1)]}{(\sigma_1 + j\omega_1)[(\sigma_1 + j\omega_1) - (\sigma_1 - j\omega_1)]}\,e^{(\sigma_1 + j\omega_1)t}$$

$$= \frac{2\,\sigma_1}{j\,\omega_1}\,e^{\sigma_1 t}\,e^{j\omega_1 t} \tag{2.4.57}$$

$$\text{res}_2 = \lim_{s\to s_2}(s - s_2)\left[\frac{(s - s_3)\,(s - s_4)}{s\,(s - s_1)\,(s - s_2)}\,e^{st}\right] = \frac{(s_2 - s_3)(s_2 - s_4)}{s_2(s_2 - s_1)}\,e^{s_2 t}$$

$$= \frac{[(\sigma_1 - j\omega_1) - (-\sigma_1 + j\omega_1)][(\sigma_1 - j\omega_1) - (-\sigma_1 - j\omega_1)]}{(\sigma_1 - j\omega_1)[(\sigma_1 - j\omega_1) - (\sigma_1 + j\omega_1)]}\,e^{(\sigma_1 - j\omega_1)t}$$

$$= \frac{2\,\sigma_1}{-\,j\,\omega_1}\,e^{\sigma_1 t}\,e^{-j\omega_1 t}$$

The sum of all three residues is:

$$g(t) = 1 + \frac{2\,\sigma_1}{j\,\omega_1}\,\mathrm{e}^{\sigma_1 t}\,\mathrm{e}^{j\omega_1 t} - \frac{2\,\sigma_1}{j\,\omega_1}\,\mathrm{e}^{\sigma_1 t}\,\mathrm{e}^{-j\omega_1 t}$$

$$= 1 + \frac{4\,\sigma_1}{\omega_1}\,\mathrm{e}^{\sigma_1 t}\left(\frac{\mathrm{e}^{j\omega_1 t} - \mathrm{e}^{-j\omega_1 t}}{2j}\right) = 1 + \frac{4\,\sigma_1}{\omega_1}\,\mathrm{e}^{\sigma_1 t}\sin\omega_1 t \qquad (2.4.58)$$

For critical damping (CD) both zeros and both poles are real. Then, $s_1 = s_2$ and $s_3 = s_4 = -s_1$. There are only two residues, which are calculated in two different ways (because the residue of the double pole must be calculated from the first derivative):

$$\mathrm{res}_0 = \lim_{s\to 0} s\left[\frac{(s-s_3)^2}{s\,(s-s_1)^2}\,\mathrm{e}^{st}\right] = \frac{s_3^2}{s_1^2} = 1 \qquad \text{(because } s_3 = -s_1\text{)}$$

$$\mathrm{res}_1 = \lim_{s\to s_1}\frac{d}{ds}\left[(s-s_1)^2\,\frac{(s-s_3)^2}{s\,(s-s_1)^2}\,\mathrm{e}^{st}\right]$$

$$= \lim_{s\to s_1}\frac{d}{ds}\left[\frac{(s-s_3)^2}{s}\,\mathrm{e}^{st}\right]$$

$$= \lim_{s\to s_1}\left[\mathrm{e}^{st} + s\,t\,\mathrm{e}^{st} - 2\,s_3\,t\,\mathrm{e}^{st} + s_3^2\,\frac{s\,t\,\mathrm{e}^{st} - \mathrm{e}^{st}}{s^2}\right]$$

$$= 4\,s_1 t\,\mathrm{e}^{s_1 t} \qquad \text{(because } s_3 = -s_1\text{)} \qquad (2.4.59)$$

The sum of both residues is the time response sought. We insert the normalized poles and put $t/RC = t/T$ to obtain:

a) for Butterworth poles (MFA), where $k = 0.3\dot{3}$ and $C_\mathrm{b} = C/8$:

$$g_a(t) = 1 - 4\,\mathrm{e}^{-2\,t/T}\sin(2\,t/T) \qquad (2.4.60)$$

b) for Bessel poles (MFED), where $k = 0.5$ and $C_\mathrm{b} = C/12$:

$$g_b(t) = 1 - 4\sqrt{3}\;\mathrm{e}^{-3\,t/T}\sin(\sqrt{3}\;t/T) \qquad (2.4.61)$$

c) for critical damping (CD), where $k = 0.6$ and $C_\mathrm{b} = C/16$:

$$g_c(t) = 1 - 16(t/T)\,\mathrm{e}^{-4\,t/T} \qquad (2.4.62)$$

d) for the case when $k = 0$ and $C_\mathrm{b} = C/4$:

$$g_d(t) = 1 - \frac{4}{\sqrt{3}}\,\mathrm{e}^{-t/T}\sin(\sqrt{3}\;t/T) \qquad (2.4.63)$$

All four plots are shown in Fig. 2.4.9. Note the initial transition owing to the bridge capacitance C_b at high frequencies, the dip where the phase inversion between the high pass and low pass section occurs, and the transition to the final value.

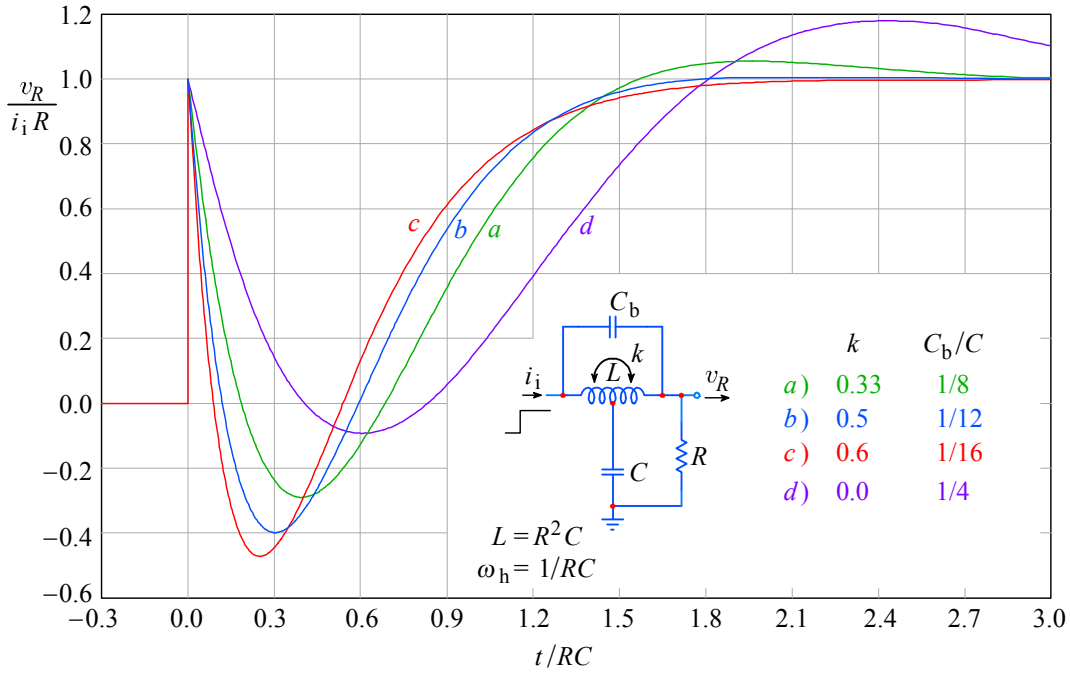

Fig. 2.4.9: The step response of the T-coil circuit, but now with the output from the loading resistor R (this is interesting for cascading stages, as explained later). As before, ***a)*** MFA, ***b)*** MFED, ***c)*** CD, and ***d)*** $k = 0$. The system has the characteristics of an all pass filter.

All the significant data of the T-coil peaking circuit are collected in the Table 2.4.1.

Table 2.4.1

response type	k	C_b/C	η_b	η_r	δ [%]
a) MFA	0.33	1/8	2.82	2.89	4.30
b) MFED	0.50	1/12	2.72	2.79	0.43
c) CD	0.60	1/16	2.57	2.62	0.00
d) $k = 0$	0.00	1/4	2.54	2.68	16.3

Table 2.4.1: Two-pole T-coil circuit parameters

2.4.6 A T-coil application example

One interesting application example of a T-coil all pass network is shown in Fig. 2.4.10. The signal coming out of a TV camera via a 75 Ω cable must be controlled by the monitor and by the vectorscope before it enters the video modulator. The video monitor and the vectorscope should not cause any reflections in the interconnecting cables. Reflections would be caused mostly by the input capacitances of these devices, since their input resistances R_1 , R_2 , $R_3 \gg 75\,\Omega$ and we shall neglect them in our calculations.

To avoid reflections we must connect an impedance matching circuit to each of these inputs and the T-coil circuit can do well, as shown in Fig. 2.4.11. The signal from the TV camera will pass any of three T-coils without reflections. However, the last T-coil in the chain (at the video modulator) must be terminated by the characteristic impedance of the cable, which is 75 Ω. We will take the output for the three devices from their input capacitances C_1, C_2, and C_3. This will cause a slight decrease in bandwidth, but — as we

will see later — the decrease introduced by T-coils will not harm the operation of the total system in any way.

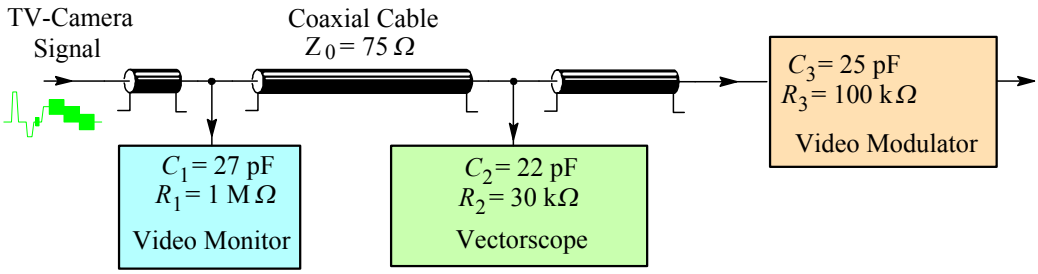

Fig. 2.4.10: An example of a system with different input impedances (TV studio equipment). The signal from a color TV camera is controlled on the monitor screen, the RGB color vectors are measured by the vectorscope, and, finally, the signal is sent to the video modulator for broadcasting. All interconnections are made by a coaxial cable with the characteristic impedance of 75Ω. With long cables, adding considerable delay, the input capacitances can affect the highest frequencies, causing reflections.

On the basis of the data in Fig. 2.4.10 we will calculate the T-coil for each of the three devices. In addition we will calculate the bandwidth at each input. Since the whole system must faithfully transmit pulses, we will consider Bessel poles for all three T-coils.

We use the following four relations:

$$L = R^2 C \qquad \text{(Eq. 2.4.19)}$$

$$C_\mathrm{b} = C/12 \qquad \text{(Eq. 2.4.32)}$$

$$k = 0.5 \qquad \text{(Eq. 2.4.37)}$$

$$\eta_\mathrm{b} = 2.72 \qquad \text{(Table 2.4.1)}$$

$$f_\mathrm{H} = \eta_\mathrm{b} f_\mathrm{h} = \frac{\eta_\mathrm{b}\omega_\mathrm{h}}{2\pi} = \frac{\eta_\mathrm{b}}{2\pi RC} \quad \text{(from Eq. 2.2.29)} .$$

So we calculate:

a) for the monitor,

$$L_1 = 152\,\mathrm{nH}, \qquad C_{\mathrm{b}1} = 2.25\,\mathrm{pF}, \qquad f_{\mathrm{h}1} = 78.6\,\mathrm{MHz}, \qquad f_{\mathrm{H}1} = 231\,\mathrm{MHz};$$

b) for the vectorscope,

$$L_2 = 124\,\mathrm{nH}, \qquad C_{\mathrm{b}2} = 1.83\,\mathrm{pF}, \qquad f_{\mathrm{h}2} = 96.5\,\mathrm{MHz}, \qquad f_{\mathrm{H}2} = 262\,\mathrm{MHz};$$

c) for the video modulator,

$$L_3 = 141\,\mathrm{nH}, \qquad C_{\mathrm{b}3} = 2.08\,\mathrm{pF}, \qquad f_{\mathrm{h}3} = 84.9\,\mathrm{MHz}, \qquad f_{\mathrm{H}3} = 230\,\mathrm{MHz}.$$

The bandwidths are far above the requirement of the system, which is about 6 MHz for either a color or a black and white signal. Fig. 2.4.11 shows the schematic diagram in which the calculated component values are implemented.

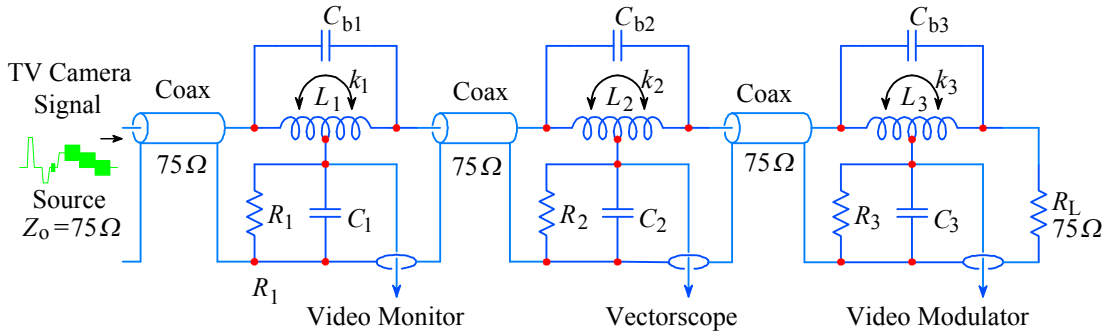

Fig. 2.4.11: Input impedance compensation by T-coil sections prevents signal reflections. Each section of the coaxial cable sees the terminating 75 Ω resistor at the end of the chain. The bandwidth is affected only slightly. The circuit values are shown in the text above.

Since a properly designed T-coil circuit has a constant input impedance, it may be used in connection with a series peaking circuit in order to improve further the system bandwidth, as we shall see in Sec. 2.6. But first we shall examine a 3-pole T-coil system.

2.5 Three-Pole T-coil Peaking Circuit

As in the three-pole series peaking circuit of Fig. 2.3.1, an input capacitance C_i is also always present at the input of the two-pole T-coil circuit, changing it into a three-pole network. This C_i can be a sum of the driving circuit capacitance and the stray input capacitance of the T-coil circuit itself. Actually, as shown in Fig. 2.5.1, the total capacitance of the non-peaking circuit is split by the T-coil into the capacitance of the driving node (C_i) and that of the output stage (C).

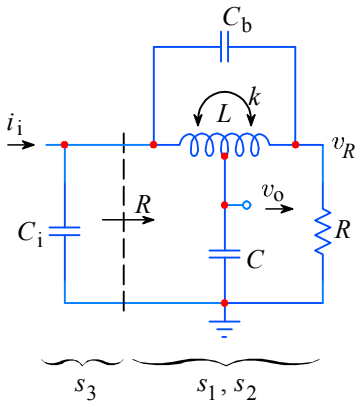

Fig. 2.5.1: The three-pole T-coil network.

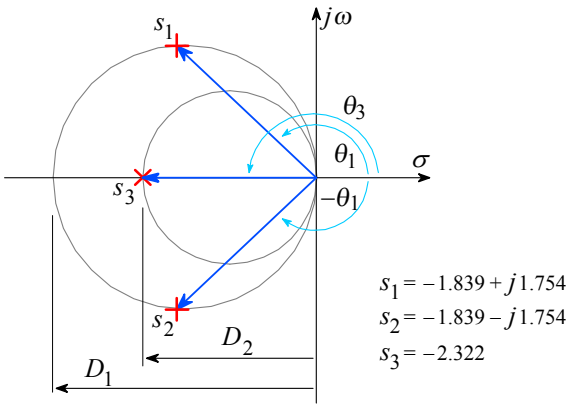

Fig. 2.5.2: Bessel pole layout for the Fig. 2.5.1.

If properly designed, the basic two-pole T-coil circuit will have a constant input impedance R, independent of frequency. This property allows a great simplification of the three-pole network analysis. To both poles of the T-coil, s_1 and s_2 , we only need to add the third input pole $s_3 = -1/RC_i$. In order to design an efficient peaking circuit, the tap of the coil must feed a greater capacitance, so $C_i < C$, because the T-coil has no influence on the input pole s_3. Since the network is reciprocal (the current input and voltage output nodes can be exchanged without affecting the response) we can always fulfill this requirement. Also, because of the constant input impedance we can obtain the expression for the transfer function from that of a two-pole T-coil circuit (Eq. 2.4.25) by adding to it the influence of the third pole s_3 (resulting in a simple multiplication of the first-order and second-order transfer function):

$$F(s) = \frac{V_o}{I_1 R} = \frac{1}{\left(s + \frac{1}{RC_i}\right)\left(s^2 R^2 C C_b + s\frac{RC}{2} + 1\right)} \qquad (2.5.1)$$

We shall resist the temptation to perform the suggested multiplication in the denominator, since we would obtain a third-order equation and needlessly complicate the analysis. Owing to the capacitance C_i we have a real pole in addition to the two complex conjugate poles which the T-coil circuit has (in wideband application). With the input capacitance C_i the input impedance is not constant any longer. Its value is equal to R at DC and approaches that of C_i at frequencies beyond ω_H. As before, our task is to select such parameters of the Eq. 2.5.1 that the network will have either Bessel or Butterworth poles. We shall do this by using the trigonometrical relations as indicated in Fig. 2.5.3. The T-coil parameters will carry an index '1' (D_1, θ_1, σ_1, and ω_1).

From the analysis of a two-pole T-coil circuit we remember that the diameter of the circle on which both poles s_1 and s_2 lie is $D_1 = 4/RC$ (see Fig. 2.4.3 or 2.4.8). The diameter D_2 of the circle which goes through the real pole $s_3 = \sigma_2$ is simply $-1/RC_\mathrm{i}$ (the reason why we have drawn the circle through this pole also, will become obvious later, when we shall analyze the four-pole L+T circuits). We introduce a new parameter:

$$n = \frac{C}{C_\mathrm{i}} \tag{2.5.2}$$

The ratio of the diameters of these circles going through the poles and the origin is then:

$$\frac{D_2}{D_1} = \frac{\dfrac{1}{RC_\mathrm{i}}}{\dfrac{4}{RC}} = \frac{\dfrac{n}{RC}}{\dfrac{4}{RC}} = \frac{n}{4} \tag{2.5.3}$$

From this we obtain:

$$\frac{C}{C_\mathrm{i}} = n = 4\,\frac{D_2}{D_1} \tag{2.5.4}$$

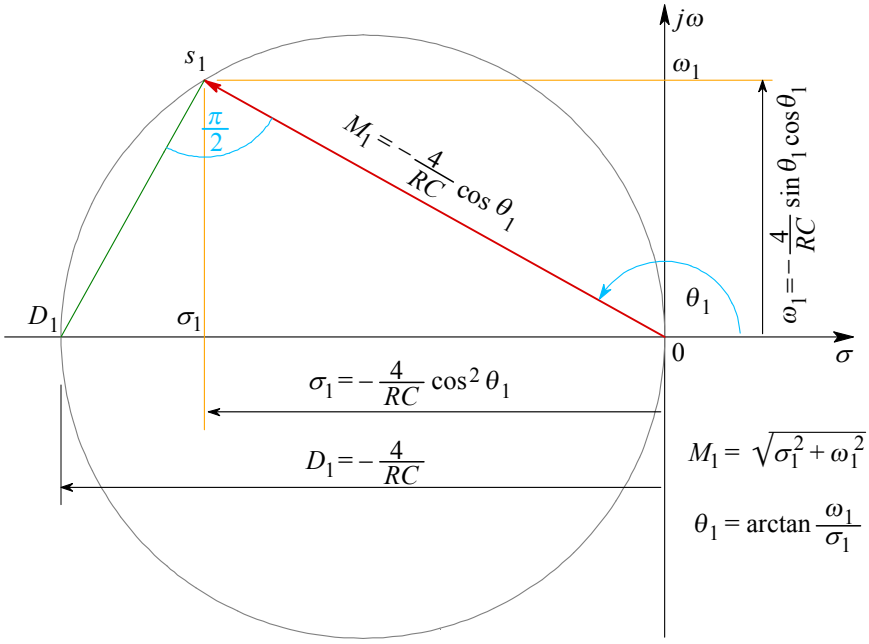

Fig. 2.5.3: The basic trigonometric relations of the main parameters for one of the poles of the T-coil circuit. Knowing one pair of parameters, it is possible to calculate the rest by these simple relations.

Fig. 2.5.3 illustrates some basic trigonometric relations between the polar and Cartesian expression of the poles by taking into account the similarity relationship between the two right angle triangles: $\triangle 0\,\sigma_1\,s_1$ and $\triangle 0\,s_1\,D_1$:

$$\Re\{s_1\} = \sigma_1 = D_1 \cos^2\theta_1 = -\frac{4}{RC}\cos^2\theta_1 \tag{2.5.5}$$

where D_1 is the circle diameter, $D_1 = -4/RC$. Likewise:

$$\Im\{s_1\} = \omega_1 = D_1 \cos\theta_1 \sin\theta_1 = -\frac{4}{RC}\cos\theta_1 \sin\theta_1 \tag{2.5.6}$$

From these equations we can calculate the coupling factor k and the bridging capacitance C_b.

Since:

$$\tan\theta_1 = \frac{\Im\{s_1\}}{\Re\{s_1\}} = \frac{\omega_1}{\sigma_1} \tag{2.5.7}$$

the corresponding coupling factor, according Eq. 2.4.36, is:

$$k = \frac{3 - \tan^2\theta_1}{5 + \tan^2\theta_1}$$

and, as before in Eq. 2.4.31, the bridging capacitance is:

$$C_\mathrm{b} = C\,\frac{1 + \tan^2\theta_1}{16}$$

Next we must calculate the parameter n from the table of poles in Part 4. For Butterworth poles, listed in Table 4.3.1, the values for order $n = 3$ are:

$$\begin{aligned} s_{1t,2t} &= \sigma_{1t} \pm j\,\omega_{1t} = -\frac{1}{2} \pm j\,\frac{\sqrt{3}}{2} \\ s_{3t} &= \sigma_{3t} = -1 \\ \theta_1 &= \pm 120^\circ = 2\pi/3\ [\mathrm{rad}] \end{aligned} \tag{2.5.8}$$

From Eq. 2.5.5 it follows that:

$$D_1 = \frac{\sigma_{1t}}{\cos^2\theta_1} \tag{2.5.9}$$

Since $D_2 = \sigma_{1t}$ the ratio D_2/D_1 is:

$$\frac{D_2}{D_1} = \frac{\sigma_{3t}\cos^2\theta_1}{\sigma_{1t}} = \frac{-1\cdot\cos^2 120^\circ}{-0.5} = 0.5 \tag{2.5.10}$$

Since $n = 4\,D_2/D_1$ we obtain:

$$n = C/C_\mathrm{i} = 2 \qquad \Rightarrow \qquad C_\mathrm{i} = C/2 \tag{2.5.11}$$

Returning to the equations for k and C_b we find $k = 0$ (no coupling !!!) and $C_\mathrm{b} = 0.25\,C$. Just as it was for a two-pole T-coil circuit, here, too, $L = R^2C$. So we have all the circuit parameters for the Butterworth poles.

We can take the values for Bessel poles for order $n = 3$ either from Table 4.4.3 in Part 4, or by running the BESTAP routine (Part 6):

$$\begin{aligned} s_{1t,2t} &= \sigma_{1t} \pm j\,\omega_{1t} = -1.8389 \pm j\,1.7544 \\ s_{3t} &= \sigma_{3t} = -2.3221 \\ \theta_1 &= \pm 136.35^\circ \end{aligned} \tag{2.5.12}$$

In a similar way as before, we obtain:

$$k = 0.3536 \qquad C_\mathrm{b} = 0.12\,C \qquad C_\mathrm{i} = 0.38\,C \tag{2.5.13}$$

To calculate the normalized transfer function we normalize the frequency variable as ω/ω_h, where ω_h is the upper cut off frequency of the non-peaking amplifier ($L = 0$):

$$\omega_\mathrm{h} = \frac{1}{R(C + C_\mathrm{i})} = \frac{1}{RC_\mathrm{c}} \tag{2.5.14}$$

This is important, because if the coil is replaced by a short circuit both capacitances appear in parallel with the loading resistor R. Since $C_\mathrm{i} = C/n$, we may express both capacitances with the total capacitance $C_\mathrm{c} = C + C_\mathrm{i}$ and obtain:

$$C = C_\mathrm{c}\frac{n}{n+1} \qquad \text{and} \qquad C_\mathrm{i} = C_\mathrm{c}\,\frac{1}{n+1} \tag{2.5.15}$$

So far we have used the pole data from tables, since we needed only the ratios of these poles. But, to calculate the frequency, phase, envelope delay, and step response we shall need the actual values of the poles. We have calculated the poles of the T-coil circuit by Eq. 2.4.29, which we repeat here for convenience:

$$s_{1,2} = -\frac{1}{4RC_\mathrm{b}}\left(1 \pm \sqrt{1 - \frac{16\,C_\mathrm{b}}{C}}\right)$$

We shall use the Butterworth poles to explain the procedure. For these poles we have $C_\mathrm{b} = C/4$ and $n = 2$. By inserting these values in the above formula we obtain:

$$s_{1,2} = -\frac{1}{RC}\left(1 \pm j\sqrt{3}\right) \tag{2.5.16}$$

Now let us express the capacitance C by C_c according to Eq. 2.5.15. Then:

$$s_{1,2} = -\frac{1}{RC_\mathrm{c}} \cdot \frac{n+1}{n}\left(1 \pm j\sqrt{3}\right) = -\frac{1}{RC_\mathrm{c}} \cdot \frac{3}{2}\left(1 \pm j\sqrt{3}\right)$$

$$= -\frac{1}{RC_\mathrm{c}}(1.5 \pm j\,2.5981) \tag{2.5.17}$$

The input pole is real:

$$s_3 = -\frac{1}{RC_\mathrm{i}} = -\frac{1}{RC_\mathrm{c}}(n+1) = -\frac{3}{RC_\mathrm{c}} \tag{2.5.18}$$

In a similar way we also calculate the values for Bessel poles and obtain:

$$s_{1,2} = -\frac{1}{RC_\mathrm{c}}(2.8860 \pm j\,2.7532) \qquad \text{and} \qquad s_3 = -\frac{3.6447}{RC_\mathrm{c}} \tag{2.5.19}$$

When calculating the values for the critical damping case (CD) we must consider that the imaginary values of the poles s_1 and s_2 must be zero. This gives $C_\mathrm{b} = C/16$. Here we may choose $n = 2$, and this means that $C_\mathrm{i} = C/2$. The corresponding poles, which are all real, are:

$$s_{1,2} = -\frac{6}{RC_\mathrm{c}} \qquad \text{and} \qquad s_3 = -\frac{3}{RC_\mathrm{c}} \tag{2.5.20}$$

2.5.1 Frequency Response

To calculate the frequency response, we can use Eq. 2.2.27 for a two-pole series peaking circuit and add the effect of the additional input real pole, σ_3. We insert the

normalized poles ($RC_c = 1$) and the normalized frequency ω/ω_h. Thus we obtain the following expression:

$$|F(\omega)| = \frac{(\sigma_{1n}^2 + \omega_{1n}^2)\,\sigma_3}{\sqrt{\left[\sigma_{1n}^2 + \left(\frac{\omega}{\omega_h} + \omega_{1n}\right)^2\right]\left[\sigma_{1n}^2 + \left(\frac{\omega}{\omega_h} - \omega_{1n}\right)^2\right]\left[\sigma_{3n}^2 + \left(\frac{\omega}{\omega_h}\right)^2\right]}} \tag{2.5.21}$$

The plot for all three types of poles is shown in Fig. 2.5.4. By comparing the curve *a*, MFA, where $k = 0$, with the curve *a* in Fig. 2.4.5, where also $k = 0$, we realize that we have achieved a bandwidth extension just by splitting the total circuit capacitance into the input capacitance C_i and the coil loading capacitance C.

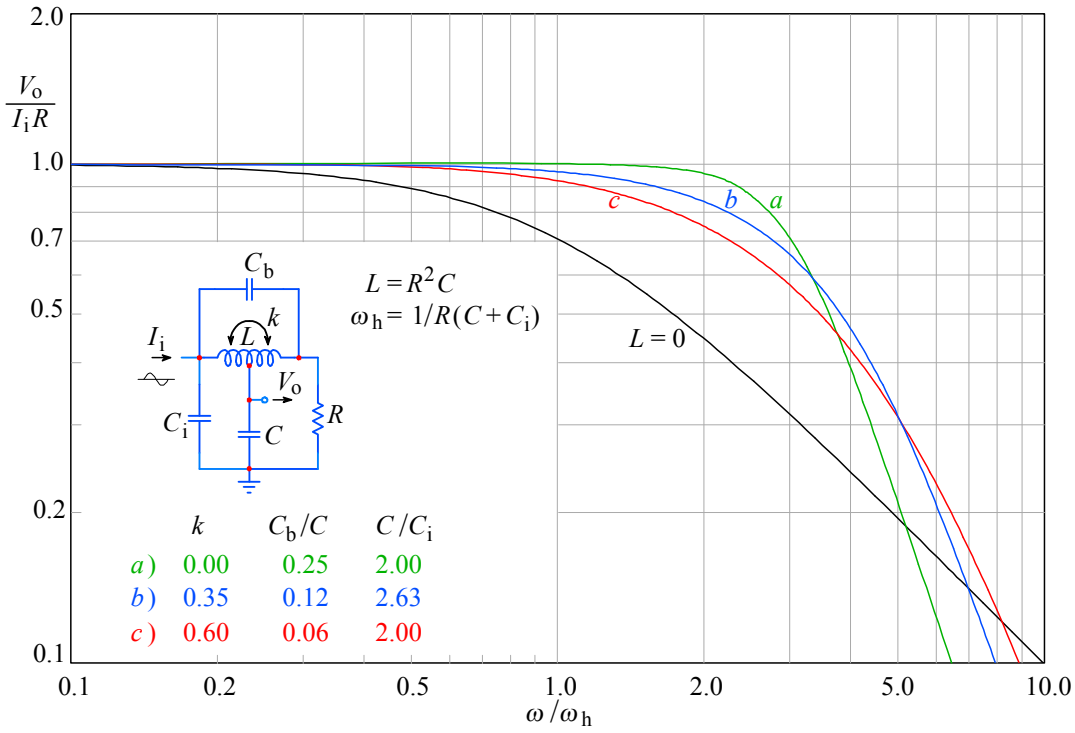

Fig. 2.5.4: Three-pole T-coil network frequency response: ***a)*** MFA; ***b)*** MFED; ***c)*** CD case. The non-peaking response ($L = 0$) is the reference. The MFA bandwidth is larger then that of the two-pole circuit in Fig.2.4.5; in contrast, MFED bandwidth is nearly the same, but the circuit can be realized more easily, owing to the lower magnetic coupling factor required. Note also that, owing to the possibility of separating the total capacitance into a driving and loading part, the reference non-peaking cut off frequency ω_h must be defined as $1/R(C + C_i)$.

2.5.2 Phase Response

For the phase response we can use Eq. 2.3.25 again, and, by inserting the values for the poles we can plot the responses as shown in Fig. 2.5.5:

$$\varphi = \arctan\frac{\frac{\omega}{\omega_h} - \omega_{1n}}{\sigma_{1n}} + \arctan\frac{\frac{\omega}{\omega_h} + \omega_{1n}}{\sigma_{1n}} + \arctan\frac{\frac{\omega}{\omega_h}}{\sigma_{3n}}$$

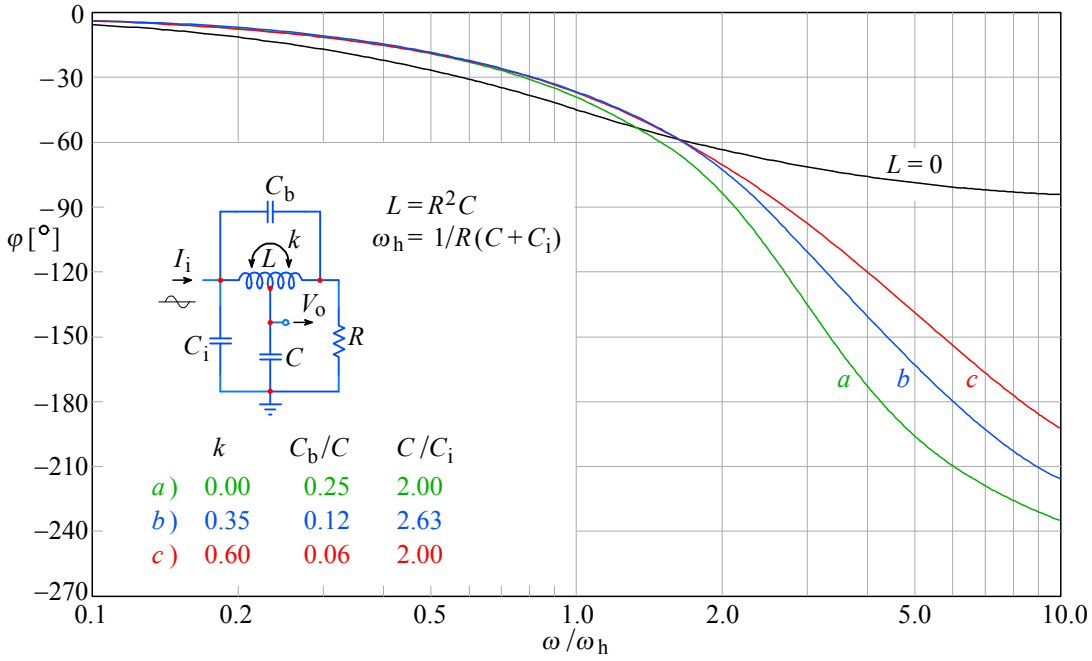

Fig. 2.5.5: Three-pole T-coil network phase response: ***a)*** MFA; ***b)*** MFED; ***c)*** CD case. Note that at high frequencies the 3-pole system phase asymptote is $-270°$ ($3 \times 90°$).

2.5.3 Envelope Delay

We take Eq. 2.3.26 again, and by inserting the values for poles we can plot the envelope delay, as in Fig. 2.5.6:

$$\tau_e\,\omega_h = \frac{\sigma_{1n}}{\sigma_{1n}^2 + \left(\frac{\omega}{\omega_h} - \omega_{1n}\right)^2} + \frac{\sigma_{1n}}{\sigma_{1n}^2 + \left(\frac{\omega}{\omega_h} + \omega_{1n}\right)^2} + \frac{\sigma_{3n}}{\sigma_{3n}^2 + \left(\frac{\omega}{\omega_h}\right)^2}$$

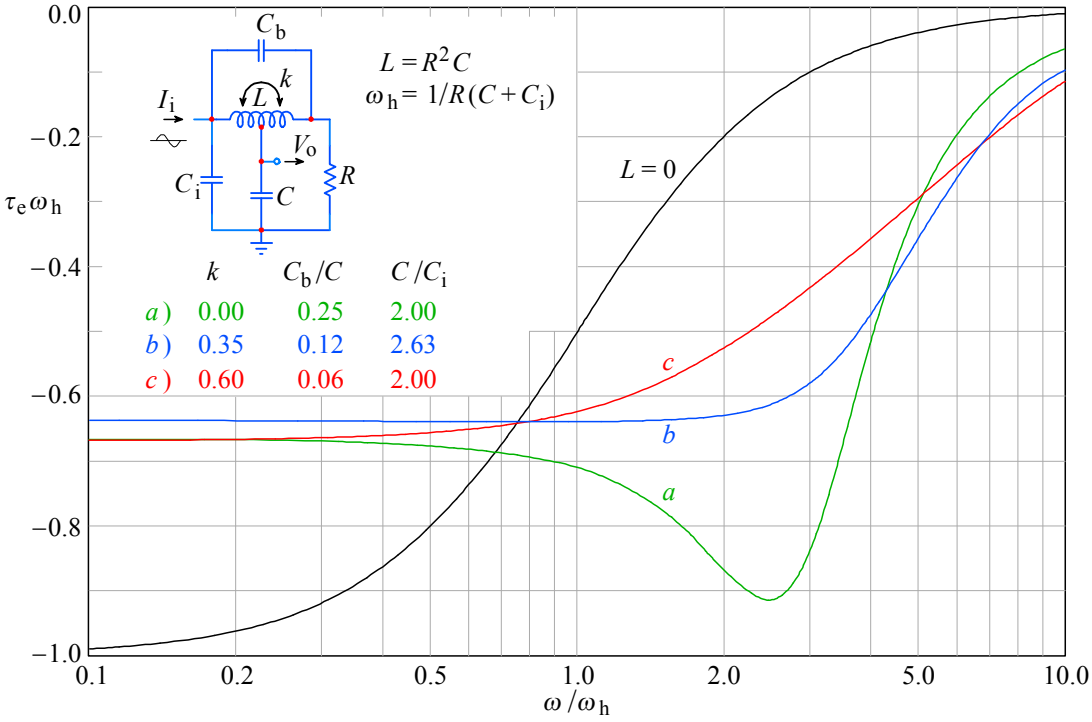

Fig. 2.5.6: Three-pole T-coil network envelope delay: ***a)*** MFA; ***b)*** MFED; ***c)*** CD case. Note that the MFED flatness now extends to nearly $1.5\,\omega_h$.

2.5.4 Step Response

We shall use again Eq. 2.3.27 and Eq. 2.3.28 (see Appendix 2.3, Sec. A2.3.1 for complete derivation). By inserting the values for poles we can calculate the responses and plot them, as shown in Fig. 2.5.7*a* and 2.5.7*b*:

a) from Eq. 2.5.8 for MFA:

$$g_a(t) = 1 + 1.1547\,\mathrm{e}^{-1.5\,t/T}\sin(2.5981\;t/T + 0 + \pi) - \mathrm{e}^{-3\,t/T} \tag{2.5.22}$$

b) from Eq. 2.5.12 for MFED:

$$g_b(t) = 1 + 1.8489\,\mathrm{e}^{-2.886\,t/T}\sin(2.7532\;t/T - 0.5400 + \pi) - 1.9507\,\mathrm{e}^{-3.6447\,t/T} \tag{2.5.23}$$

For the CD case, where we have a double real pole ($s_2 = s_1 = \sigma_1$), the calculation is different (see Eq. 1.11.12 in Part 1). The general expression:

$$F(s) = \frac{-\,s_1^2\,s_3}{(s - s_1)^2(s - s_3)} \tag{2.5.24}$$

(where $s_1 = \sigma_1$ and $s_3 = \sigma_3$) must be multiplied by the unit step operator $1/s$ to obtain the form appropriate for $\mathcal{L}^{-1}$ transform:

$$G(s) = \frac{-\,s_1^2\,s_3}{s\,(s - s_1)^2(s - s_3)} \tag{2.5.25}$$

and the step response is the inverse Laplace transform of $G(s)$, which in turn is equal to the sum of its residues:

$$g(t) = \mathcal{L}^{-1}\{G(s)\} = \sum \mathrm{res}\,\frac{-\,s_1^2\,s_3\,\mathrm{e}^{st}}{s\,(s - s_1)^2\,(s - s_3)} \tag{2.5.26}$$

We have three residues:

$$\mathrm{res}_0 = \lim_{s\to 0} s\left[\frac{-\,s_1^2\,s_3\,\mathrm{e}^{st}}{s\,(s - s_1)^2(s - s_3)}\right] = \frac{-\,s_1^2\,s_3\,\mathrm{e}^{0t}}{s_1^2(-\,s_3)} = 1$$

$$\mathrm{res}_1 = \lim_{s\to s_1}\frac{d}{ds}\left[(s - s_1)^2\,\frac{-\,s_1^2\,s_3\,\mathrm{e}^{st}}{s(s - s_1)^2(s - s_3)}\right] = \lim_{s\to s_1}\frac{d}{ds}\left[\frac{-\,s_1^2\,s_3\,\mathrm{e}^{st}}{s\,(s - s_3)}\right]$$

$$= \lim_{s\to s_1}\left[s_1^2\,s_3\,\frac{s_3(s\,t - 1) - s\,(s\,t - 2)}{s^2\,(s_3 - s)^2}\,\mathrm{e}^{st}\right]$$

$$= s_1^2\,s_3\,\frac{s_3 s_1\,t - s_3 - s_1^2\,t + 2s_1}{s_1^2\,(s_3 - s_1)^2}\,\mathrm{e}^{s_1 t} = s_3\,\frac{s_1(s_1 - s_3)\,t + 2s_1 - s_3}{(s_1 - s_3)^2}\,\mathrm{e}^{s_1 t}$$

$$\mathrm{res}_2 = \lim_{s\to s_3}(s - s_3)\left[\frac{-\,s_1^2\,s_3\,\mathrm{e}^{st}}{s\,(s - s_1)^2(s - s_3)}\right] = \frac{-\,s_1^2}{(s_3 - s_1)^2}\,\mathrm{e}^{s_3 t} \tag{2.5.27}$$

The sum of all three residues is the sought step response:

$$g_c(t) = 1 + s_3 \frac{s_1(s_1 - s_3)\,t + 2s_1 - s_3}{(s_1 - s_3)^2}\,\mathrm{e}^{s_1 t} - \frac{s_1^2}{(s_3 - s_1)^2}\,\mathrm{e}^{s_3 t} \qquad (2.5.28)$$

By inserting $s_1 = \sigma_1$ and $s_3 = \sigma_3$ we obtain:

$$g_c(t) = 1 + \sigma_3 \frac{\sigma_1(\sigma_1 - \sigma_3)\,t + 2\sigma_1 - \sigma_3}{(\sigma_1 - \sigma_3)^2}\,\mathrm{e}^{\sigma_1 t} - \frac{\sigma_1^2}{(\sigma_3 - \sigma_1)^2}\,\mathrm{e}^{\sigma_3 t} \qquad (2.5.29)$$

Finally, we normalize the poles (Eq. 2.5.20), $\sigma_{1n} = -6$ and $\sigma_{3n} = -3$ and normalize the time as t/T, where $T = R(C_i + C)$, to obtain the formula by which the plot *c* in Fig. 2.5.7 is calculated:

$$g_c(t) = 1 + 3\,(1 + 2\,t/T)\,\mathrm{e}^{-6t/T} - 4\,\mathrm{e}^{-3t/T} \qquad (2.5.30)$$

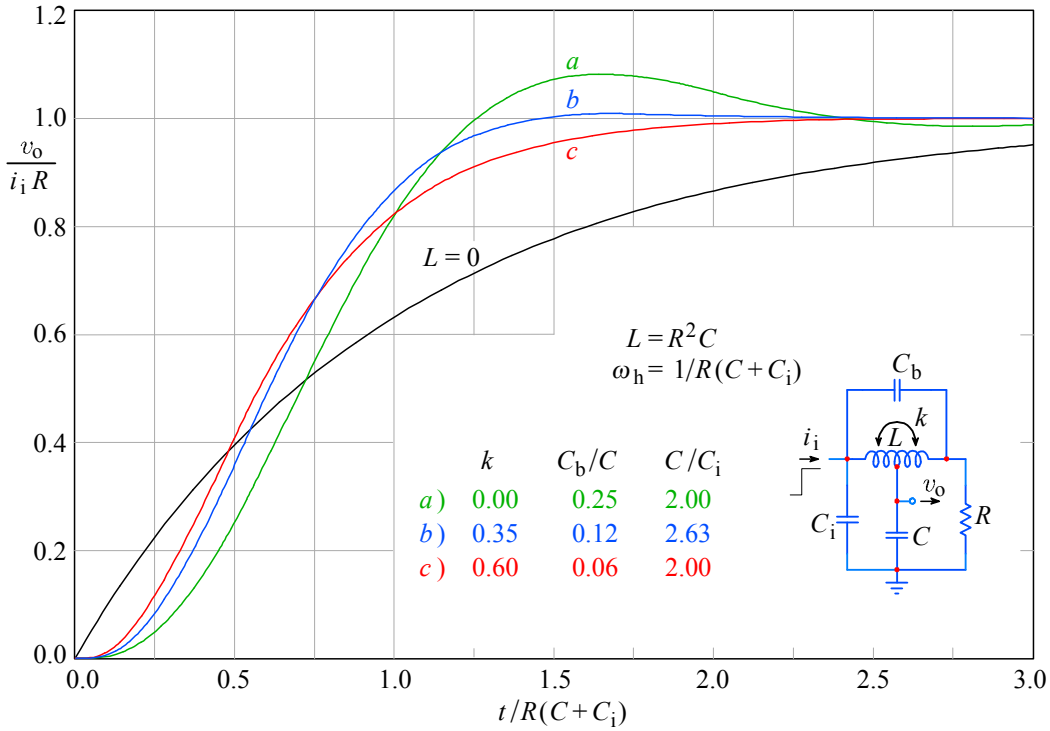

Fig. 2.5.7: The step response of the three-pole T-coil circuit: ***a)*** MFA; ***b)*** MFED; ***c)*** CD. The non-peaking case ($L = 0$) is the reference. Since the total capacitance $C + C_i$ is equal to C of the two-pole T-coil circuit, the MFED rise time is also nearly identical. However, the three-pole circuit is much easier to realize in practice, owing to the lower k required .

2.5.5. Low coupling cases

In the practical realization of a T-coil the toughest problem is to achieve a high coupling factor k. Even $k = 0.5$, as is needed for the two-pole circuit MFED response, is not easy to achieve if we do not want to increase the bridging capacitance C_b excessively. The three-pole T-coil circuits are easy to realize in practice, because of the low coupling required (no coupling for MFA, and only $k = 0.35$ for MFED).

We have also seen that the low coupling factor required is achieved by simply splitting the total circuit capacitance into C and C_i. Therefore it might be useful to further investigate the effects of low coupling. Let us calculate the frequency and the step responses, making three plots each, with a different ratio $C_i/C = n$. In the first group we shall put $k = 0.3\dot{3}$ and in the second group $k = 0.2$.

The corresponding poles are:

Group 1: $k = 0.3\dot{3}$, $C_b = C/8$

a) $n = 2.5$
$s_{1n,2n} = -2.8 \pm j2.8$
$s_{3n} = -3.5$

b) $n = 2$
$s_{1n,2n} = -3 \pm j3$
$s_{3n} = -3$

c) $n = 1.5$
$s_{1n,2n} = -3.3\dot{3} \pm j3.3\dot{3}$
$s_{3n} = -2.5$

The poles are selected so that the sum of $C + C_i$ is the same for all three cases. In this way we have the same upper half power frequency ω_h for any set of poles. This is necessary in order to have the same scale for all three plots. For the above poles we obtain the frequency response as in Fig. 2.5.8 and the step response as in Fig. 2.5.9.

Group 2: $k = 0.2$, $C_b = 0.17\,C$

a) $n = 2$
$s_{1n,2n} = -2.5 \pm j2.908$
$s_{3n} = -3$

b) $n = 1.5$
$s_{1n,2n} = -2.5 \pm j3.227$
$s_{3n} = -2.5$

c) $n = 1$
$s_{1n,2n} = -3 \pm j3.837$
$s_{3n} = -2$

The corresponding frequency response plots are displayed in Fig. 2.5.10 and the step responses in Fig. 2.5.11. From Fig. 2.5.11 it is evident that we have decreased the coupling factor in the second group too much. Nor is a single curve in this figure suitable for the peaking circuit of a pulse amplifier. In curve *a* the overshoot is excessive, whilst the curve *c* exhibits too slow a response. The curve *b* rounds off too soon, reaching the final value with a much slower slope. In a plot with a coarser time scale this curve would clearly show a missing chunk of the step response. Needless to say, it would be very annoying if an oscilloscope amplifier were to have such a step response.

All the important data for the three-pole T-coil peaking circuits are collected in Table 2.5.1. It is worth noting that we achieve a three-pole MFED response with the coupling factor $k = 0.35$ ($\eta_r = 2.78$), whilst for a two-pole T-coil MFED response the $k = 0.5$ was necessary (for a similar $\eta_r = 2.76$). If we are satisfied with a slightly smaller bandwidth it is possible to use the parameters of Group 1, where the coupling factor is $0.3\dot{3}$ only. Such a small coupling factor is much easier to achieve than $k = 0.5$. So for the practical construction of a wideband amplifier we find the three-pole T-coil circuits very convenient.

Table 2.5.1

response type	k	C_b/C	C/C_i	η_b	η_r	δ[%]
MFA	0	0.25	2	2.99	2.89	8.08
MFED	0.35	0.125	2.645	2.75	2.78	0.75
CD	0.60	0.063	2	2.22	2.26	0.00
Group 1, a	0.33	0.125	2.5	2.75	2.77	0.80
Group 1, b	0.33	0.125	2	2.59	2.63	0.00
Group 1, c	0.33	0.125	1.5	2.34	2.39	0.00
Group 2, a	0.2	0.167	2	2.70	2.72	1.85
Group 2, b	0.2	0.167	1.5	2.59	2.62	0.00
Group 2, c	0.2	0.167	1	2.11	2.16	0.00

Table 2.5.1: Three-pole T-coil circuit parameters.

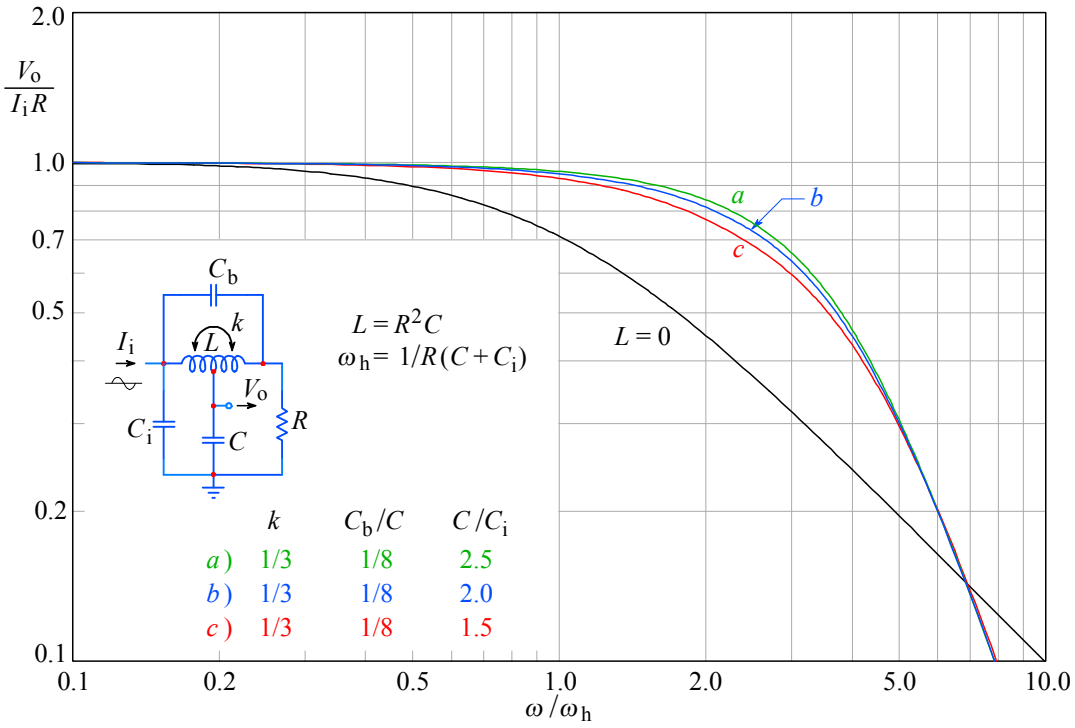

Fig. 2.5.8: Low coupling factor, Group 1: frequency response.

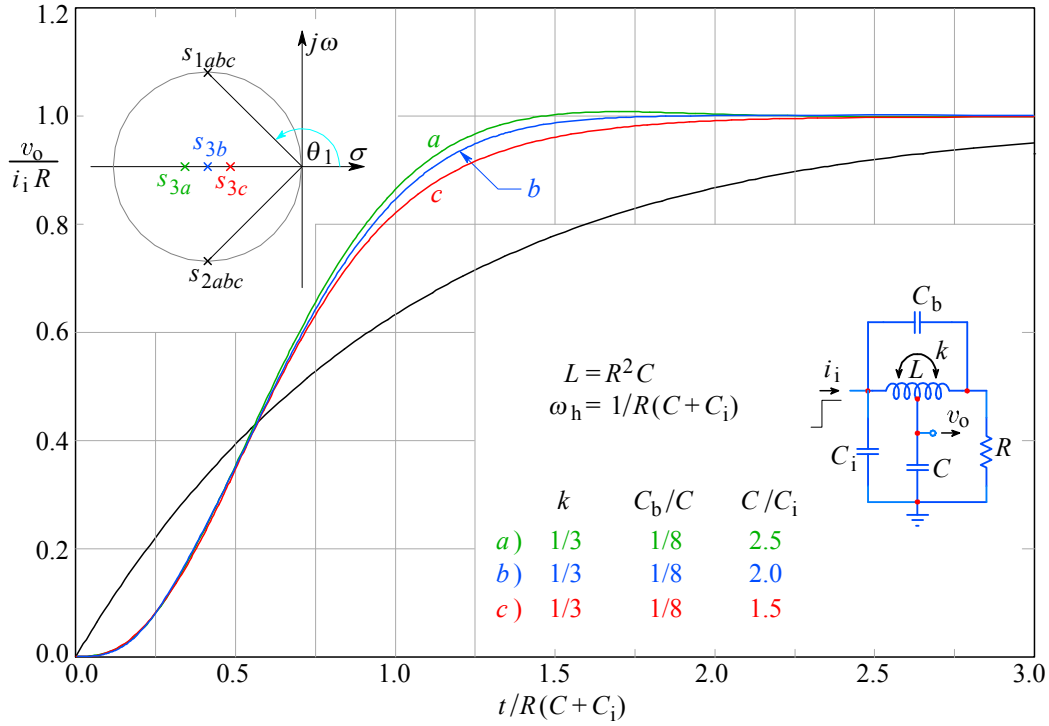

Fig. 2.5.9: Low coupling factor, Group 1: step response. In all three cases the real pole s_3 is placed closer to the origin (becoming dominant) than in the MFA and MFED case, making the responses more similar to the CD case. The characteristic circle of the complex conjugate pole pair has a slightly different diameter in each case.

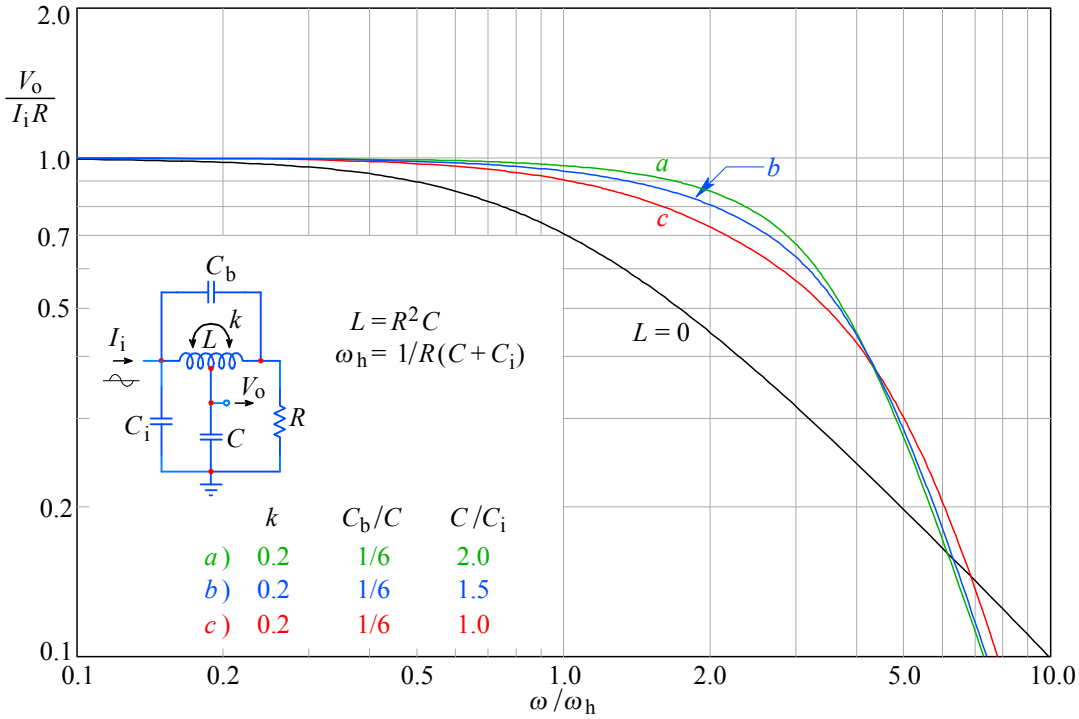

Fig. 2.5.10: Low coupling factor, Group 2: frequency response.

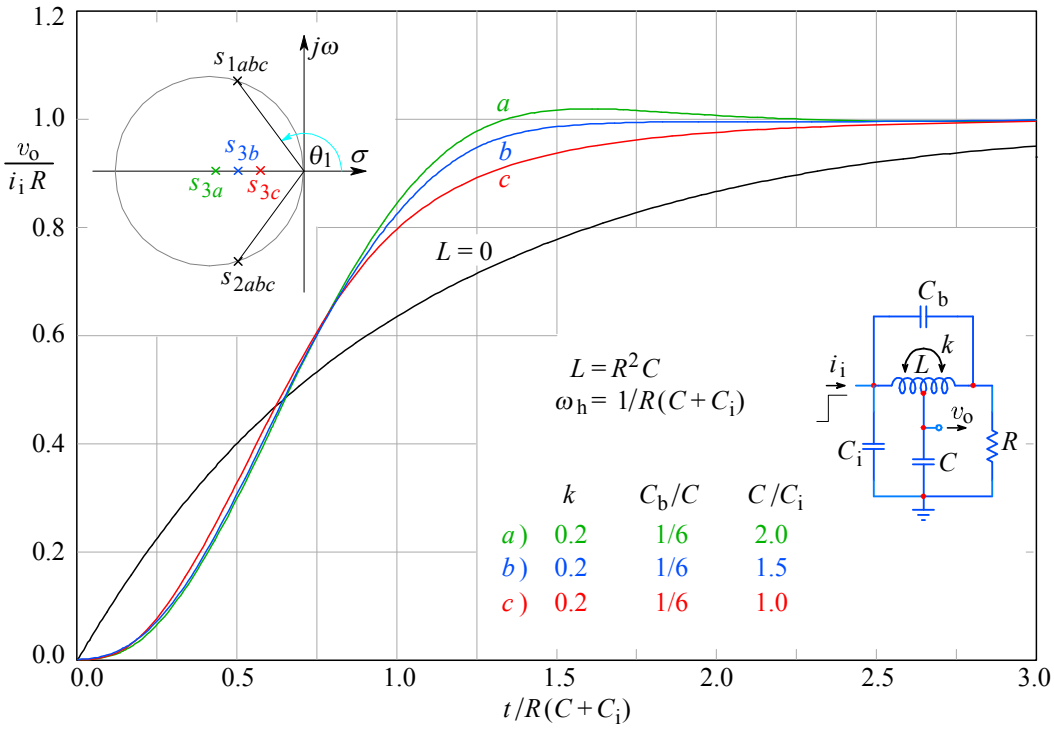

Fig. 2.5.11: Low coupling factor, Group 2: step response. The pole s_{3a} is slightly further away from the real axis than s_{3b} or s_{3c}, therefore causing an overshoot larger than in the MFED case. Both responses *b* and *c* are over-damped, reaching the final value much later than in the MFED case.

(blank page)

2.6 Four-pole L+T Peaking Circuit

Instead of leaving the input capacitance C_i without any peaking coil, as it was in the three-pole T-coil circuit, we can add another coil between C_i and the T-coil. This is the same as adding the series peaking components to the T-coil (it can be done since the input impedance of the T-coil is resistive, if properly designed). In this way, the MFA bandwidth can be extended by over 4 times, compared with the simple RC system. This is substantially more than the 2.75 times found in the two-pole T-coil circuit, where there was only one capacitance. In Fig. 2.6.1 we see such a circuit. The price to pay for such an improvement is a coupling factor $k > 0.5$, which is difficult, but possible, to achieve.

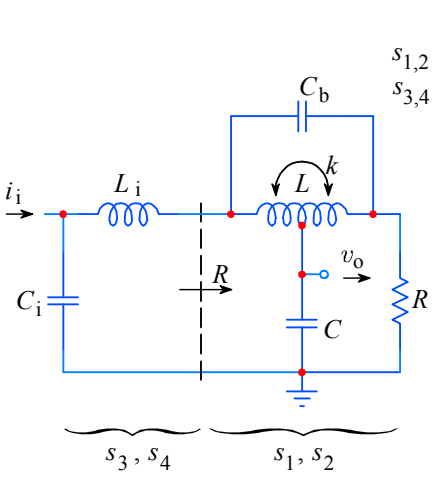

Fig. 2.6.1: The four-pole L+T network.

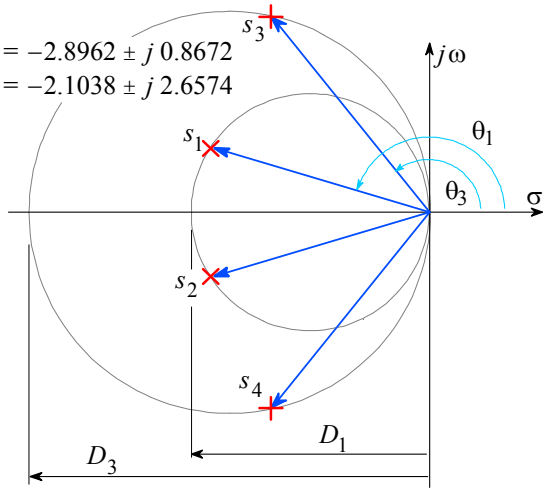

Fig. 2.6.2: The Bessel four-pole pattern of L+T.

Here we utilize the basic property of a T-coil circuit — its constant and real input impedance, presenting the loading resistor to the input series peaking section. Since the input capacitance C_i and the input inductance L_i form a letter 'L' (inverted), we call the network in Fig. 2.6.1 the L+T circuit. This is a four-pole network and **its input impedance is not constant**, but it is similar to the series peaking system, which we have already calculated (Eq. 2.2.44 — 2.2.48, plots in Fig. 2.2.9).

The transfer function of the L+T network is simply the product of the transfer function for a two-pole series peaking circuit (Eq. 2.2.4) and the transfer function for a two-pole T-coil circuit (Eq. 2.4.25). Explicitly:

$$F(s) = \frac{\dfrac{1}{mR^2C_i^2}}{s^2 + \dfrac{s}{mRC_i} + \dfrac{1}{mR^2C_i^2}} \cdot \frac{\dfrac{R}{R^2CC_b}}{s^2 + \dfrac{s}{RC_b} + \dfrac{1}{R^2CC_b}} \tag{2.6.1}$$

Both polynomials in the denominator are written in the canonical form. It would be useless to multiply them, because this would make the analysis very complicated. If we replace R in the later numerator by 1, a normalized equation results.

The T-coil section has two poles, which we can rewrite from Eq. 2.4.28:

$$s_{1,2} = \sigma_1 \pm j\omega_1 = -\frac{1}{4\,RC_b} \pm \sqrt{\frac{1}{(4\,RC_b)^2} - \frac{1}{R^2CC_b}} \tag{2.6.2}$$

whilst the input section L has two poles, rewritten from Eq. 2.2.5:

$$s_{3,4} = \sigma_3 \pm j\omega_3 = -\frac{1}{2mRC_\mathrm{i}} \pm \sqrt{\frac{1}{4m^2R^2C_\mathrm{i}^2} - \frac{1}{mR^2C_\mathrm{i}^2}} \qquad (2.6.3)$$

The T-coil circuit extends the bandwidth twice as much as the series peaking circuit, so in order to extend the bandwidth of the L+T-network as much as possible, the T-coil tap must be connected to whichever capacitance is greater. Thus $C_\mathrm{i} < C$. Therefore, the circle with the diameter D_1 and the angle θ_1, corresponding to the T-coil circuit poles $s_{1,2}$, are smaller than the circle with the diameter D_3 and the angle θ_3 corresponding to the poles $s_{3,4}$ of the L branch of the circuit.

Our task is to calculate the circuit parameters for the Bessel pole pattern shown in Fig. 2.6.2, which gives an MFED response. The corresponding values for Bessel poles, shown in Table 4.4.3 in Part 4, order $n = 4$, are:

$$s_{1t,2t} = \sigma_{1t} \pm j\omega_{1t} = -2.8962 \pm j0.8672 \quad \Rightarrow \quad \theta_1 = 163.33°$$
$$s_{3t,4t} = \sigma_{3t} \pm j\omega_{3t} = -2.1038 \pm j2.6574 \quad \Rightarrow \quad \theta_3 = 128.37°$$

As indicated in Fig. 2.5.3, the circle diameters are:

$$D_1 = \frac{|s_{1t}|}{\cos\theta_1} = \frac{\sqrt{\sigma_{1t}^2 + \omega_{1t}^2}}{\cos\theta_1} \quad \text{and} \quad D_3 = \frac{|s_{3t}|}{\cos\theta_3} = \frac{\sqrt{\sigma_{3t}^2 + \omega_{3t}^2}}{\cos\theta_3} \qquad (2.6.4)$$

The diameter ratio is:

$$\frac{D_3}{D_1} = \frac{\sqrt{\sigma_{3t}^2 + \omega_{3t}^2}\,\cos\theta_1}{\sqrt{\sigma_{1t}^2 + \omega_{1t}^2}\,\cos\theta_3} = \frac{\sqrt{2.1038^2 + 2.6574^2}}{\sqrt{2.8962^2 + 0.8672^2}} \cdot \frac{\cos 163.33°}{\cos 128.37°} = 1.7304 \qquad (2.6.5)$$

From Fig. 2.2.2 it is evident that the diameter of the circle, on which the poles of the series peaking circuit lie, is $2/RC_\mathrm{i}$. But from Fig. 2.4.3, in the case of a two-pole T-coil circuit, the circle diameter is $4/RC$. Furthermore it is:

$$\frac{C}{C_\mathrm{i}} = n \quad \text{or} \quad C_\mathrm{i} = \frac{C}{n} \qquad (1.6.6)$$

From this we derive:

$$\frac{D_3}{D_1} = \frac{\frac{2}{RC_\mathrm{i}}}{\frac{4}{RC}} = \frac{\frac{2n}{RC}}{\frac{4}{RC}} = \frac{n}{2} \quad \Rightarrow \quad n = 2\frac{D_3}{D_1} = 2 \cdot 1.7304 = 3.4608 \qquad (2.6.7)$$

As for the three-pole T-coil analysis, here, too, we express the upper half power frequency of the uncompensated circuit (without coils) as a function of the total capacitance C_c:

$$\omega_\mathrm{h} = \frac{1}{R\,(C + C_\mathrm{i})} = \frac{1}{RC_\mathrm{c}}$$

We can define the capacitors in relation to their sum, like in Eq. 2.5.15:

$$C = C_\mathrm{c}\frac{n}{n+1} \quad \text{and} \quad C_\mathrm{i} = C_\mathrm{c}\frac{1}{n+1}$$

With $n = 3.4608$ form Eq. 2.6.7 we obtain:

$$C = \frac{C_c}{1.2890} \qquad \text{and} \qquad C_i = \frac{C_c}{4.4608} \tag{2.6.8}$$

Now we can calculate all other parameters of the L+T circuit and also the actual values of the poles:

a) Coupling factor (Eq. 2.4.36):

$$k = \frac{3 - \tan^2\theta_1}{5 + \tan^2\theta_1} = \frac{3 - \tan^2 163.33°}{5 + \tan^2 163.33°} = 0.5718$$

b) Bridging capacitance (Eq. 2.4.31):

$$C_b = C\,\frac{1 + \tan^2\theta_1}{16} = C\,\frac{1 + \tan^2 163.33°}{16} = 0.0681\,C$$

c) The parameter m (Eq. 2.2.26):

$$m = \frac{1 + \tan^2\theta_3}{4} = \frac{1 + \tan^2 128.37°}{4} = 0.6488$$

d) Input inductance L_i (Eq. 2.2.14):

$$L_i = mR^2C_i = 0.6488\,R^2C_i$$

e) Real part of the pole s_1, $\Re\{s_1\} = \sigma_1$, (Eq. 2.5.5 and Fig. 2.5.3):

$$\sigma_1 = -\frac{4}{RC}\cos^2\theta_1 = -\frac{4 \cdot 1.2890}{RC_c}\cos^2 163.33° = -\frac{4.7317}{RC_c}$$

f) Imaginary part of the pole s_1, $\Im\{s_1\} = \omega_1$, (Eq. 2.5.6 and Fig. 2.5.3):

$$\omega_1 = -\frac{4}{RC}\cos\theta_1 \sin\theta_1 = -\frac{4 \cdot 1.2890}{RC_c}\cos 163.33° \sin 163.33° = \frac{1.4167}{RC_c}$$

g) Real part of the pole s_3, $\Re\{s_3\} = \sigma_3$, (Eq. 2.5.5 and Fig. 2.5.3):

$$\sigma_3 = -\frac{2}{RC_i}\cos^2\theta_3 = -\frac{2 \cdot 4.4608}{RC_c}\cos^2 128.37° = -\frac{3.4376}{RC_c}$$

h) Imaginary part of the pole s_3, $\Im\{s_3\} = \omega_3$, (Eq. 2.5.6 and Fig. 2.5.3):

$$\omega_3 = -\frac{2}{RC_i}\cos\theta_3 \sin\theta_3 = -\frac{2 \cdot 4.4608}{RC_c}\cos 128.37° \sin 128.37° = \frac{4.3419}{RC_c}$$

As above, we can calculate the parameters for the MFA response from normalized ($RC_c = 1$) values of the 4th-order Butterworth system (Table 4.3.1, BUTTAP, Part 6):

$$s_{1n,2n} = \sigma_{1n} \pm j\,\omega_{1n} = -4.1213 \pm j\,1.7071 \qquad \text{and} \qquad \theta_1 = 157.50°$$
$$s_{3n,4n} = \sigma_{3n} \pm j\,\omega_{3n} = -1.7071 \pm j\,4.1213 \qquad \text{and} \qquad \theta_3 = 112.50°$$

The L+T network parameters for some other types of poles are given in Table 2.6.1 at the end of this section.

For Butterworth poles (and only for these!) it is very easy to calculate the upper half power frequency ω_H: it is equal to the radius of the circle centered at the origin, on which all four poles lie, which in turn is equal to the absolute value of any one of the four poles. If we use the normalized pole values, the circle radius is also equal to the factor of bandwidth improvement, η_b. By dividing this value by RC_c, we obtain ω_H. We can use any one of the four poles, e.g. s_{1n}:

$$\eta_b = \frac{\omega_H}{\omega_h} = |s_{1n}| = \sqrt{\sigma_{1n}^2 + \omega_{1n}^2} = \sqrt{4.1213^2 + 1.7071^2} = 4.4609 \qquad (2.6.9)$$

and this is a really impressive bandwidth improvement.

2.6.1 Frequency Response

Let us compose a general expression for the frequency response for our L+T circuit. The formula with normalized values is very similar to Eq. 2.5.21, except that here we have two pairs of poles, $\sigma_{1n} \pm j\omega_{1n}$ and $\sigma_{3n} \pm j\omega_{3n}$:

$$|F(\omega)| = \frac{(\sigma_{1n}^2 + \omega_{1n})^2}{\sqrt{\left[\sigma_{1n}^2 + \left(\frac{\omega}{\omega_h} + \omega_{1n}\right)^2\right]\left[\sigma_{1n}^2 + \left(\frac{\omega}{\omega_h} - \omega_{1n}\right)^2\right]}}$$

$$\cdot \frac{(\sigma_{3n}^2 + \omega_{3n})^2}{\sqrt{\left[\sigma_{3n}^2 + \left(\frac{\omega}{\omega_h} + \omega_{3n}\right)^2\right]\left[\sigma_{3n}^2 + \left(\frac{\omega}{\omega_h} - \omega_{3n}\right)^2\right]}} \qquad (2.6.10)$$

Since we have inserted the normalized poles, the frequency, too, had to be normalized as ω/ω_h. Fig. 2.6.3 shows the frequency response for *a*) MFA and *b*) MFED and also for two other pole placements, reported in [Ref. 2.28], the data of which are:

The curve *c*) corresponds to the poles of Group C of [Ref. 2.28]:

$$s_{1n,2n} = \sigma_{1n} \pm j\omega_{1n} = -3.3252 \pm j0.5863 \quad \text{and} \quad \theta_1 = 170.00°$$
$$s_{3n,4n} = \sigma_{3n} \pm j\omega_{3n} = -1.7071 \pm j4.1213 \quad \text{and} \quad \theta_3 = 112.50°$$

The curve *d*) corresponds to the poles of Group A of [Ref. 2.28]:

$$s_{1n,2n} = \sigma_{1n} \pm j\omega_{1n} = -3.8332 \pm j1.7874 \quad \text{and} \quad \theta_1 = 155.00°$$
$$s_{3n,4n} = \sigma_{3n} \pm j\omega_{3n} = -2.1024 \pm j5.0013 \quad \text{and} \quad \theta_3 = 112.80°$$

Whilst *c* and *d* offer an improvement in η_b and η_r, their step response is far from optimum.

In Fig. 2.6.4, the plot *e*) is the Chebyshev response, $\Delta\varphi = \pm 0.05°$ [Ref. 2.24, 2.30]:

$$s_{1n,2n} = \sigma_{1n} \pm j\omega_{1n} = -3.7912 \pm j1.8656 \quad \text{and} \quad \theta_1 = 153.80°$$
$$s_{3n,4n} = \sigma_{3n} \pm j\omega_{3n} = -2.4861 \pm j4.6755 \quad \text{and} \quad \theta_3 = 118.00°$$

The plot *f*) is the Gaussian frequency response (to $-12\,\mathrm{dB}$) [Ref. 2.24, 2.30]:

$$s_{1n,2n} = \sigma_{1n} \pm j\omega_{1n} = -3.3835 \pm j2.0647 \quad \text{and} \quad \theta_1 = 148.83°$$

$$s_{3n,4n} = \sigma_{3n} \pm j\omega_{3n} = -3.4150 \pm j6.2556 \quad \text{and} \quad \theta_3 = 118.60°$$

The plot *g*) corresponds to a double pair of Bessel poles, with the following data:

$$s_{1n,2n} = s_{3n,4n} = \sigma_{1n} \pm j\omega_{1n} = -4.5000 \pm j2.5981 \quad \text{and} \quad \theta_1 = 150.00°$$

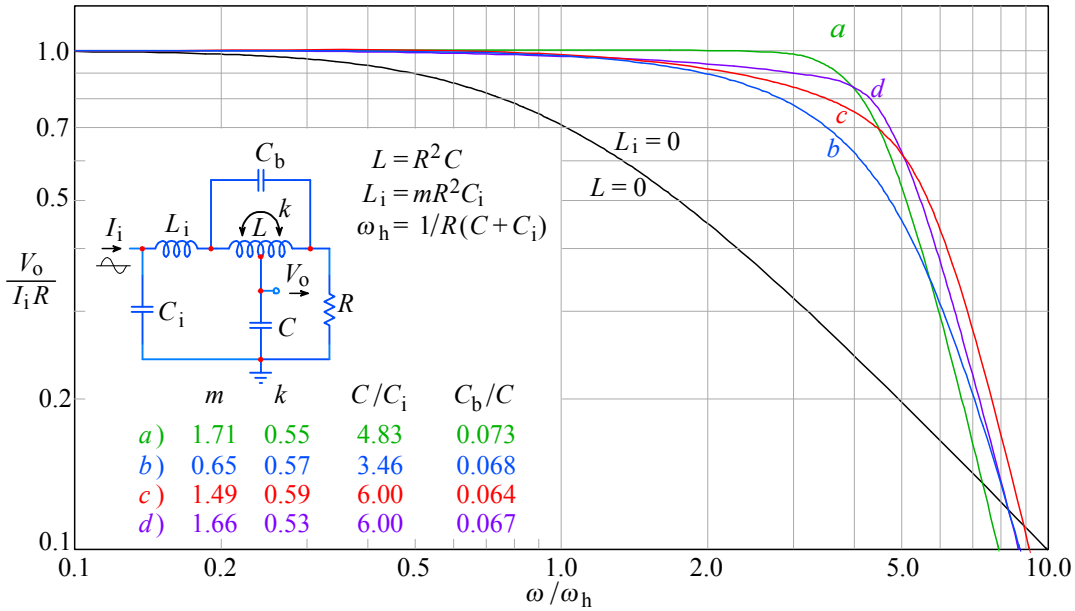

Fig. 2.6.3: Four-pole L+T peaking circuit frequency-response: ***a)*** MFA; ***b)*** MFED; ***c)*** Group C; ***d)*** Group A. In the non-peaking reference case both inductances are zero.

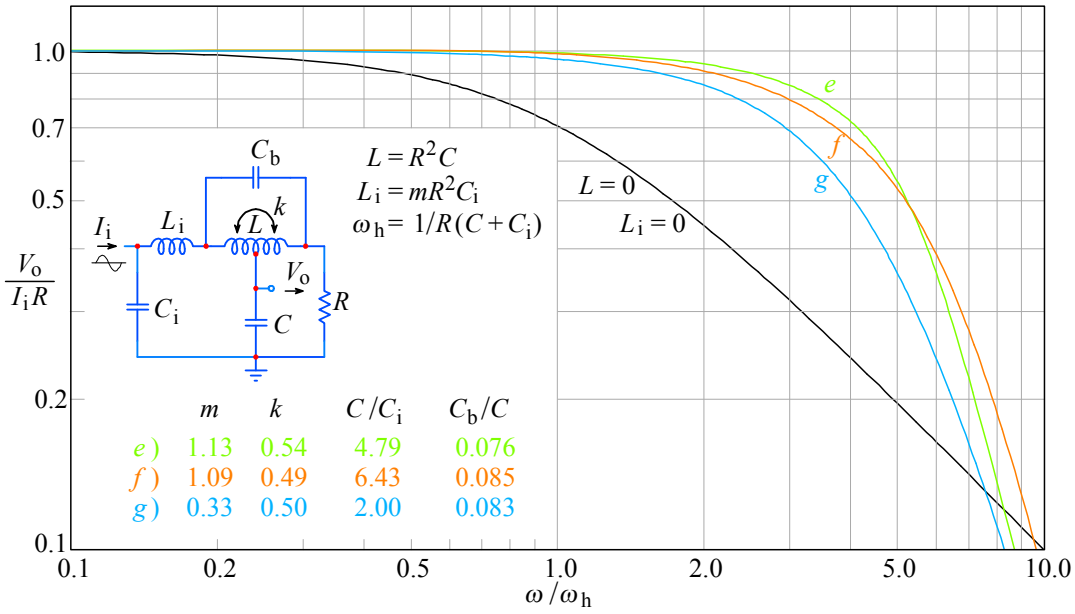

Fig. 2.6.4: Some additional frequency response plots of the four-pole L+T peaking circuit: ***e)*** Chebyshev with 0.05° phase ripple, ***f)*** Gaussian to −12dB, ***g)*** double 2nd-order Bessel. Note the lower bandwidth of *g*) ($2.9\,\omega_h$) compared with *b*) in Fig. 2.6.3 ($3.47\,\omega_h$). This clearly shows that the bandwidth of a cascade of identical stages is lower than if the stages have staggered poles.

Note: The lower bandwidth ($\omega_H = 2.9\,\omega_h$) of the system with repeated poles, plot *g*, compared with the staggered pole placement Fig. 2.6.3, plot *b* ($\omega_H = 3.47\,\omega_h$), clearly shows that using repeated poles is not a clever idea! See also the step response plots.

All these groups of poles can be found in the tables [Ref. 2.30]. Here we can see the extreme adaptability of the calculation method based on the trigonometric relations as shown in Fig. 2.5.2, 2.5.3, 2.6.2, and the corresponding formulae. We call this method *geometrical synthesis*. By this method, the calculation of circuit parameters for the inductive peaking amplifier with any suitable pole placement is very easy and we will use it extensively throughout the rest of the book.

2.6.2 Phase Response

We use Eq. 2.2.30 for each of the four poles:

$$\varphi = \arctan\frac{\frac{\omega}{\omega_h} - \omega_{1n}}{\sigma_{1n}} + \arctan\frac{\frac{\omega}{\omega_h} + \omega_{1n}}{\sigma_{1n}} + \arctan\frac{\frac{\omega}{\omega_h} - \omega_{3n}}{\sigma_{3n}} + \arctan\frac{\frac{\omega}{\omega_h} + \omega_{3n}}{\sigma_{3n}} \qquad (2.6.11)$$

The phase response plots for the first four groups of the poles are shown in Fig. 2.6.5. Although the vertical scale ends at $-300°$, the phase asymptote at high frequencies is $-360°$ for all 4th-order responses.

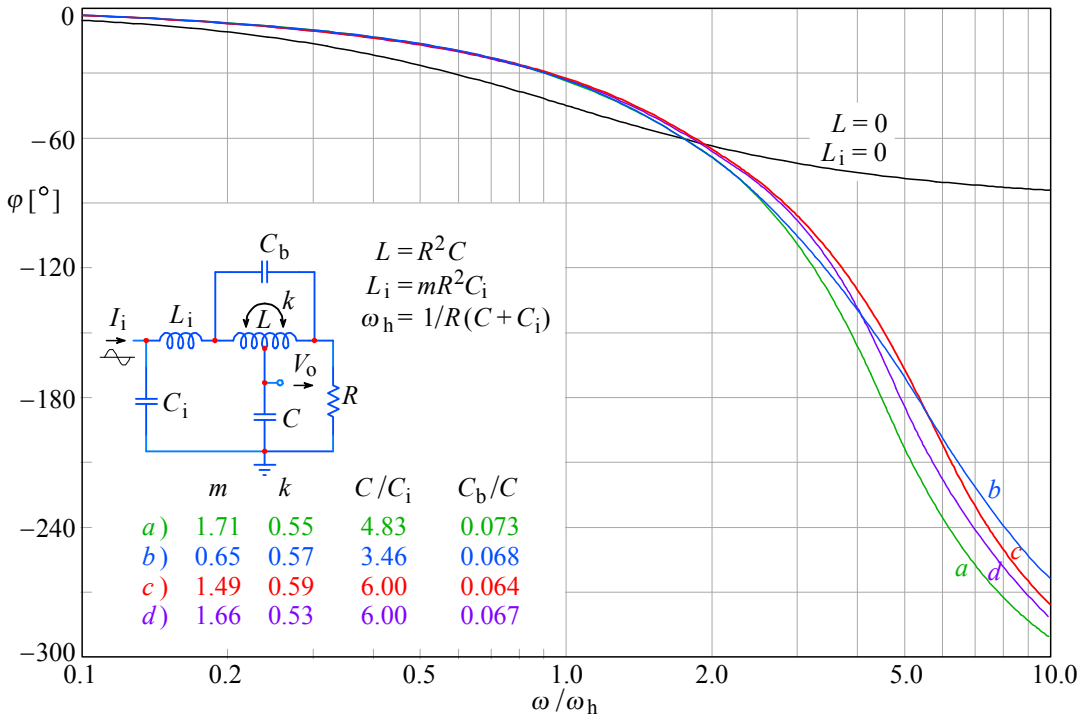

Fig. 2.6.5: Four-pole L+T peaking circuit phase response: ***a)*** MFA; ***b)*** MFED; ***c)*** Group C; ***d)*** Group A. The non-peaking case, in which both inductors are zero, has a 90° maximum phase shift; all other cases, being of 4th-order, have a 360° maximum phase shift.

2.6.3 Envelope Delay

We apply Eq. 2.2.34 for each of the four poles:

$$\tau_e\omega_h = \frac{\sigma_{1n}}{\sigma_{1n}^2 + \left(\frac{\omega}{\omega_h} - \omega_{1n}\right)^2} + \frac{\sigma_{1n}}{\sigma_{1n}^2 + \left(\frac{\omega}{\omega_h} + \omega_{1n}\right)^2} + \frac{\sigma_{3n}}{\sigma_{3n}^2 + \left(\frac{\omega}{\omega_h} - \omega_{3n}\right)^2} + \frac{\sigma_{3n}}{\sigma_{3n}^2 + \left(\frac{\omega}{\omega_h} + \omega_{3n}\right)^2} \tag{2.6.12}$$

The corresponding plots for the first four groups of poles are displayed in Fig. 2.6.6. Note that the value of the delay at low frequency is slightly different for each pole group. This is owed to a different normalization for each circuit.

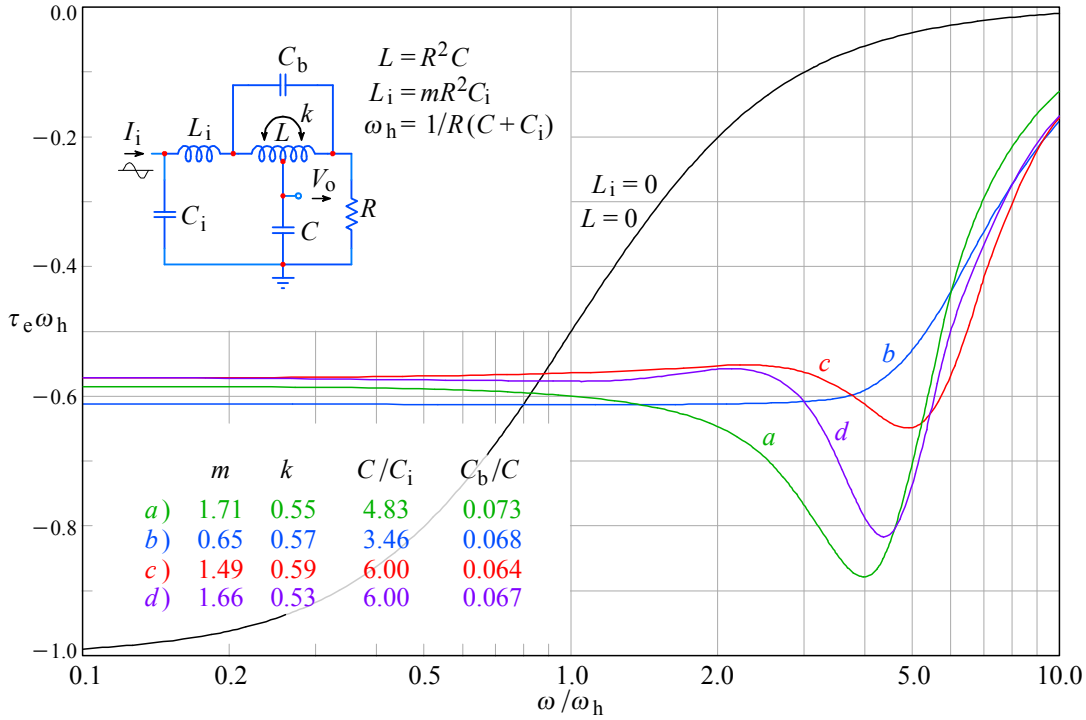

Fig. 2.6.6: Four-pole L+T peaking circuit envelope delay: ***a)*** MFA; ***b)*** MFED; ***c)*** Group C; ***d)*** Group A. For the non-peaking case at DC. the envelope delay is 1; all other cases have a larger bandwidth and consequently a lower delay. Note the MFED flatness up to nearly 3.3 ω_h.

2.6.4 Step Response

A general expression of a four-pole normalized complex frequency response is:

$$F(s) = \frac{s_1\, s_2\, s_3\, s_4}{(s - s_1)(s - s_2)(s - s_3)(s - s_4)} \tag{2.6.13}$$

The $\mathcal{L}$ transform of the step response is obtained by multiplying this function by the unit step operator $1/s$, resulting in a new, five-pole function:

$$G(s) = \frac{s_1\, s_2\, s_3\, s_4}{s\,(s - s_1)(s - s_2)(s - s_3)(s - s_4)} \tag{2.6.14}$$

and to obtain the step response in the time domain, we calculate the $\mathcal{L}^{-1}$ transform:

$$g(t) = \mathcal{L}^{-1}\{G(s)\} = \sum_{i=0}^{4} res_i \{G(s)\} \tag{2.6.15}$$

The analytical calculation is a pure routine of algebra, but it would require some 8 pages to present each step. Readers who are interested in the details, can find it in Appendix 2.3 (on the disk). Here we will write only the result:

$$g(t) = 1 + \frac{K_1}{\omega_1}\, e^{\sigma_1 t} \sqrt{(\sigma_1 A - \omega_1^2 B)^2 + \omega_1^2 (A + \sigma_1 B)^2}\ \sin(\omega_1 t + \theta_1)$$
$$+ \frac{K_3}{\omega_3}\, e^{\sigma_3 t} \sqrt{(\sigma_3 C + \omega_3^2 B)^2 + \omega_3^2 (C - \sigma_3 B)^2}\ \sin(\omega_3 t + \theta_3) \tag{2.6.16}$$

where:

$$A = (\sigma_1 - \sigma_3)^2 - (\omega_1^2 - \omega_3)^2 \qquad K_1 = \frac{\sigma_3^2 + \omega_3^2}{A^2 + \omega_1^2 B^2}$$

$$B = 2(\sigma_1 - \sigma_3)$$

$$C = (\sigma_1 - \sigma_3)^2 + (\omega_1^2 - \omega_3)^2 \qquad K_3 = \frac{\sigma_1^2 + \omega_1^2}{C^2 + \omega_3^2 B^2}$$

$$\theta_1 = \arctan \frac{-\omega_1 (A + \sigma_1 B)}{\sigma_1 A - \omega_1^2 B} \qquad \theta_3 = \arctan \frac{-\omega_3 (C - \sigma_3 B)}{\sigma_3 C + \omega_3^2 B} \tag{2.6.17}$$

Note: The angles θ_1 and θ_3 calculated by the *arctangent* will not always give a correct result. Depending on the pole pattern, one or both will require an addition of π radians, as we show in Appendix 2.3. In the following relations we give the correct values.

By inserting the normalized values for poles, and the normalized time t/T, where $T = R(C_i + C)$, we obtain the following step response functions:

a) MFA response (Butterworth poles)

$$g(t) = 1 + 2.4142\, e^{-4.1213\, t/T} \sin(1.7071\, t/T + 0.7854 + \pi)$$
$$+ 0.9968\, e^{-1.7071\, t/T} \sin(4.1213\, t/T - 0.7854 + \pi)$$

b) MFED response (Bessel poles)

$$g(t) = 1 + 5.6632\, e^{-4.7317\, t/T} \sin(1.4167\, t/T + 0.4866 + \pi)$$
$$+ 1.6484\, e^{-3.4376\, t/T} \sin(4.3419\, t/T + 1.5389)$$

c) Response for the poles of Group A

$$g(t) = 1 + 2.7233\, e^{-3.8332\, t/T} \sin(1.7874\, t/T + 0.6807 + \pi)$$
$$+ 0.7587\, e^{-2.1024\, t/T} \sin(5.0013\, t/T - 1.2250 + \pi)$$

d) Response for the poles of Group C

$$g(t) = 1 + 5.9875\, e^{-3.3252\, t/T} \sin(0.5863\, t/T + 0.2843 + \pi)$$
$$+ 0.7310\, e^{-1.7284\, t/T} \sin(3.8475\, t/T - 1.1920 + \pi)$$

e) Chebyshev poles with 0.05° phase ripple

$$g(t) = 1 + 3.0807\,\mathrm{e}^{-3.7912\,t/T}\sin(1.8565\,t/T + 0.6915 + \pi) + \\ + 0.9744\,\mathrm{e}^{-2.4861\,t/T}\sin(4.6775\,t/T - 1.4289 + \pi)$$

f) Gaussian response to − 12 dB

$$g(t) = 1 + 2.8084\,\mathrm{e}^{-3.3835\,t/T}\sin(2.0467\,t/T + 0.5403 + \pi) + \\ + 0.5098\,\mathrm{e}^{-3.4150\,t/T}\sin(6.2556\,t/T + 1.0598)$$

g) Double 2nd-order Bessel pole pairs

$$g(t) = 1 - \mathrm{e}^{-4.5\,t/T}\left[2\sin(2.5981\,t/T + 0.5236) + \right. \\ \left. + 4\sin(2.5981\,t/T)\cos(0.5236) - 10.3923\,(t/T)\cos(2.5981\,t/T + 0.5236)\right]$$

The last response was calculated by convolution. We will not repeat it here, because it is a very lengthy procedure and it has already been published [Ref. 2.5]. As with any function with repeating poles, the resulting step response is slow compared with the function with the same number of poles but in an optimized pattern. Fig. 2.6.7 shows the step responses of *a*), *b*), *c*) and *d*) ; Fig. 2.6.8 shows the step responses of *e*), *f*) and *g*) .

The data for the four-pole L+T peaking circuit are given in Table 2.6.1.

Table 2.6.1

response type	k	m	n	C_b/C	η_b	η_r	δ [%]
MFA	0.5469	1.7071	4.8283	0.0732	4.46	4.02	10.9
MFED (4th-order Bessel)	0.5718	0.6488	3.4608	0.0681	3.47	3.46	0.90
Group A	0.5333	1.6647	6.0000	0.1667	4.40	4.08	1.90
Group C	0.5901	1.4877	6.0000	0.0644	4.72	4.15	6.20
Chebyshev 0.05°	0.5358	1.1343	4.7902	0.2088	4.09	3.52	3.56
Gaussian to −12 dB	0.4904	1.0888	6.4357	0.1554	3.71	3.43	0.47
Double 2nd-order Bessel	0.5000	0.3333	2.0000	0.0833	2.92	2.96	0.44

Table 2.6.1: Four-pole L+T peaking circuit parameters.

Thus we have concluded the section on four-pole L+T peaking networks. Here we have discussed the geometrical synthesis in a very elementary way, which can be briefly explained as follows:

If the main capacitance C loading the T-coil network tap is known and the loading resistor R is selected upon the required gain, we can — based on the pole data and the geometrical relations of their real and imaginary parts — calculate all the remaining circuit parameters for the complete L+T network.

As we shall see later in the book, the same procedure can be used to calculate the circuit parameters for a multi-stage amplifier by implementing the peaking networks described so far.

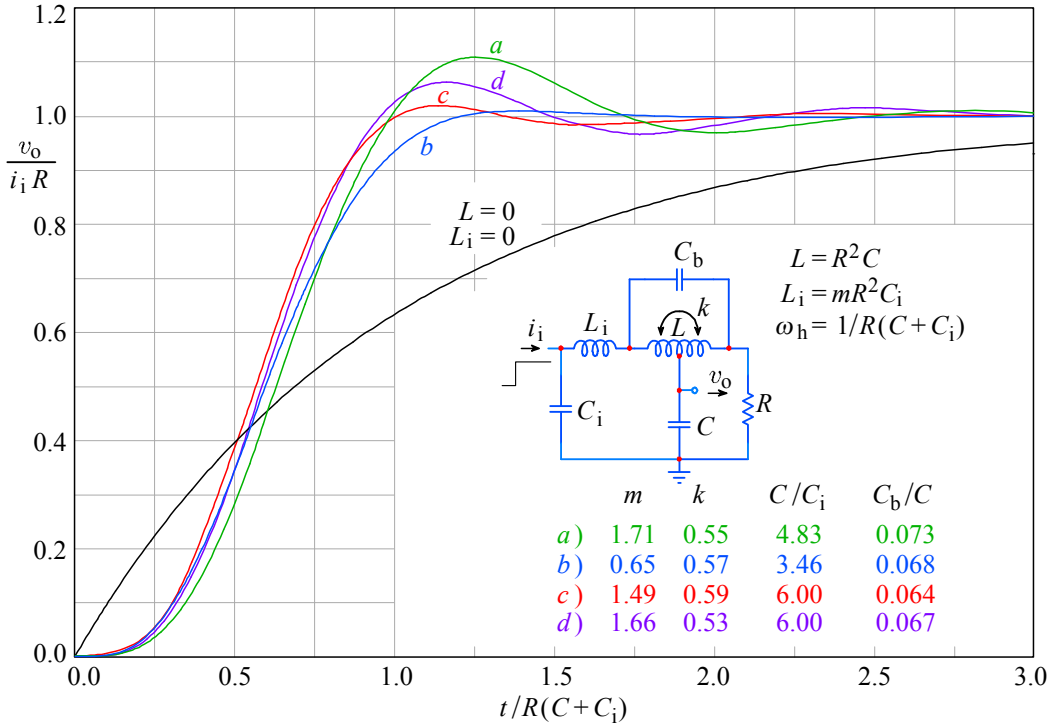

Fig. 2.6.7: Four-pole L+T circuit step response: ***a)*** MFA; ***b)*** MFED; ***c)*** Group C; ***d)*** Group A.

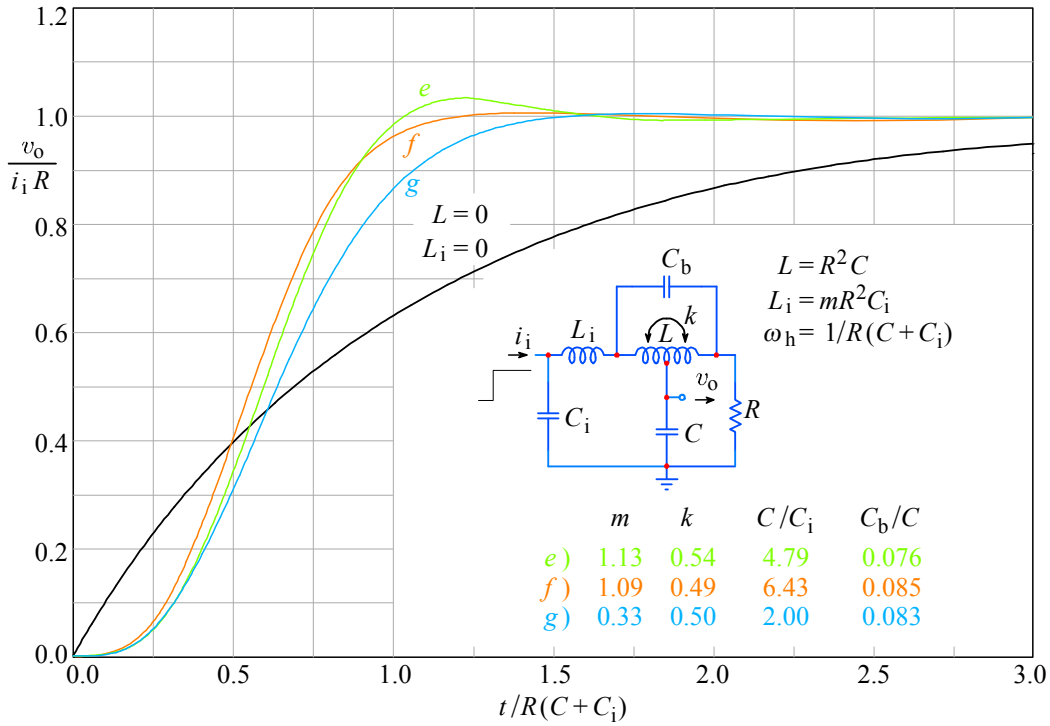

Fig. 2.6.8: Some additional four-pole L+T circuit step responses: ***e)*** Chebyshev 0.05°; ***f)*** Gaussian to − 12dB; ***g)*** double 2nd-order Bessel. Again, the step response confirms that repeating the poles is not optimal; compare the rise times of *g*) and *b*) in Fig. 2.6.7.

2.7 Two-Pole Shunt Peaking Circuit

In some cases, when a single amplifying stage is sufficient, we can use a very simple and efficient shunt peaking circuit, shown in Fig. 2.7.1. This is equivalent to the Fig. 2.1.3, but with the output taken from the capacitor C. Because shunt peaking networks are very simple to make and their bandwidth extension and risetime improvement surpass their series peaking counterparts, they have found very broad application in single stage amplifiers, e.g., in TV receivers.

As the following analysis will show, the two-pole shunt peaking circuit in Fig. 2.7.1 also has one zero. Likewise, the three-pole shunt peaking circuit, which we will discuss in Sec. 2.8, has two zeros. These zeros prevent us from using the geometrical synthesis method for shunt peaking circuits.

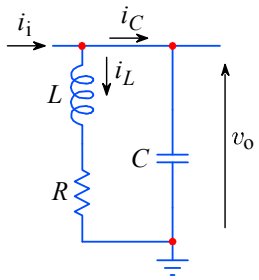

Fig. 2.7.1: A shunt peaking network. It has two poles and one zero.

If we were to compensate the zeros (by intentionally adding a network containing poles coincident with those zeros), we could still use the geometrical synthesis, but that would spoil the optimum performance of the amplifier. Whilst there are no restrictions in using the shunt peaking circuit in a multi-stage amplifier, the total bandwidth and rise time improvement of such amplifier is lower than if the complete amplifier were designed on the basis of the geometrical synthesis. Sometimes a shunt peaking circuit amplifier, designed independently, may be used as an addition to a multi-stage amplifier with series peaking and T-coil peaking circuits in order to shape the starting portion of the amplified pulse to achieve a more symmetrical step response.

The output voltage V_o of the network in Fig. 2.7.1 is:

$$V_o = I_i Z = I_i \frac{\dfrac{R + j\omega L}{j\omega C}}{R + j\omega L + \dfrac{1}{j\omega C}} \tag{2.7.1}$$

This gives the input impedance:

$$Z(\omega) = \frac{R + j\omega L}{1 + j\omega RC - \omega^2 LC} \tag{2.7.2}$$

We introduce the parameters m and ω_h:

$$L = m\,R^2 C \qquad \text{and} \qquad \omega_h = \frac{1}{RC}$$

We insert these parameters into Eq. 2.7.2 to obtain:

$$Z(\omega) = \frac{R + j\omega mR^2C}{1 + \dfrac{j\omega}{\omega_h} - \omega^2 mR^2C^2} = R\,\frac{1 + m\,\dfrac{j\omega}{\omega_h}}{1 + \dfrac{j\omega}{\omega_h} - m\left(\dfrac{\omega}{\omega_h}\right)^2} \tag{2.7.3}$$

2.7.1 Frequency Response

To obtain the normalized frequency response magnitude, we normalize the impedance ($R = 1$), then square the real and imaginary parts in both the numerator and the denominator, and take a square root of the whole fraction:

$$\left|F(\omega)\right| = \sqrt{\frac{1 + m^2\left(\dfrac{\omega}{\omega_h}\right)^2}{1 + (1 - 2m)\left(\dfrac{\omega}{\omega_h}\right)^2 + m^2\left(\dfrac{\omega}{\omega_h}\right)^4}} \tag{2.7.4}$$

We shall first find the value of the parameter m for the MFA response. In this case the factors at $(\omega/\omega_h)^2$ in the numerator and in the denominator must be equal [Ref. 2.4]:

$$1 - 2m = m^2 \qquad \Rightarrow \qquad m = \sqrt{2} - 1 = 0.4141 \tag{2.7.5}$$

If we put this value into Eq. 2.7.4 we obtain:

$$\left|F(\omega)\right| = \sqrt{\frac{1 + 0.1716\left(\dfrac{\omega}{\omega_h}\right)^2}{1 + 0.1716\left(\dfrac{\omega}{\omega_h}\right)^2 + 0.1716\left(\dfrac{\omega}{\omega_h}\right)^4}} \tag{2.7.6}$$

The corresponding plot is shown in Fig. 2.7.2, curve *a*.

For the MFED response, we have to first find the envelope delay.

2.7.2 Phase Response And Envelope Delay

We calculate the value of the parameter m for the MFED response from the envelope delay response, which we derive from the phase angle $\varphi(\omega)$:

$$\varphi(\omega) = \arctan\frac{\Im\{F(\omega)\}}{\Re\{F(\omega)\}}$$

where $F(\omega)$ can be derived from Eq. 2.7.3 by making the denominator real. This is done by multiplying both the numerator and the denominator by the complex conjugate value of the denominator: $1 - m(\omega/\omega_h) - j\,(\omega/\omega_h)$.

The result is:

$$F(\omega) = \frac{\left[1 + jm\left(\frac{\omega}{\omega_h}\right)\right]\left[1 - m\left(\frac{\omega}{\omega_h}\right)^2 - j\left(\frac{\omega}{\omega_h}\right)\right]}{\left[1 - m\left(\frac{\omega}{\omega_h}\right)^2\right]^2 + \left(\frac{\omega}{\omega_h}\right)^2} = \frac{\mathcal{N}}{\mathcal{D}} \qquad (2.7.7)$$

Next we multiply the brackets in the numerator and separate the real and imaginary parts:

$$\mathcal{N} = 1 + j\left[(m-1)\left(\frac{\omega}{\omega_h}\right) - m^2\left(\frac{\omega}{\omega_h}\right)^3\right] \qquad (2.7.8.)$$

By dividing the imaginary part of $F(\omega)$ by its real part, $\mathcal{D}$ cancels from the phase:

$$\boxed{\varphi = \arctan\frac{\Im\{\mathcal{N}\}}{\Re\{\mathcal{N}\}} = \arctan\left[(m-1)\left(\frac{\omega}{\omega_h}\right) - m^2\left(\frac{\omega}{\omega_h}\right)^3\right]} \qquad (2.7.9)$$

By inserting $m = 0.4141$ (Eq. 2.7.5), we would get the phase response of the MFA case, as plotted in Fig. 2.7.3, curve *a*. But for the MFED response, the correct value of m must be found from the envelope delay, so we must calculate $d\varphi/d\omega$ from Eq. 2.7.9:

$$\tau_e = \frac{d\,\varphi}{d\,\omega} = \frac{d}{d\,\omega}\left\{\arctan\left[(m-1)\left(\frac{\omega}{\omega_h}\right) - m^2\left(\frac{\omega}{\omega_h}\right)^3\right]\right\}$$

$$= \frac{(m-1) - 3\,m^2\left(\frac{\omega}{\omega_h}\right)^2}{1 + \left[(m-1)\left(\frac{\omega}{\omega_h}\right) - m^2\left(\frac{\omega}{\omega_h}\right)^3\right]^2} \cdot \frac{1}{\omega_h} \qquad (2.7.10)$$

Let us square the bracket in the denominator, factor out $(m-1)$ and multiply both sides of the equation by ω_h in order to obtain the normalized envelope delay:

$$\boxed{\tau_e\,\omega_h = \frac{(m-1)\left[1 - \frac{3m^2}{m-1}\left(\frac{\omega}{\omega_h}\right)^2\right]}{1 + (m-1)^2\left(\frac{\omega}{\omega_h}\right)^2 - 2m^2(m-1)\left(\frac{\omega}{\omega_h}\right)^4 + m^4\left(\frac{\omega}{\omega_h}\right)^6}} \qquad (2.7.11)$$

A maximally flat envelope-delay is achieved when both factors at $(\omega/\omega_h)^2$ in the numerator and in the denominator are equal [Ref. 2.4]. Taking the sign into account, we have:

$$\frac{3m^2}{1-m} = (m-1)^2 \qquad \Rightarrow \qquad 3m^2 = (m^2 - 2m + 1)(1-m) \qquad (2.7.12)$$

Finally:

$$m^3 + 3\,m - 1 = 0 \qquad \Rightarrow \qquad m = 0.3222 \qquad (2.7.13)$$

The only real solution is $m = 0.3222$. At DC $\tau_e\omega_h = m - 1 \approx -0.68$. If we put m into Eq. 2.7.4 for the frequency response, Eq. 2.7.9 for phase response and Eq. 2.7.11 for envelope delay, we can make the plots *b* in Fig. 2.7.2, Fig. 2.7.3, and FIg. 2.7.4.

Now we have enough data to calculate both poles and the zero for the MFA and MFED case, which we shall also need to calculate the step response. But we still have to find the value of m for the critical damping (CD) case. We can derive it from the fact that for CD all the poles are real and equal. To find the poles, we take Eq. 2.7.3, divide it by R, and replace the normalized frequency $j\omega/\omega_h$ with the complex variable s:

$$F(s) = \frac{Z(s)}{R} = \frac{1 + m\,s}{1 + s + m\,s^2} = \frac{s + \dfrac{1}{m}}{s^2 + s\,\dfrac{1}{m} + \dfrac{1}{m}} \tag{2.7.14}$$

We obtain the normalized poles from the denominator of $F(s)$:

$$s_{1n,2n} = \sigma_{1n} \pm j\omega_{1n} = -\frac{1}{2m} \pm \frac{1}{2m}\sqrt{1 - 4m} = \frac{1}{2m}\left(-1 \pm j\sqrt{4m - 1}\right) \tag{2.7.15}$$

and the normalized real zero from the numerator:

$$s_{3n} = -\sigma_{3n} = -\frac{1}{m} \tag{2.7.16}$$

Since the poles are usually complex, we have written the complex form in the solution of the quadratic equation (Eq. 2.7.15). However, for CD, the solution must be real, so the expression under the square root must be zero and this gives $m = 0.25$. The curves corresponding to CD in Fig. 2.7.2, 2.7.3, and 2.7.4 are marked with the letter *c*.

Note that, in spite of the higher cut off frequency, all the curves have the same high frequency asymptote as the first-order response.

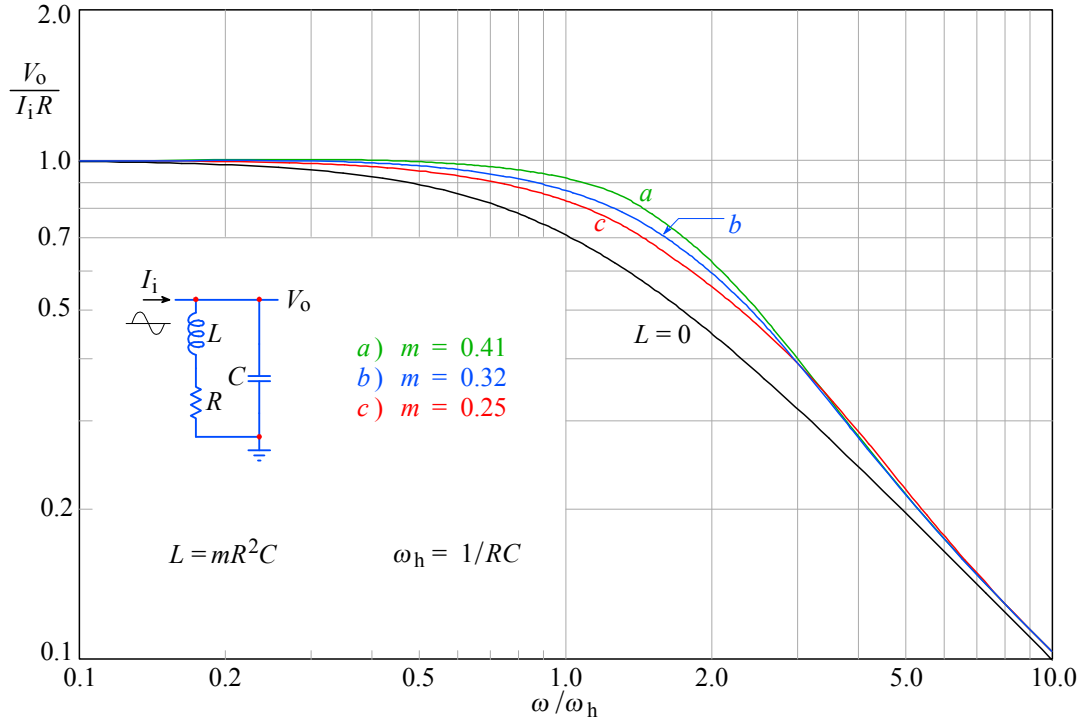

Fig. 2.7.2: Shunt peaking circuit frequency response: ***a)*** MFA; ***b)*** MFED; ***c)*** CD. As usual, the non-peaking case ($L = 0$) is the reference. The system zero causes the high-frequency asymptote to be the same as for the non-peaking system.

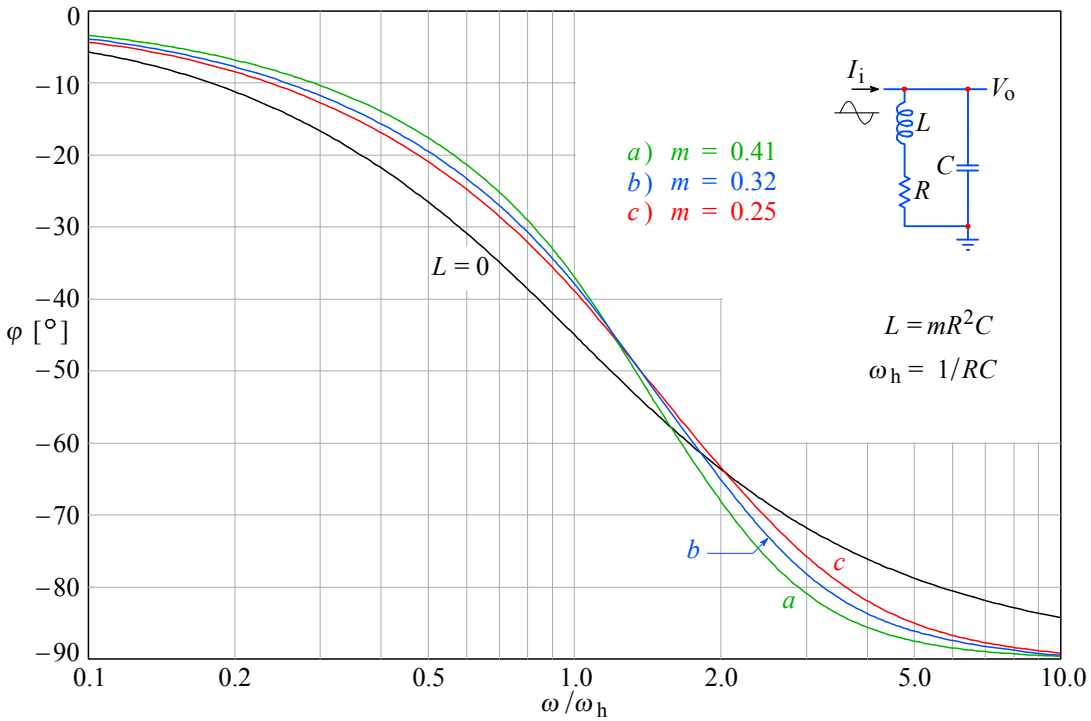

Fig. 2.7.3: Shunt peaking circuit phase response: ***a)*** MFA; ***b)*** MFED; ***c)*** CD. The non-peaking case ($L = 0$) is the reference. The system zero causes the high frequency phase to be $-90°$, the same as for the non-peaking system.

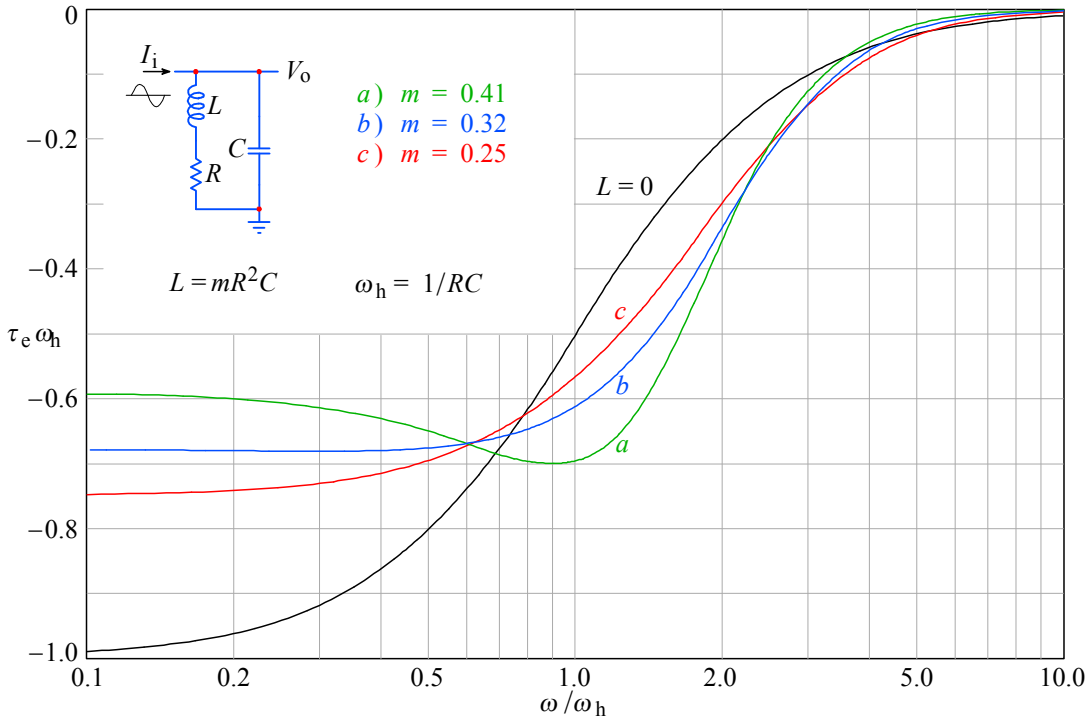

Fig. 2.7.4: Shunt peaking circuit envelope delay: ***a)*** MFA; ***b)*** MFED; ***c)*** CD. The non-peaking case ($L = 0$) is the reference. The peaking systems have a higher bandwidth, and consequently a lower delay at DC than the non-peaking system.

2.7.3 Step Response

For the calculated values of m the poles (Eq. 2.7.15) and the zero (Eq. 2.7.16) are:

a) for MFA response:

the poles $s_{1n,2n} = -1.2071 \pm j\,0.9783$ and the zero $s_{3n} = \sigma_{3n} = -2.4142$

b) for MFED response:

the poles $s_{1n,2n} = -1.5518 \pm j\,0.8340$ and the zero $s_{3n} = \sigma_{3n} = -3.1037$

c) for CD response:

the double pole $s_{1n,2n} = \sigma_{1n} = -2$ and the zero $s_{3n} = \sigma_{3n} = -4$

With these data we can calculate the step response. At first we calculate the MFA and MFED responses, where in both cases we have two complex conjugate poles and one real zero. The general expression for the frequency response is:

$$F(s) = -\frac{s_1 s_2 (s - s_3)}{s_3 (s - s_1)(s - s_2)} \tag{2.7.17}$$

We multiply this equation by the unit step operator $1/s$ and obtain a new function:

$$G(s) = \frac{-s_1 s_2 (s - s_3)}{s\, s_3 (s - s_1)(s - s_2)} \tag{2.7.18}$$

To calculate the step response in the time domain we take the $\mathcal{L}^{-1}$ transform:

$$g(t) = \mathcal{L}^{-1}\{G(t)\} = \sum \text{res}\, \frac{-s_1\, s_2\, (s - s_3)\, \mathrm{e}^{st}}{s\, s_3\, (s - s_1)\, (s - s_2)} \tag{2.7.19}$$

We have three residues:

$$\text{res}_0 = \lim_{s \to 0} s \left[\frac{-s_1\, s_2\, (s - s_3)\, \mathrm{e}^{st}}{s\, s_3\, (s - s_1)(s - s_2)} \right] = \frac{s_1\, s_2\, s_3}{s_1\, s_2\, s_3} = 1$$

$$\text{res}_1 = \lim_{s \to s_1} (s - s_1) \left[\frac{-s_1\, s_2\, (s - s_3)\, \mathrm{e}^{st}}{s\, s_3\, (s - s_1)\, (s - s_2)} \right] = \frac{-s_2\, (s_1 - s_3)}{s_3\, (s_1 - s_2)}\, \mathrm{e}^{s_1 t}$$

$$\text{res}_2 = \lim_{s \to s_2} (s - s_2) \left[\frac{-s_1\, s_2\, (s - s_3)\, \mathrm{e}^{st}}{s\, s_3\, (s - s_1)\, (s - s_2)} \right] = \frac{-s_1 (s_2 - s_3)}{s_3 (s_2 - s_1)}\, \mathrm{e}^{s_2 t} \tag{2.7.20}$$

Since the procedure is the same as for the previous circuits, we shall omit some intermediate expressions. After inserting all the pole components, the sum of residues is:

$$g(t) = 1 - \frac{A + jB}{2jB}\, \mathrm{e}^{\sigma_1 t}\, \mathrm{e}^{j\omega_1 t} - \frac{A - jB}{2jB}\, \mathrm{e}^{\sigma_1 t}\, \mathrm{e}^{-j\omega_1 t} \tag{2.7.21}$$

where $A = \omega_1^2 + \sigma_1(\sigma_1 - \sigma_3)$ and $B = \omega_1 \sigma_3$. After factoring out $-\mathrm{e}^{\sigma_1 t}/B$ we obtain:

$$g(t) = 1 - \frac{\mathrm{e}^{\sigma_1 t}}{B} \left(\frac{A + jB}{2j}\, \mathrm{e}^{j\omega_1 t} + \frac{A - jB}{2j}\, \mathrm{e}^{-j\omega_1 t} \right) \tag{2.7.22}$$

The expression in parentheses can be simplified by sorting the real and imaginary parts:

$$\frac{A + jB}{2j}\,\mathrm{e}^{j\omega_1 t} + \frac{A - jB}{2j}\,\mathrm{e}^{-j\omega_1 t} = A\,\frac{\mathrm{e}^{j\omega_1 t} - \mathrm{e}^{-j\omega_1 t}}{2j} + B\,\frac{\mathrm{e}^{j\omega_1 t} + \mathrm{e}^{-j\omega_1 t}}{2}$$

$$= A\sin\omega_1 t + B\cos\omega_1 t$$

$$= \sqrt{A^2 + B^2}\ \sin(\omega_1 t + \beta) \qquad (2.7.23)$$

where:

$$\beta = \arctan\frac{B}{A}$$

Again we have written β in order not to confuse it with the pole angle θ. And here, too, we will have to add π radians to β wherever appropriate, owing to the π period of the *arctangent* function. By entering Eq. 2.7.23 into Eq. 2.7.22 and inserting the poles, we obtain the general expression:

$$\boxed{g(t) = 1 - \frac{\sqrt{\left[\omega_1^2 + \sigma_1(\sigma_1 - \sigma_3)\right]^2 + \omega_1^2\sigma_3^2}}{\omega_1\sigma_3}\,\mathrm{e}^{\sigma_1 t}\sin(\omega_1 t + \beta)} \qquad (2.7.24)$$

where:

$$\boxed{\beta = \arctan\frac{\omega_1\sigma_3}{\omega_1^2 + \sigma_1(\sigma_1 - \sigma_3)} + \pi} \qquad (2.7.25)$$

We now need the general expression for the step response for the CD case, where we have a double real pole s_1 and a real zero s_3. We start from the normalized frequency response function:

$$F(s) = \frac{-\,s_1^2\,(s - s_3)}{s_3\,(s - s_1)^2} \qquad (2.7.26)$$

which must be multiplied by the unit step operator $1/s$, thus obtaining:

$$G(s) = \frac{-\,s_1^2\,(s - s_3)}{s\,s_3\,(s - s_1)^2} \qquad (2.7.27)$$

There are two residues:

$$\mathrm{res}_0 = \lim_{s\to 0} s\left[\frac{-\,s_1^2\,(s - s_3)\,\mathrm{e}^{st}}{s\,s_3\,(s - s_1)^2}\right] = \frac{s_1^2\,s_3}{s_1^2\,s_3} = 1$$

$$\mathrm{res}_1 = \lim_{s\to s_1}\frac{d}{ds}\left[(s - s_1)^2\,\frac{-\,s_1^2\,(s - s_3)\,\mathrm{e}^{st}}{s\,s_3\,(s - s_1)^2}\right] = \left[s_1 t\left(1 - \frac{s_1}{s_3}\right) - 1\right]\mathrm{e}^{s_1 t} \qquad (2.7.28)$$

If we express the poles in the second residue with their real and imaginary parts and take the sum of both residues, we obtain:

$$\boxed{g(t) = 1 + \mathrm{e}^{\sigma_1 t}\left[\sigma_1 t\left(1 - \frac{\sigma_1}{\sigma_3}\right) - 1\right]} \qquad (2.7.29)$$

Finally we insert the normalized numerical values for the poles, the zeros and the time variable $t/T = t/RC$. The step response is:

a) for MFA ($\sigma_{1n} = -1.2071$, $\omega_{1n} = \pm 0.9783$, $\sigma_{3n} = -2.4142$)

$$g(t) = 1 + 1.0178\,\mathrm{e}^{-1.2071\,t/T}\sin(0.9783\,t/T - 1.3622 + \pi)$$

b) for MFED ($\sigma_{1n} = -1.5518$, $\omega_{1n} = \pm 0.8340$, $\sigma_{3n} = -3.1037$)

$$g(t) = 1 + 1.1018\,\mathrm{e}^{-1.5518\,t/T}\sin(0.5374\,t/T - 0.9862 + \pi)$$

c) for CD ($\sigma_{1n} = -2$, $\sigma_{3n} = -4$)

$$g(t) = 1 - \mathrm{e}^{-2t/T}(t/T + 1)$$

The step response plots are shown in Fig. 2.7.5. By comparing them with those for the two-pole series peaking circuit in Fig. 2.2.8 we note that the step response derivative at time $t = 0$ is not zero, in contrast to those of the series peaking circuit. Instead the responses look more like the step response of the non-peaking first-order case. The reason for this is in the difference between the number of poles and zeros, which is only 1 in favor of the poles in the shunt peaking circuit.

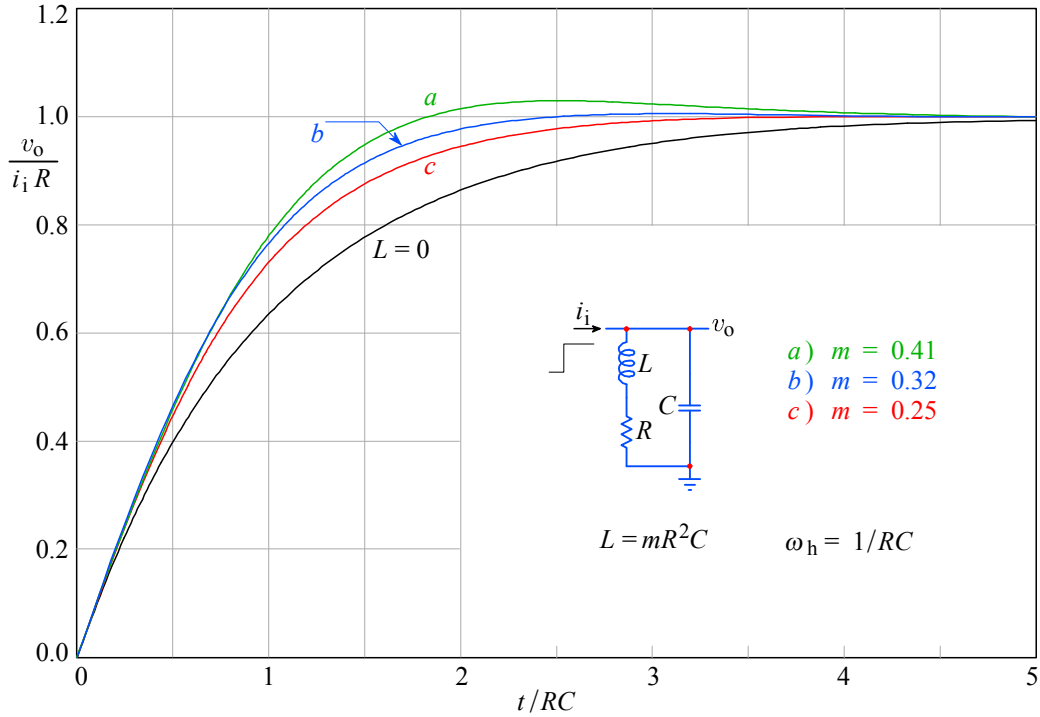

Fig. 2.7.5: Shunt peaking circuit step response: ***a)*** MFA; ***b)*** MFED; ***c)*** CD. The non-peaking case ($L = 0$) is the reference. The difference between the number of poles and the number of zeros is only 1 for the shunt peaking systems, therefore the starting slope of the step response is similar to that of the non-peaking first-order system.

Fig. 2.7.6 shows the pole placements for the three cases. Note the placement of the zero, which is farther from the origin for those systems which have the poles with lower imaginary part.

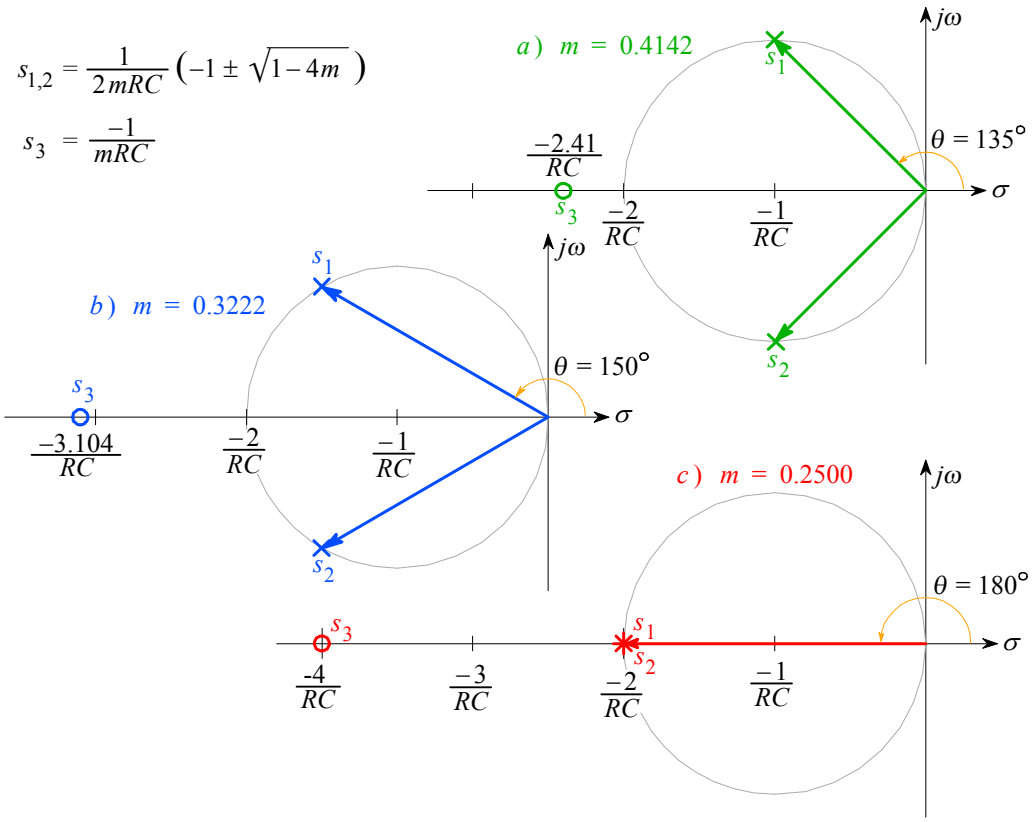

Fig. 2.7.6: Shunt peaking circuit placement of the poles and the zero: ***a)*** MFA; ***b)*** MFED; ***c)*** CD. Note the position of the zero s_3 at the far left of the real axis. Although far from the poles, its influence on the response is notable in each case.

We conclude the discussion with Table 2.7.1, in which all the important two-pole shunt peaking circuit parameters are listed.

Table 2.7.1

response type	m	η_b	η_r	δ [%]
a) MFA	0.4141	1.72	1.81	3.08
b) MFED	0.3222	1.57	1.62	0.41
c) CD	0.2500	1.41	1.43	0.00

Table 2.7.1: Two-pole shunt-peaking circuit parameters

(blank page)

2.8 Three-Pole Shunt Peaking Circuit

If we consider the self capacitance C_L of the coil L the two-pole shunt peaking circuit acquires an additional pole and an additional zero. If the value of C_L can not be neglected it must be in a well defined proportion against other circuit components in order to achieve optimum performance in the MFA or MFED sense. Fig. 2.8.1 shows the corresponding three-pole, two-zero shunt peaking circuit.

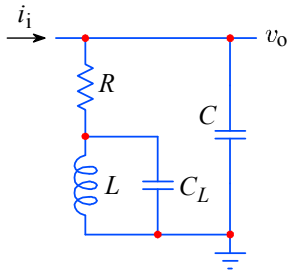

Fig. 2.8.1: The shunt peaking circuit has three poles and two zeros.

The network impedance is:

$$Z(\omega) = \frac{1}{j\omega C + \dfrac{1}{R + \dfrac{1}{j\omega C_L + \dfrac{1}{j\omega L}}}}$$

$$= \frac{R + j\omega L - \omega^2 L C_L R}{j\omega C R(1 - \omega^2 L C_L) - \omega^2 L\,(C + C_L) + 1} \qquad (2.8.1)$$

Let us introduce the following parameters:

$$L = mR^2C \qquad \omega_h = \frac{1}{RC} \qquad C_L = n\,C \qquad (2.8.2)$$

which we insert into Eq. 2.8.1. Then:

$$Z(\omega) = R\,\frac{1 - m\,n\left(\dfrac{\omega}{\omega_h}\right)^2 + j\,m\left(\dfrac{\omega}{\omega_h}\right)}{1 - m\,(1+n)\left(\dfrac{\omega}{\omega_h}\right)^2 + j\left(\dfrac{\omega}{\omega_h}\right)\left[1 - m\,n\left(\dfrac{\omega}{\omega_h}\right)^2\right]} \qquad (2.8.3)$$

2.8.1. Frequency Response

The system transfer function can be obtained easily from $Z(\omega)$. We first replace the normalized imaginary frequency $j\,(\omega/\omega_h)$ by the complex frequency variable s. Then, by realizing that the output voltage is equal to the product of input current and the system impedance: $V_o = I_i\,Z(\omega)$, we can express the transfer function by normalizing the output to the final value at DC:

$$F(s) = \frac{V_o}{I_i R} = \frac{Z(s)}{R} \qquad (2.8.4)$$

With a little rearranging we obtain:

$$F(s) = \frac{s^2 + s\frac{1}{n} + \frac{1}{m\,n}}{s^3 + s^2\frac{1+n}{n} + s\frac{1}{m\,n} + \frac{1}{m\,n}} \tag{2.8.5}$$

The magnitude $|F(s)| = \sqrt{F(s)\cdot F^*(s)}$ can be obtained more easily from the impedance magnitude. We start from Eq. 2.8.3, square the imaginary and real parts in the numerator and in the denominator and take a square root of the whole fraction:

$$|Z(\omega)| = R\sqrt{\frac{\left[1 - m\,n\left(\frac{\omega}{\omega_\mathrm{h}}\right)^2\right]^2 + m^2\left(\frac{\omega}{\omega_\mathrm{h}}\right)^2}{\left[1 - m(1+n)\left(\frac{\omega}{\omega_\mathrm{h}}\right)^2\right]^2 + \left(\frac{\omega}{\omega_\mathrm{h}}\right)^2\left[1 - m\,n\left(\frac{\omega}{\omega_\mathrm{h}}\right)^2\right]^2}} \tag{2.8.6}$$

Then we square the brackets and divide by R to obtain a normalized expression:

$$|F(\chi)| = \sqrt{\frac{1 + \left[m^2 - 2\,m\,n\right]\chi^2 + m^2n^2\chi^4}{1 + \left[1 - 2\,m(1+n)\right]\chi^2 + \left[m^2(1+n)^2 - 2\,m\,n\right]\chi^4 + m^2n^2\chi^6}} \tag{2.8.7}$$

and here we have replaced the normalized frequency ω/ω_h with the symbol χ in order to be able to write the equation on a single line.

For the MFA response the numerator and denominator factors at the same powers of $(\omega/\omega_\mathrm{h})$ in Eq. 2.8.7 must be equal [Ref. 2.4]. Thus we have two equations:

$$\begin{aligned} m^2 - 2\,m\,n &= 1 - 2m(1+n) \\ m^2n^2 &= m^2(1+n)^2 - 2\,m\,n \end{aligned} \tag{2.8.8}$$

from which we calculate the values of m and n for the MFA response:

$$m = 0.414 \qquad \text{and} \qquad n = 0.354 \tag{2.8.9}$$

For the MFED response the procedure for calculating the parameters m and n can be similar to that for the two-pole shunt peaking circuit: we would first calculate the formula for the envelope delay and equate the factors at the same powers of $(\omega/\omega_\mathrm{h})$ in the numerator and the denominator, etc. But, with the increasing number of poles, the calculation becomes more complicated. It is much simpler to compare the coefficients of the characteristic polynomial of the complex frequency transfer function Eq. 2.8.5.

The numerical values of the coefficients of the 3rd-order Bessel polynomial, sorted by the falling powers of s, are: 1, 6, 15 and 15 again. Thus, we have two equations:

$$\frac{1+n}{n} = 6 \qquad \text{and} \qquad \frac{1}{m\,n} = 15 \tag{2.8.10}$$

from which we get:

$$n = \frac{1}{5} \qquad \text{and} \qquad m = \frac{1}{3} \tag{2.8.11}$$

Compare these values to those from the work of *V.L. Krejcer* [Ref. 2.4, loc. cit.]. His values for MFED responses are:

$$m = 0.35 \qquad \text{and} \qquad n = 0.22$$

Krejcer also calculated the parameters for a "special" case circuit (SPEC):

$$m = 0.45 \qquad \text{and} \qquad n = 0.22 \tag{2.8.12}$$

By inserting the values of parameters from Eq. 2.8.9 – 2.8.12 into Eq. 2.8.7, we can calculate the corresponding frequency responses. However, for the phase, envelope delay, and step response we also need to know the values of poles and zeros. Since we know all the values of parameters m and n, we can use Eq. 2.8.5 . We equate the denominator $\mathcal{D}$ of $F(s)$ to zero and find the roots, which are the three poles of $F(s)$. Similarly, by equating the numerator $\mathcal{N}$ of $F(s)$ to zero we calculate the two zeros (for readers less experienced in mathematics we have reported the general solutions for polynomials of first, second and third order in Appendix 2.1).

a) MFA response ($m = 0.414$ and $n = 0.354$):

$\mathcal{D} \Rightarrow \quad s^3 + 3.825\,s^2 + 6.823\,s + 6.823 = 0$

The poles: $s_{1n,2n} = \sigma_{1n} \pm j\,\omega_{1n} = -0.850 \pm j\,1.577$

$s_{3n} = \sigma_{3n} = -2.125$

$\mathcal{N} \Rightarrow \quad s^2 + 2.825\,s + 6.823 = 0$

The zeros: $s_{4n,5n} = \sigma_{5n} \pm j\,\omega_{5n} = -1.412 \pm j\,2.197$

b) MFED response ($m = 0.333$ and $n = 0.200$):

$\mathcal{D} \Rightarrow \quad s^3 + 6\,s^2 + 15\,s + 15 = 0$

The poles: $s_{1n,2n} = \sigma_{1n} \pm j\,\omega_{1n} = -1.8389 \pm j\,1.7544$

$s_{3n} = \sigma_{3n} = -2.3222$

$\mathcal{N} \Rightarrow \quad s^2 + 5\,s + 15 = 0$

The zeros: $s_{4n,5n} = \sigma_{5n} \pm j\,\omega_{5n} = -2.500 \pm j\,2.958$

c) Special case ($m = 0.45$ and $n = 0.22$):

$\mathcal{D} \Rightarrow \quad s^3 + 5.545\,s^2 + 10.101\,s + 10.101 = 0$

The poles: $s_{1n,2n} = \sigma_{1n} \pm j\,\omega_{1n} = -1.035 \pm j\,1.355$

$s_{3n} = \sigma_{3n} = -3.475$

$\mathcal{N} \Rightarrow \quad s^2 + 4,545\,s + 10.101 = 0$

The zeros: $s_{4n,5n} = \sigma_{5n} \pm j\,\omega_{5n} = -2.237 \pm j\,2.222$

By inserting the values of m and n in Eq. 2.8.7 we can calculate the frequency response magnitude of the three cases. The resulting plots are shown in Fig. 2.8.2. Note the high frequency asymptote, which is the same as for the non-peaking single-pole case.

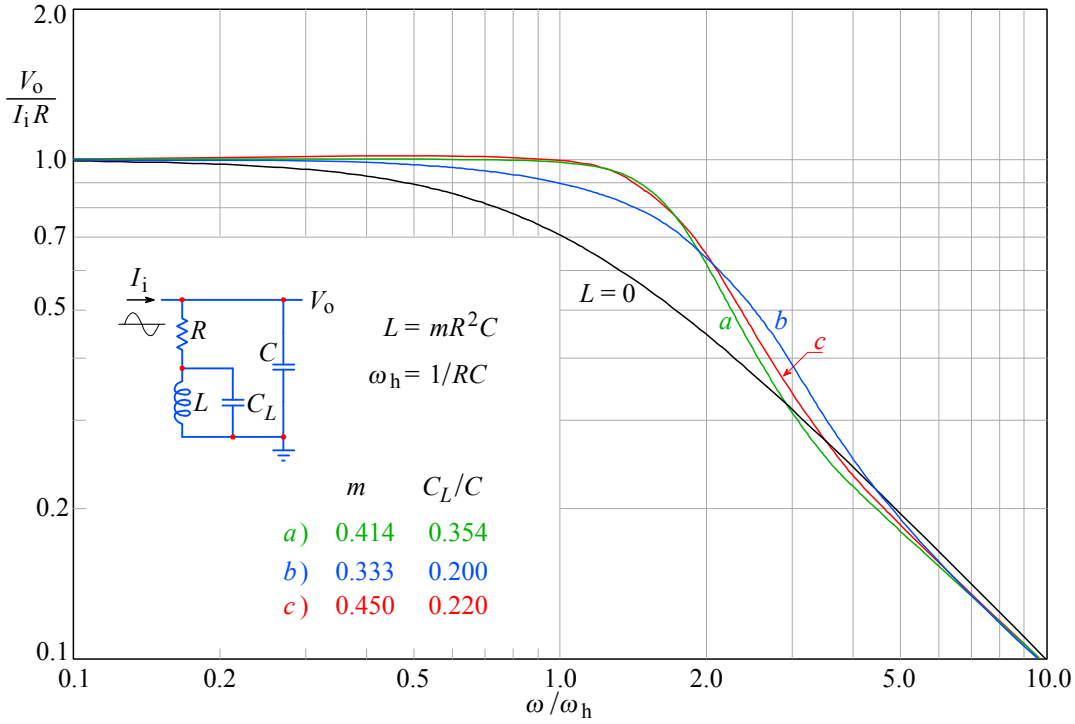

Fig. 2.8.2: Three-pole shunt peaking circuit frequency response: ***a)*** MFA; ***b)*** MFED; ***c)*** SPEC. The non-peaking case ($L = 0$) is the reference. The difference of the number of poles and the number of zeros is only 1 for peaking systems, therefore the ending slope of the frequency response is similar to that of the non-peaking system.

2.8.2 Phase Response

We use Eq. 2.2.30 positive for each pole and negative for each zero and sum them:

$$\varphi = \arctan\frac{\frac{\omega}{\omega_h} - \omega_{1n}}{\sigma_{1n}} + \arctan\frac{\frac{\omega}{\omega_h} + \omega_{1n}}{\sigma_{1n}} + \arctan\frac{\frac{\omega}{\omega_h}}{\sigma_{3n}} + \\ - \arctan\frac{\frac{\omega}{\omega_h} - \omega_{5n}}{\sigma_{5n}} - \arctan\frac{\frac{\omega}{\omega_h} + \omega_{5n}}{\sigma_{5n}} \tag{2.8.13}$$

By entering the numerical values of poles and zeros we obtain the phase response equations for each case. In Fig. 2.8.3 the corresponding plots are shown.

2.8.3 Envelope Delay

We use Eq. 2.2.34, adding a term for each pole and subtracting for each zero:

$$\tau_e\omega_h = \frac{\sigma_{1n}}{\sigma_{1n}^2 + \left(\frac{\omega}{\omega_h} + \omega_{1n}\right)^2} + \frac{\sigma_{1n}}{\sigma_{1n}^2 + \left(\frac{\omega}{\omega_h} - \omega_{1n}\right)^2} + \frac{\sigma_{3n}}{\sigma_{3n}^2 + \left(\frac{\omega}{\omega_h}\right)^2} \\ - \frac{\sigma_{5n}}{\sigma_{5n}^2 + \left(\frac{\omega}{\omega_h} + \omega_{5n}\right)^2} - \frac{\sigma_{5n}}{\sigma_{5n}^2 + \left(\frac{\omega}{\omega_h} - \omega_{5n}\right)^2} \tag{2.8.14}$$

Again we insert the numerical values for poles and zeros in Eq. 2.8.14 to plot the envelope delay as shown in Fig. 2.8.4. As we have explained in Fig. 2.2.6, there is an envelope advance (owed to system zeros) in the high frequency range.

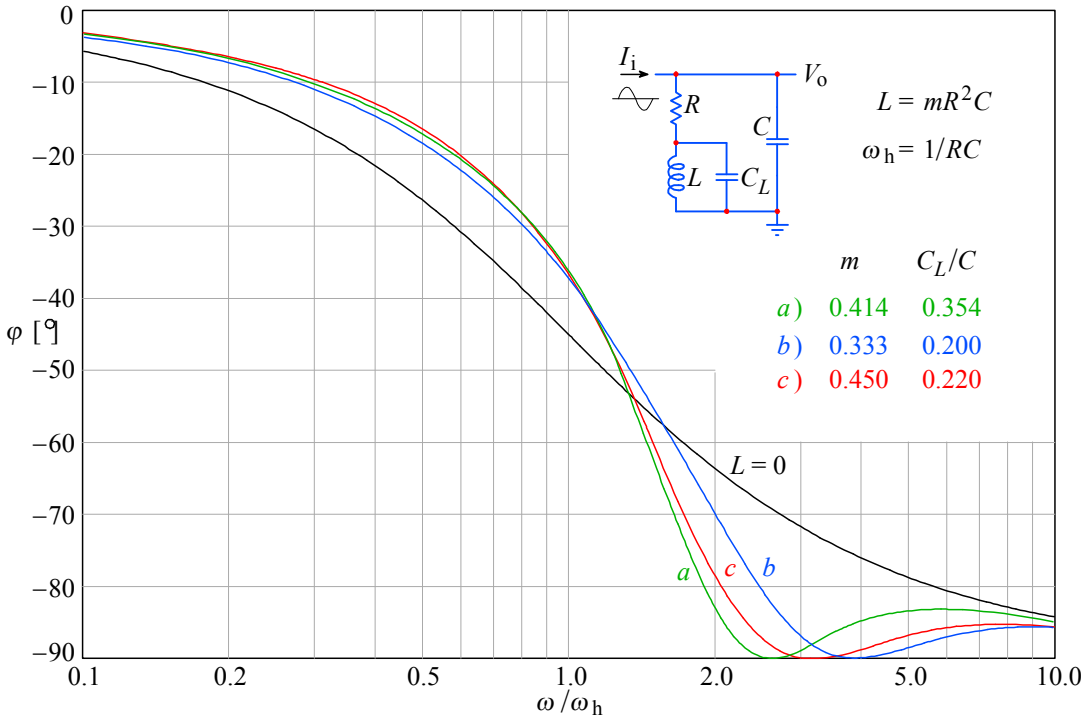

Fig. 2.8.3: Three-pole shunt peaking circuit phase response: ***a)*** MFA; ***b)*** MFED; ***c)*** SPEC. The non-peaking case ($L = 0$) is the reference. The system zeros cause the phase response bouncing up at the $-90°$ boundary and then returning back.

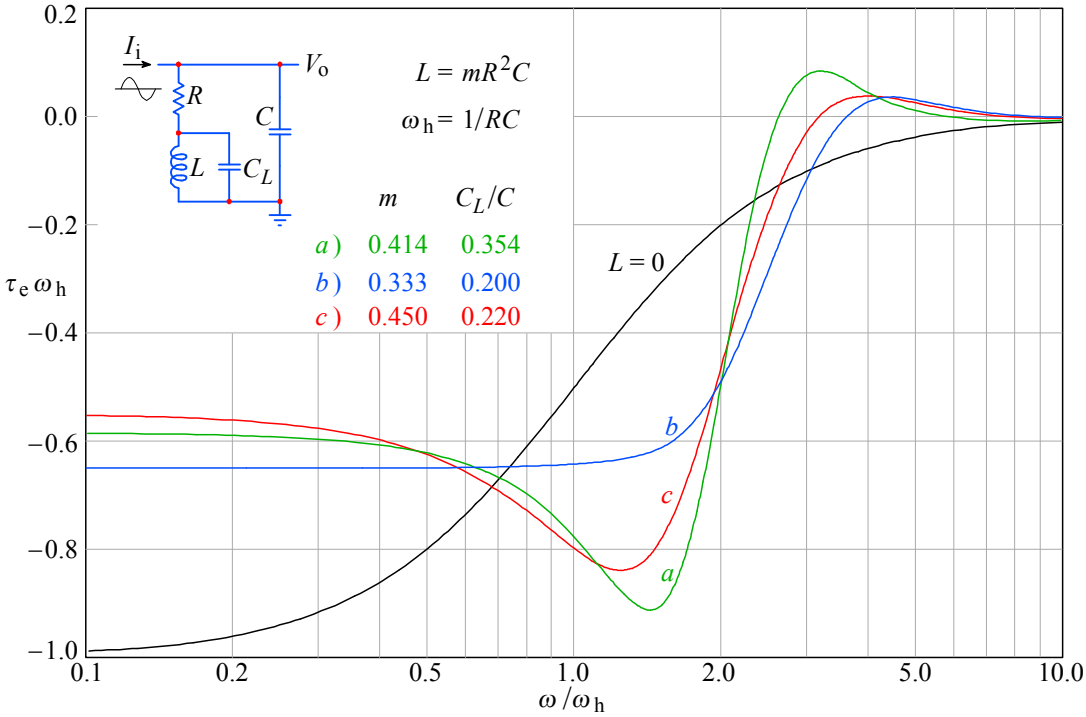

Fig. 2.8.4: Three-pole shunt peaking circuit envelope delay: ***a)*** MFA; ***b)*** MFED; ***c)*** SPEC. The non-peaking ($L = 0$) case is shown as the reference. Note the envelope advance in the high frequency range, owed to system zeros.

2.8.4 Step Response

For the step response we use the general transfer function for three poles and two zeros, which we shall reshape to suit a solution in the Laplace Transform Tables.

$$F(s) = \frac{-\,s_1 s_2\, s_3\,(s - s_4)(s - s_5)}{s_4\, s_5\,(s - s_1)(s - s_2)(s - s_3)} \tag{2.8.15}$$

We multiply this function by the unit step operator $1/s$ and obtain a new equation:

$$G(s) = \frac{1}{s} \cdot \frac{-\,s_1 s_2\, s_3\,(s - s_4)(s - s_5)}{s_4\, s_5\,(s - s_1)(s - s_2)(s - s_3)} \tag{2.8.16}$$

The step response $g(t)$ is fully derived in Appendix 2.3 (on the disk). The result is:

$$\boxed{g(t) = 1 - \frac{K_1}{\omega_1}\, \mathrm{e}^{\sigma_1 t/T} \sqrt{A^2 + \omega_1^2 B^2}\ \sin(\omega_1 t/T + \beta) - K_3\, \mathrm{e}^{\sigma_3 t/T}} \tag{2.8.17}$$

Besides the usual time normalization $T = RC$, here we have:

$$A = [\sigma_1(\sigma_1 - \sigma_3) - \omega_1^2][\sigma_1^2 - \omega_1^2 + \sigma_5^2 + \omega_5^2 - 2\,\sigma_5\,\sigma_1] - 2\,\sigma_5\,\omega_1^2\,(2\,\sigma_1 - \sigma_3)$$

$$B = (2\,\sigma_1 - \sigma_3)[\sigma_1^2 - \omega_1^2 + \sigma_5^2 + \omega_5^2 - 2\,\sigma_5\sigma_1] + 2\,\sigma_5[\sigma_1(\sigma_1 - \sigma_3) - \omega_1^2]$$

$$\beta = \arctan\left(\frac{-\,\omega_1 B}{A}\right) + \pi$$

$$K_1 = \frac{\sigma_3}{(\sigma_5^2 + \omega_5^2)[(\sigma_1 - \sigma_3)^2\ + \omega_1^2]}$$

$$K_3 = \frac{(\sigma_1^2 + \omega_1^2)[(\sigma_3 - \sigma_5)^2 + \omega_5^2]}{(\sigma_5^2 + \omega_5^2)[(\sigma_3 - \sigma_1)^2 + \omega_1^2]} \tag{2.8.18}$$

By inserting the numerical values of the poles and zeros we obtain the following relations:

a) MFA response ($m = 0.414$ and $n = 0.354$):

$$g(t) = 1 + 0.5573\,\mathrm{e}^{-0.850\,t/T}\,\sin(1.577\,t/T + 0.7741 + \pi) - 0.6104\,\mathrm{e}^{-2.125\,t/T}$$

b) MFED response ($m = 0.333$ and $n = 0.200$):

$$g(t) = 1 + 0.8054\,\mathrm{e}^{-1.839\,t/T}\,\sin(1.754\,t/T - 0.1772 + \pi) - 1.1420\,\mathrm{e}^{-2.322\,t/T}$$

c) Special case ($m = 0.45$ and $n = 0.22$):

$$g(t) = 1 + 0.8814\,\mathrm{e}^{-1.035\,t/T}\,\sin(1.355\,t/T + 1.0333 + \pi) - 0.2429\,\mathrm{e}^{-3.475\,t/T}$$

The plots of these responses can be seen in Fig. 2.8.5. Because the difference between the number of poles and zeros is one only, the initial slope of the response is the same as for the non-peaking response.

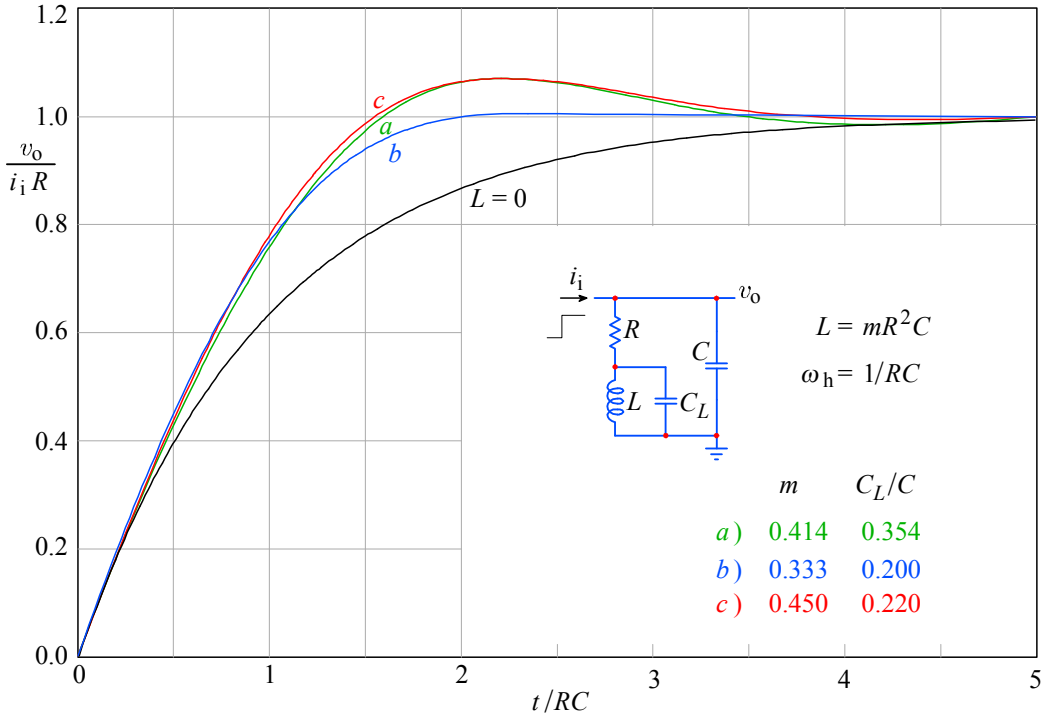

Fig. 2.8.5: Three-pole shunt peaking circuit step response: ***a)*** MFA; ***b)*** MFED; ***c)*** SPEC. The non-peaking case ($L = 0$) is the reference. The initial slope is similar to the non-peaking response, since the difference between the number of system poles and zeros is one only.

We conclude the discussion of the three-pole and two-zero shunt peaking circuit by the Table 2.8.1, which gives all the important circuit parameters.

Table 2.8.1

response type	m	n	η_b	η_r	δ [%]
a) MFA	0.414	0.354	1.84	1.85	7.1
b) MFED	0.333	0.200	1.72	1.74	0.37
c) SPEC	0.450	0.220	1.84	1.91	7.0

Table 2.8.1: Three-pole shunt-peaking circuit parameters

(blank page)

2.9 Shunt–Series Peaking Circuit

In those cases in which the amplifier capacitance may be split into two parts, C_i and C, we can combine the shunt and the series peaking to form a network, shown in Fig. 2.9.1, named the shunt–series peaking circuit. The bandwidth of the shunt–series circuit is increased further than can be achieved by each system alone.

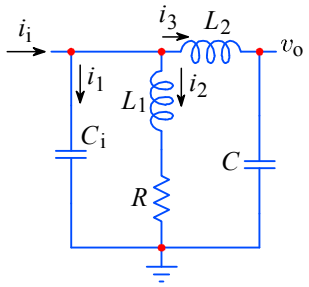

Fig. 2.9.1: The shunt–series peaking circuit.

Although the improvement of the bandwidth and rise time in a shunt–series peaking circuit exceeds that of a pure series or pure shunt peaking circuit, the improvement factors just barely reach the values offered by the three-pole T-coil circuit, which is analytically and practically much easier to deal with; not to speak of the improvement offered by the L+T network, which is substantially greater. This circuit has been extensively treated in literature [Ref. 2.4, 2.25, 2.26]. The calculation of the step response for this circuit can be found in Appendix 2.3, so we shall give only the essential relations.

We start the analysis by calculating the input impedance:

$$Z_i = \frac{V_i}{I_i} = \frac{V_i}{I_1 + I_2 + I_3} \tag{2.9.1}$$

where:

$$I_1 = \frac{V_i}{\frac{1}{s\,C_i}} \qquad I_2 = \frac{V_i}{R + s\,L_1} \qquad I_3 = \frac{V_i}{\frac{1}{s\,C} + sL_2} \tag{2.9.2}$$

By introducing this into Eq. 2.9.1 and eliminating the double fractions we get:

$$Z_i = \frac{(R + s\,L_1)(1 + s^2 L_2 C)}{s\,C_i(R + s\,L_1)(1 + s^2 L_2 C) + s^2 L_2 C + 1 + s\,C(R + s\,L_1)} \tag{2.9.3}$$

The output voltage is:

$$V_o = V_i \frac{\frac{1}{s\,C}}{s\,L_2 + \frac{1}{s\,C}} = I_i\,Z_i \frac{1}{s^2 L_2 C + 1} \tag{2.9.4}$$

We insert Eq. 2.9.3 for Z_i, cancel the $s^2 L_2 C + 1$ terms and extract R from the numerator:

$$V_o = I_i R \frac{1 + s\,L_1/R}{s\,C_i(R + s\,L_1)(1 + s^2 L_2 C) + s^2 L_2 C + 1 + s\,C(R + s\,L_1)} \tag{2.9.5}$$

We divide this by $I_i R$ to get the transfer function normalized in amplitude. Also we multiply all the terms in parentheses and rearrange the result to obtain the canonical form

(divide by the coefficient at the highest power of s) first in the numerator (because it is easy) and then in the denominator:

$$\frac{V_o}{I_i R} = \frac{\frac{L_1}{R}\left(s+\frac{R}{L_1}\right)}{(s\,C_i R + s^2\,C_i L_1)(1+s^2 L_2 C) + s^2 L_2 C + 1 + s\,C(R+s\,L_1)} \tag{2.9.6}$$

$$= \frac{\frac{L_1}{R}\left(s+\frac{R}{L_1}\right)}{s^4 L_1 L_2 C C_i + s^3 L_2 C C_i R + s^2\,C_i L_1 + s^2 L_2 C + s^2\,L_1 C + s\,C R + s\,C_i R + 1}$$

$$= \frac{\frac{1}{L_1 L_2\,C\,C_i}\cdot\frac{L_1}{R}\left(s+\frac{R}{L_1}\right)}{s^4 + s^3\frac{R}{L_1} + s^2\,\frac{L_2 C + L_1 C_i + L_1 C}{L_1 L_2\,C\,C_i} + s\,\frac{R\,(C_i + C)}{L_1 L_2\,C\,C_i} + \frac{1}{L_1 L_2\,C\,C_i}}$$

Since we would like to know how much we can improve the bandwidth with respect to the non-peaking circuit (inductances shorted), let us normalize the transfer function to $\omega_h = 1/R(C_i + C)$ by putting $R = 1$ and $C_i + C = 1$. To simplify the expressions, we introduce the following parameters:

$$n = \frac{C}{C + C_i} \qquad m_1 = \frac{L_1}{R^2(C + C_i)} \qquad m_2 = \frac{L_2}{R^2(C + C_i)} \tag{2.9.7}$$

and by using the normalization we have:

$$C \Rightarrow n \qquad C_i \Rightarrow (1-n) \qquad L_1 \Rightarrow m_1 \qquad L_2 \Rightarrow m_2 \tag{2.9.8}$$

With these expressions the frequency response Eq. 2.9.6 becomes:

$$F(s) = \frac{\frac{1}{m_1 m_2\,n\,(1-n)}\,m_1\left(s+\frac{1}{m_1}\right)}{s^4 + s^3\frac{1}{m_1} + s^2\,\frac{m_2\,n + m_1}{m_1 m_2\,n\,(1-n)} + s\,\frac{1}{m_1 m_2\,n\,(1-n)} + \frac{1}{m_1 m_2\,n\,(1-n)}} \tag{2.9.9}$$

Now we compare this with the generalized four-pole one-zero transfer function:

$$F(s) = \frac{(-1)^4\,s_1 s_2 s_3 s_4}{(s-s_1)(s-s_2)(s-s_3)(s-s_4)}\cdot\frac{s-s_5}{-s_5} \tag{2.9.10}$$

From the numerator it is immediately clear that the zero is:

$$s_5 = -\frac{1}{m_1} \tag{2.9.11}$$

and the product of the poles is:

$$s_1 s_2 s_3 s_4 = \frac{1}{m_1 m_2\,n\,(1-n)} \tag{2.9.12}$$

Next we transform the denominator of Eq. 2.9.10 into a canonical form:

$$(s-s_1)(s-s_2)(s-s_3)(s-s_4) = s^4 + as^3 + bs^2 + cs + d \tag{2.9.13}$$

where:

$$\begin{aligned} a &= -(s_1 + s_2 + s_3 + s_4) \\ b &= s_1 s_2 + s_1 s_3 + s_1 s_4 + s_2 s_3 + s_2 s_4 + s_3 s_4 \\ c &= -(s_1 s_2 s_3 + s_1 s_2 s_4 + s_1 s_3 s_4 + s_2 s_3 s_4) \\ d &= s_1 s_2 s_3 s_4 \end{aligned} \tag{2.9.14}$$

By comparing the coefficients at equal powers of s, we note that:

$$a = \frac{1}{m_1} \qquad b = \frac{m_2\, n + m_1}{m_1 m_2\, n\,(1-n)} \qquad c = d = \frac{1}{m_1 m_2\, n\,(1-n)} \tag{2.9.15}$$

For the MFED response the coefficients of the fourth-order Bessel polynomial (which we obtain by running the BESTAP routine in Part 6) have the following numerical values:

$$a = 10 \qquad b = 45 \qquad c = 105 \qquad d = 105 \tag{2.9.16}$$

So, from a:

$$m_1 = 0.1 \tag{2.9.17}$$

From b and c:

$$b = (m_2\, n + m_1)\, c \qquad \Rightarrow \qquad m_2 = \frac{\dfrac{b}{c} - m_1}{n} \tag{2.9.18}$$

From c or d:

$$\begin{aligned} n(1-n) = \frac{1}{c\, m_1 m_2} \qquad &\Rightarrow \qquad n - n^2 - \frac{n}{105 \cdot 0.1 \cdot \left(\dfrac{45}{105} - 0.1\right)} = 0 \\ &\Rightarrow \qquad n - n^2 - \frac{n}{3.45} = 0 \\ &\Rightarrow \qquad n\left(1 - n - \frac{1}{3.45}\right) = 0 \end{aligned} \tag{2.9.19}$$

And, since $n \neq 0$:

$$n = 1 - \frac{1}{3.45} = 0.7101 \tag{2.9.20}$$

With this we calculate m_2:

$$m_2 = \frac{\dfrac{b}{c} - m_1}{n} = \frac{\dfrac{45}{105} - 0.1}{0.7101} = 0.4627 \tag{2.9.21}$$

The component values for the MFED transfer function will be:

$$\begin{aligned} C &= n(C_\mathrm{i} + C) = 0.7101\,(C_\mathrm{i} + C) \\ C_\mathrm{i} &= (1-n)(C + C_\mathrm{i}) = 0.2899\,(C_\mathrm{i} + C) \\ L_1 &= m_1 R^2 (C + C_\mathrm{i}) = 0.1\, R^2 (C_\mathrm{i} + C) \\ L_2 &= m_2\, R^2 (C + C_\mathrm{i}) = 0.4627\, R^2 (C_\mathrm{i} + C) \end{aligned} \tag{2.9.22}$$

The MFED poles s_{1-4} (BESTAP routine, Part 6) and the zero s_5 (Eq. 2.9.11) are:

$$\begin{aligned} s_{1n,2n} &= s_{1t,2t} = -2.8962 \pm j\,0.8672 \\ s_{3n,4n} &= s_{3t,4t} = -2.1038 \pm j\,2.6574 \\ s_{5n} &= -10.000 \end{aligned} \tag{2.9.23}$$

For the MFA we can use the same procedure as in Sec.2.3.1, but since we have a system of 4th-order we would get an 8th-order polynomial and, consequently, a complicated set of equations to solve. Instead we shall use a simpler approach (which, by the way, can be used in any other case). We must first consider that our system will have a bandwidth larger than the normalized Butterworth system. Let η_b be the proportionality factor between each normalized Butterworth pole and the shunt–series peaking system pole:

$$s_k = \eta_b\, s_{kt} \tag{2.9.24}$$

The normalized 4th-order Butterworth system poles (see Part 6, BUTTAP routine) are:

$$\begin{aligned} s_{1t,2t} &= -0.3827 \pm j\,0.9239 \\ s_{3t,4t} &= -0.9239 \pm j\,0.3827 \end{aligned} \tag{2.9.25}$$

and the values of the characteristic polynomial coefficients are:

$$1.0000 \quad 2.6131 \quad 3.4142 \quad 2.6131 \quad 1.0000 \tag{2.9.26}$$

The polynomial coefficients a, b, c and d of the shunt-series peaking system are then:

$$\begin{aligned} a &= -\eta_b\,(s_{1t} + s_{2t} + s_{3t} + s_{4t}) = \eta_b \cdot 2.6131 \\ b &= \eta_b^2(s_{1t}s_{2t} + s_{1t}s_{3t} + s_{1t}s_{4t} + s_{2t}s_{3t} + s_{2t}s_{4t} + s_{3t}s_{4t}) = \eta_b^2 \cdot 3.4142 \\ c &= -\eta_b^3(s_{1t}s_{2t}s_{3t} + s_{1t}s_{2t}s_{4t} + s_{1t}s_{3t}s_{4t} + s_{2t}s_{3t}s_{4t}) = \eta_b^3 \cdot 2.6131 \\ d &= \eta_b^4 s_{1t}s_{2t}s_{3t}s_{4t} = \eta_b^4 \end{aligned} \tag{2.9.27}$$

Since the coefficients a, b, c and d are the same as in Eq. 2.9.15, we get four equations form which we will extract the values of factors η_b, m_1, m_2 and n:

$$\begin{aligned} \eta_b \cdot 2.6131 &= \frac{1}{m_1} & \eta_b^2 \cdot 3.4142 &= \frac{m_2\,n + m_1}{m_1 m_2\,n\,(1-n)} \\ \eta_b^3 \cdot 2.6131 &= \frac{1}{m_1 m_2\,n\,(1-n)} & \eta_b^4 &= \frac{1}{m_1 m_2\,n\,(1-n)} \end{aligned} \tag{2.9.28}$$

From the last two equations we immediately find the value of η_b:

$$\eta_b^3 \cdot 2.6131 = \eta_b^4 \quad \Rightarrow \quad \boxed{\eta_b = 2.6131} \tag{2.9.29}$$

Effectively, the pole multiplication factor is equal to the MFA bandwidth extension. From the first equation of 2.9.28 we can now calculate m_1:

$$m_1 = \frac{1}{2.6131\,\eta_b} = \frac{1}{\eta_b^2} = 0.1464 \tag{2.9.30}$$

From the last equation of 2.9.28 we can establish the relationship between m_2 and n:

$$\eta_b^4 = \frac{1}{m_1 m_2\, n\,(1-n)} \qquad \Rightarrow \qquad m_2 = \frac{1}{\eta_b^2\, n\,(1-n)} \tag{2.9.31}$$

Finally, from the second equation we can derive n:

$$\eta_b^2 \cdot 3.4142 = \frac{m_2\, n + m_1}{m_1 m_2\, n\,(1-n)} \tag{2.9.32}$$

$$\Rightarrow \quad \eta_b^2 \cdot 3.4142\; m_1 m_2\, n\,(1-n) = m_2\, n + m_1$$

Here we substitute m_1 with $1/\eta_b^2$ and m_2 with $1/\eta_b^2\, n\,(1-n)$:

$$\Rightarrow \quad 3.4142\,\frac{1}{\eta_b^2} = \frac{n}{\eta_b^2\, n\,(1-n)} + \frac{1}{\eta_b^2}$$

$1/\eta_b^2$ cancels, as well as n:

$$\Rightarrow \quad 3.4142 = \frac{1}{(1-n)} + 1$$

$$\Rightarrow \quad n = 1 - \frac{1}{(3.4142-1)} = 0.5858 \tag{2.9.33}$$

And now we can calculate m_2:

$$m_2 = \frac{1}{\eta_b^2\, n\,(1-n)} = 0.6036 \tag{2.9.34}$$

The MFA poles and the zero are:

$$\begin{aligned} s_{1n,2n} &= -2.4142 \pm j\,1.0000 \\ s_{3n,4n} &= -1.0000 \pm j\,2.4142 \\ s_{5n} &= -6.8283 \end{aligned} \tag{2.9.35}$$

and the MFA coefficients are:

$$1.0000 \quad 6.8284 \quad 23.3132 \quad 46.6260 \quad 46.6260 \tag{2.9.36}$$

In addition to the numerical values of parameters m_1 , m_2 and n just calculated, we will also show the results for MFED obtained from two other sources, Braude [Ref. 2.25] and Shea [Ref. 2.26, loc. cit.], to illustrate the possibility of different optimization strategies.

All the design parameters and performance indicators are in Table 2.9.1 at the end of this section.

Let us insert these data into Eq. 2.9.9 and calculate the poles and the zero :

a) MFA by PS/EM ($m_1 = 0.1464$, $m_2 = 0.6036$, and $n = 0.5858$):

$$s^4 + 6.8284\,s^3 + 23.3132\,s^2 + 46.6260\,s + 46.6260 = 0$$

The poles are: $s_{1n,2n} = \sigma_{1n} \pm j\,\omega_{1n} = -2.4142 \pm j\,1.0000$

$s_{3n,4n} = \sigma_{3n} \pm j\,\omega_{3n} = -1.0000 \pm j\,2.4142$

and the zero: $s_{5n} = \sigma_{5n} = -6.8284$

b) MFED by PS/EM ($m_1 = 0.1000$, $m_2 = 0.4627$, and $n = 0.7101$):

$$s^4 + 10.0000\,s^3 + 44.9933\,s^2 + 104.9863\,s + 104.9863 = 0$$

The poles are: $s_{1n,2n} = \sigma_{1n} \pm j\,\omega_{1n} = -2.8976 \pm j\,0.8649$

$s_{3n,4n} = \sigma_{3n} \pm j\,\omega_{3n} = -2.1024 \pm j\,2.6573$

and the zero: $s_{5n} = \sigma_{5n} = -10.0000$

c) MFED by Shea ($m_1 = 0.133$, $m_2 = 0.467$ and $n = 0.667$):

$$s^4 + 7.5188\,s^3 + 32.2198\,s^2 + 72.4872\,s + 72.4872 = 0$$

The poles are: $s_{1n,2n} = \sigma_{1n} \pm j\,\omega_{1n} = -2.1360 \pm j\,1.0925$

$s_{3n,4n} = \sigma_{3n} \pm j\,\omega_{3n} = -1.6234 \pm j\,3.1556$

and the zero: $s_{5n} = \sigma_{5n} = -7.5188$

d) MFED by Braude ($m_1 = 0.122$, $m_2 = 0.511$, and $n = 0.656$):

$$s^4 + 8.1967\,s^3 + 32.4996\,s^2 + 71.0816\,s + 71.0816 = 0$$

The poles are: $s_{1n,2n} = \sigma_{1n} \pm j\,\omega_{1n} = -2.6032 \pm j\,0.9618$

$s_{3n,4n} = \sigma_{3n} \pm j\,\omega_{3n} = -1.4951 \pm j\,2.6446$

and the zero: $s_{5n} = \sigma_{5n} = -8.1967$

2.9.1 Frequency Response

We shall use the normalized formula which we developed for the 4-pole L+T circuit, (Eq. 2.6.10), to which we must include the influence of the zero. The magnitude of the transfer function (to shorten the expression, we will omit the index 'n' here) is:

$$|F(\omega)| = \frac{\left(\sigma_1^2 + \omega_1^2\right)\left(\sigma_3^2 + \omega_3^2\right)\frac{1}{\sigma_5}\sqrt{\sigma_5^2 + \chi^2}}{\sqrt{\left[\sigma_1^2 + (\chi + \omega_1)^2\right]\left[\sigma_1^2 + (\chi - \omega_1)^2\right]\left[\sigma_3^2 + (\chi + \omega_3)^2\right]\left[\sigma_3^2 + (\chi - \omega_3)^2\right]}} \tag{2.9.37}$$

where again $\chi = \omega/\omega_h$. In Fig. 2.9.2 we have plotted the responses resulting from this equation by inserting the values of the poles and the zero for our MFA and MFED.

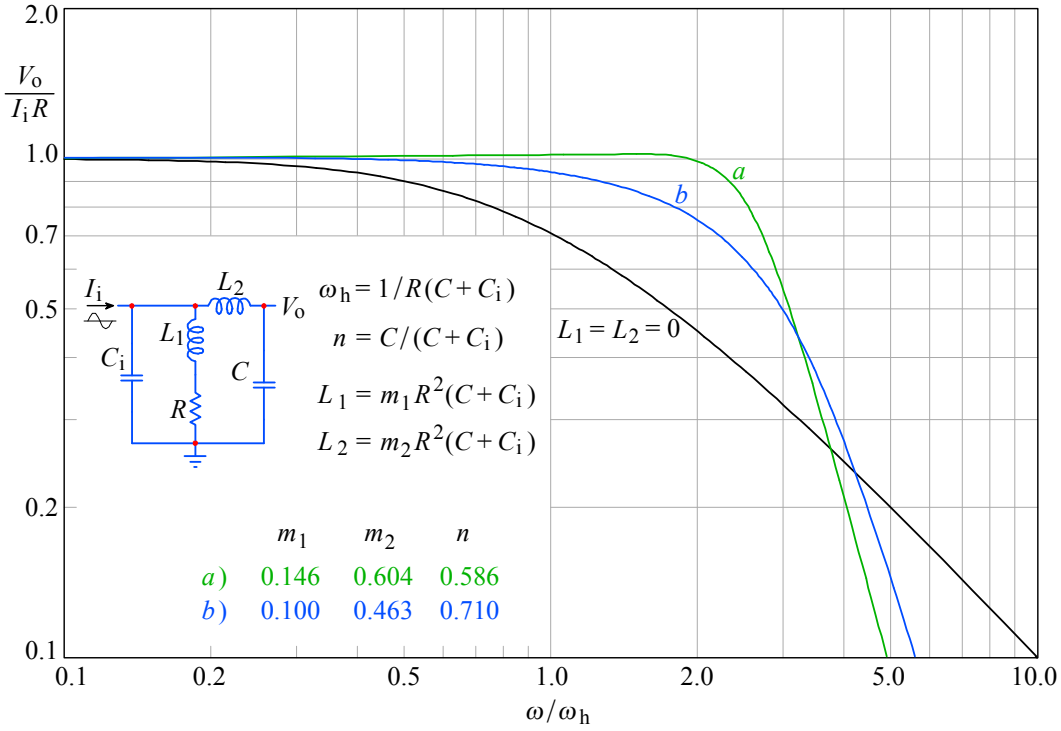

Fig. 2.9.2: The shunt–series peaking circuit frequency-response: ***a)*** MFA; ***b)*** MFED. Note the MFA not being exactly maximally flat, owing to the system zero.

2.9.2 Phase Response

As before, we apply Eq. 2.2.30 for each pole and (negative) for the zero:

$$\varphi(\omega) = \arctan\frac{\frac{\omega}{\omega_h} - \omega_{1n}}{\sigma_{1n}} + \arctan\frac{\frac{\omega}{\omega_h} + \omega_{1n}}{\sigma_{1n}}$$
$$+ \arctan\frac{\frac{\omega}{\omega_h} - \omega_{3n}}{\sigma_{3n}} + \arctan\frac{\frac{\omega}{\omega_h} + \omega_{3n}}{\sigma_{3n}} - \arctan\frac{\frac{\omega}{\omega_h}}{\sigma_{5n}} \qquad (2.9.38)$$

By inserting the values for the poles and the zero from the equations above, we obtain the responses shown in Fig. 2.9.3 .

2.9.3 Envelope Delay

By Eq. 2.2.34, for responses *a*) and *b*) we obtain:

$$\tau_e \omega_h = \frac{\sigma_{1n}}{\sigma_{1n}^2 + \left(\frac{\omega}{\omega_h} + \omega_{1n}\right)^2} + \frac{\sigma_{1n}}{\sigma_{1n}^2 + \left(\frac{\omega}{\omega_h} - \omega_{1n}\right)^2}$$
$$+ \frac{\sigma_{3n}}{\sigma_{3n}^2 + \left(\frac{\omega}{\omega_h} + \omega_{3n}\right)^2} + \frac{\sigma_{3n}}{\sigma_{3n}^2 + \left(\frac{\omega}{\omega_h} - \omega_{3n}\right)^2} - \frac{\sigma_{5n}}{\sigma_{5n}^2 + \left(\frac{\omega}{\omega_h}\right)^2} \qquad (2.9.39)$$

By inserting the values for the poles and the zero from the equations above, we obtain the responses shown in Fig. 2.9.4. Again, as in pure shunt peaking, we have different low frequency delays for each type of poles, owing to the different normalization.

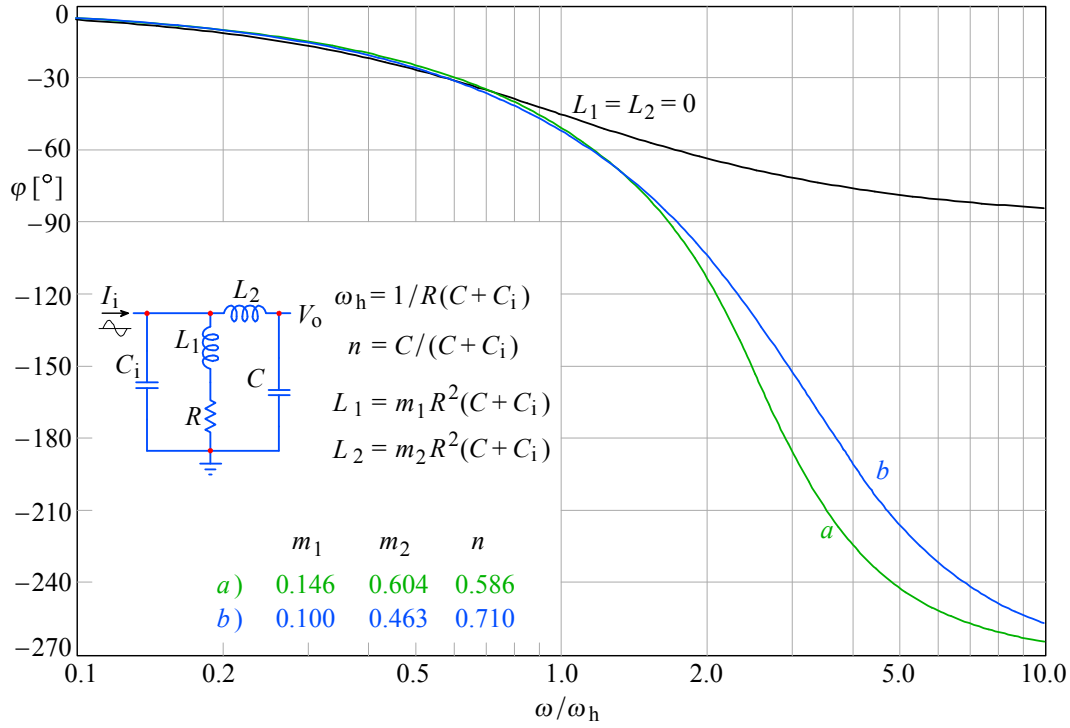

Fig. 2.9.3: The shunt–series peaking circuit phase response: ***a)*** MFA; ***b)*** MFED.

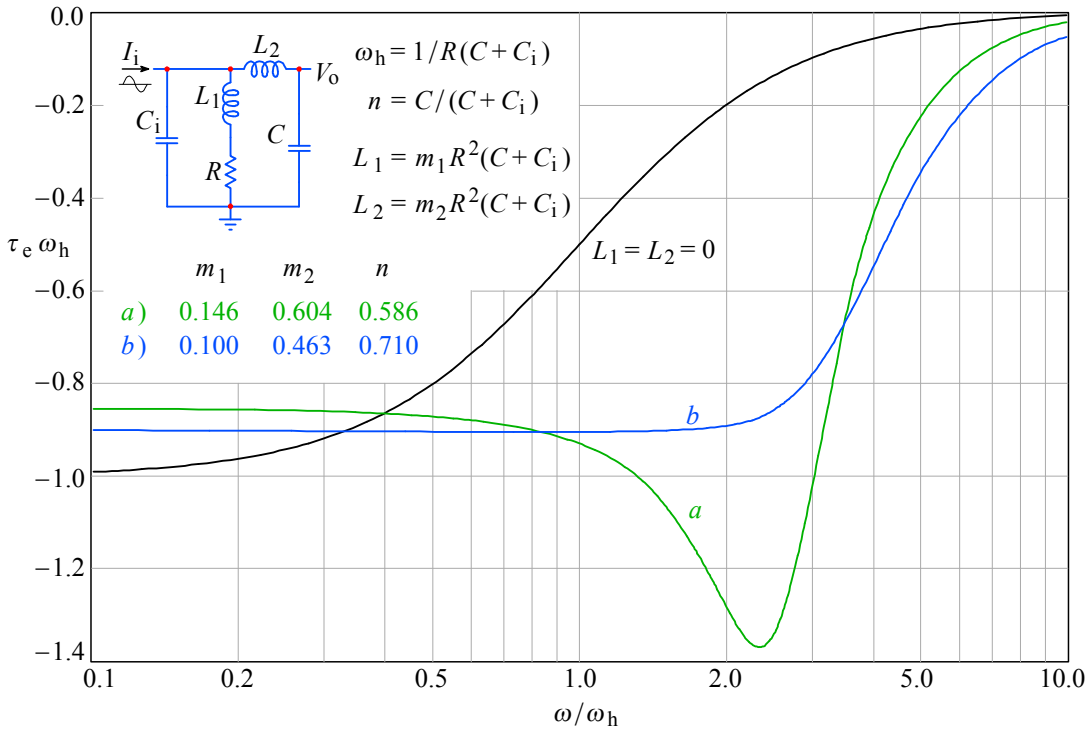

Fig. 2.9.4: The shunt–series peaking circuit envelope delay: ***a)*** MFA; ***b)*** MFED.

2.9.4 Step Response

The normalized general expression for four poles and one zero in the frequency domain is:

$$F(s) = \frac{s_1\, s_2\, s_3\, s_4\, (s - s_5)}{-\, s_5\, (s - s_1)(s - s_2)(s - s_3)(s - s_4)} \tag{2.9.40}$$

To get the step response in the s domain, we multiply $F(s)$ by the unit step operator $1/s$:

$$G(s) = \frac{s_1\, s_2\, s_3\, s_4\, (s - s_5)}{-\, s\, s_5\, (s - s_1)(s - s_2)(s - s_3)(s - s_4)} \tag{2.9.41}$$

The step response in the time domain is obtained by taking the $\mathcal{L}^{-1}$ transform:

$$g(t) = \mathcal{L}^{-1}\{G(s)\} = \sum \text{res}\, \frac{s_1\, s_2\, s_3\, s_4\, (s - s_5)\, e^{st}}{-\, s\, s_5\, (s - s_1)(s - s_2)(s - s_3)(s - s_4)} \tag{2.9.42}$$

This formula requires even more effort than was spent for the L+T network. We shall skip the lengthy procedure (which is presented in Appendix 2.3) and give only the solution, which for all the listed poles and zeros is:

$$g(t) = 1 - \frac{K_1}{\sigma_5\, \omega_1}\, e^{\sigma_1 t}[M \sin(\omega_1 t/T) + \omega_1 N \cos(\omega_1 t/T)]$$

$$- \frac{K_3}{\sigma_5\, \omega_3}\, e^{\sigma_3 t}[P \sin(\omega_3\, t/T) + \omega_3\, Q \cos(\omega_3\, t/T)] \tag{2.9.43}$$

where:

$$\begin{aligned} M &= (\sigma_1 - \sigma_5)[\sigma_1 A - \omega_1^2 B] + \omega_1^2 (A + \sigma_1 B) \\ N &= [\sigma_1 A - \omega_1^2 B] - (\sigma_1 - \sigma_5)(A + \sigma_1 B) \\ P &= (\sigma_3 - \sigma_5)[\sigma_3 C + \omega_3^2 B] + \omega_3^2 (C - \sigma_3 B) \\ Q &= [\sigma_3 C + \omega_3^2 B] - (\sigma_3 - \sigma_5)(C - \sigma_3 B) \end{aligned} \tag{2.9.44}$$

whilst A, B, C, K_1 and K_3 are the same as for the L+T network (Eq. 2.6.17).

The plots in Fig. 2.9.5 and Fig. 2.9.6 were calculated and drawn by using these formulae.

Let us now compare the MFED response with those obtained by Braude and Shea. The step response relation is the same for all three systems (Eq. 2.9.43, 2.9.44), but the pole and zero values are different. As it appears from the comparison of the characteristic polynomial coefficients and even more so from the comparison of the poles and zeros, the three systems were optimized in different ways. This is evident from Fig. 2.9.7.

Although at first glance all three step responses look very similar (Fig. 2.9.6), a closer look reveals that the Braude case has an excessive overshoot. The Shea case has the steepest slope (largest bandwidth), but this is paid for by an extra overshoot and ringing. The Bessel system has the lowest transient slope; however, it has the minimal overshoot and it is the first to settle to $<0.1\%$ of the final amplitude value (in about $2.7\, t/T$).

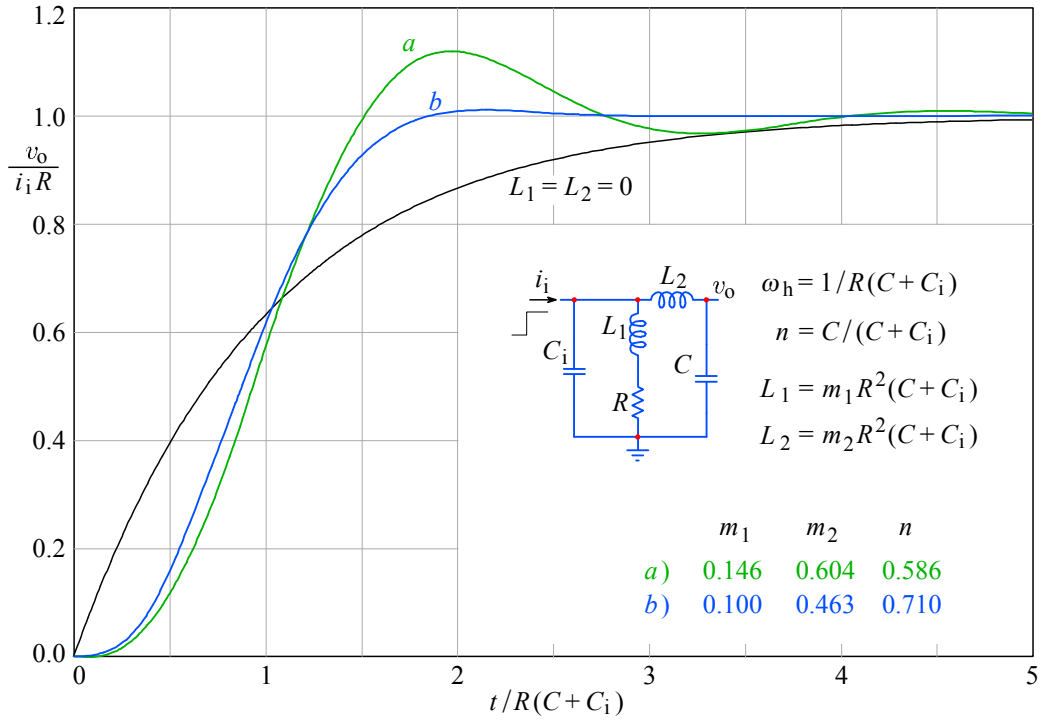

Fig. 2.9.5: The shunt–series peaking circuit step response: ***a)*** MFA; ***b)*** MFED.

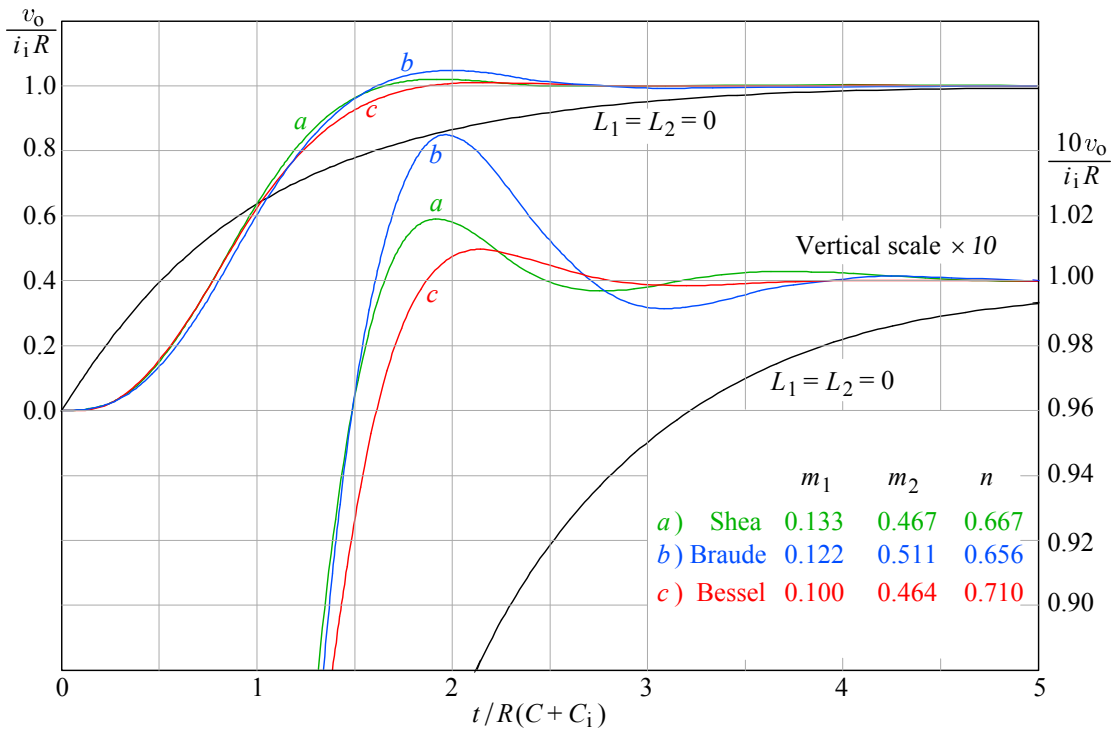

Fig. 2.9.6: The MFED shunt–series peaking circuit step response: ***a)*** by Shea; ***b)*** by Braude; ***c)*** a true Bessel system. The ×10 vertical scale expansion shows the top 10 % of the response. The overshoot in the Braude case is excessive, whilst the Shea version has a prolonged ringing. Although slowest, the Bessel system is the first to settle to < 0.1 % of the final value.

The pole layout in Fig. 2.9.7 confirms the statements above. In the Braude case the two poles with the smaller imaginary part are too far from the imaginary axis to compensate

the peaking of the two poles closer, so the overshoot is inevitable. The Shea case has the widest pole spread and consequently the largest bandwidth, but the two poles with the lower imaginary part are too close to the imaginary axis (this is needed in order to level out the peaks and deeps in the frequency response). As a consequence, whilst the overshoot is just acceptable, there is some long term ringing, impairing the system's settling time. The Bessel system pole layout follows the theoretical requirement. In spite of the presence of the zero (located far from the poles, the farthest of all three systems), the system performance is optimal.

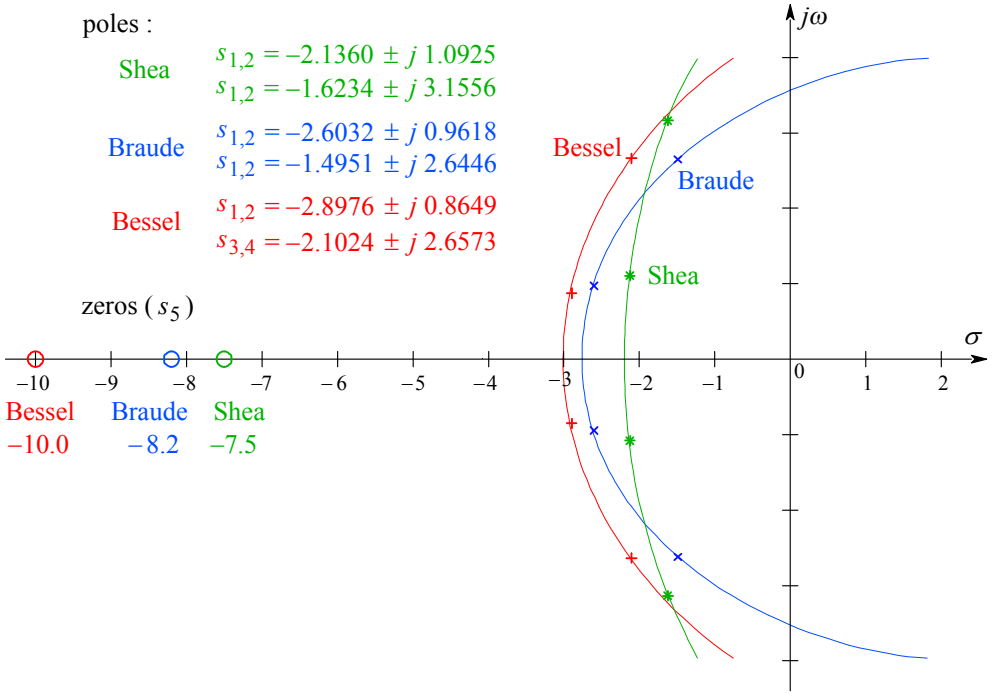

Fig. 2.9.7: The MFED shunt–series peaking circuit pole loci of the three different systems. The zero of each system is too far from the poles to have much influence. It is interesting how a similar step response can be obtained using three different optimization strategies. Strictly speaking, only the Bessel system is optimal.

Let us conclude this section with Table 2.9.1, in which we have collected all the design parameters, in addition to the bandwidth and rise time improvements and the overshoots for the cases discussed.

Table 2.9.1

response type	author	m_1	m_2	n	η_b	η_r	δ [%]
a) MFA	PS/EM	0.1464	0.6036	0.5858	2.61	2.72	12.23
b) MFED	PS/EM	0.1000	0.4627	0.7101	2.18	2.21	0.90
c) MFED	Shea	0.133	0.467	0.667	2.44	2.39	1.86
d) MFED	Braude	0.122	0.511	0.656	2.50	2.36	4.45

Table 2.9.1: Series–shunt peaking circuit parameters.

This completes our discussion of inductive peaking circuits.

We have deliberately omitted the analysis of the combination of a 3-pole + 1-zero shunt peaking, combined with a two-pole series peaking circuit. This network, introduced by *R.L. Dietzold*, was thoroughly analyzed in 1948 in the book *Vacuum Tube Amplifiers* [Ref. 2.2] (the reader who is interested in following the analysis there should consider that several printing mistakes crept into some of the formulae). In those days that circuit represented the ultimate in inductive peaking circuits. Today we achieve a much better bandwidth and rise time improvement with the L+T circuit, discussed in Sec. 2.6, which is easier to realize in practice and also requires substantially less mathematical work.

With shunt–series peaking it is sometimes not possible to achieve the required ratio of stray capacitances n as in Table 2.9.1; but by adding an appropriate damping resistor across the series peaking coil it is possible to adapt the shunt–series peaking circuit also to an awkward ratio n. This is well described in [Ref. 2.2]. However the bandwidth and the rise time improvement of such circuits may be either similar to that of a three-pole shunt peaking circuit, or even worse than that, so we will not discuss them.

To summarize: in view of the advanced T-coil circuits, the shunt–series peaking circuit may be considered obsolete. This is why we have not discussed it as extensive as all the other inductive peaking circuits. On the other hand, by omitting the shunt–series peaking circuit entirely, the discussion of the inductive peaking circuits would not be complete.

2.10 Comparison of MFA Frequency Responses and of MFED Step Responses

In an actual process of amplifier design the choice of circuits used in different amplifying stages is not just a matter of a designer's personal taste or a simple collection of best performing circuits. Rather, it is a process of carefully balancing the advantages and disadvantages both at the system level and at each particular stage.

To help the designer in making a decision, now that we have analyzed the frequency responses and step responses of the most important types of inductive peaking circuits, we compare their performance in the following two plots.

We have drawn all the MFA frequency responses in Fig. 2.10.1 and all the MFED step responses in Fig. 2.10.2.

On the basis of both figures we conclude that T-coil circuits surpass all the other types of inductive peaking circuits.

In addition we have collected all the data for the circuit parameters corresponding to both figures in the table in Appendix 2.4 (on the disk). The table contains the circuit schematic diagram, the relations between the component values, the normalized pole and zero values, the formulae for the frequency responses and the step responses, as well as the bandwidth and the rise time enhancement and the step response overshoot.

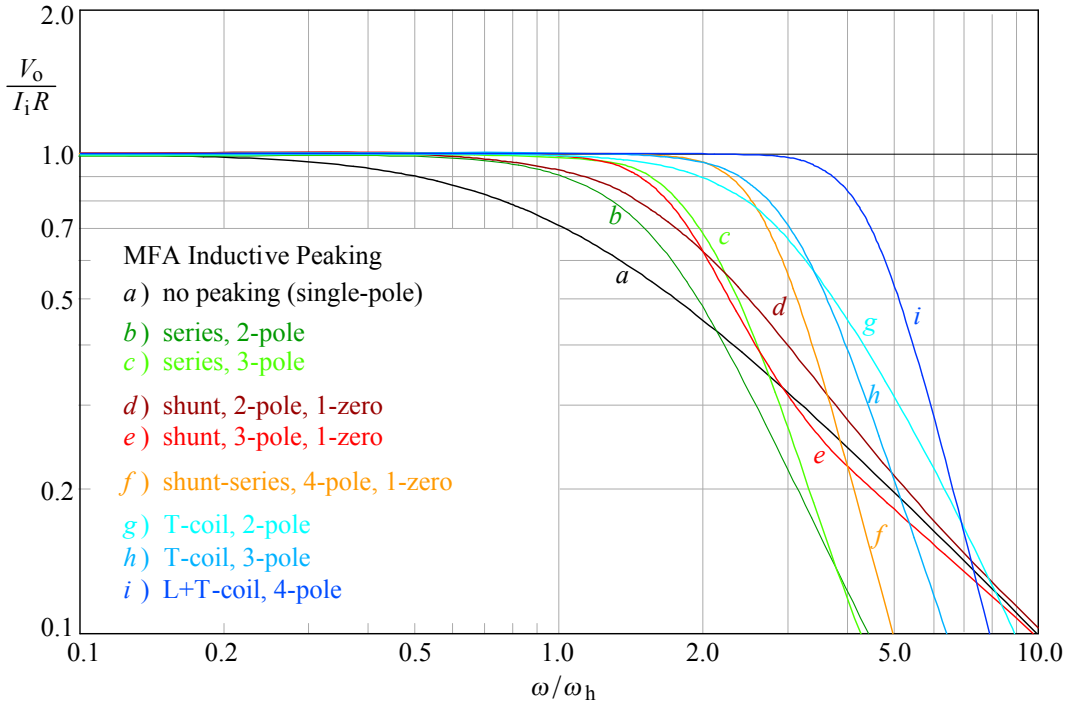

Fig. 2.10.1: MFA frequency responses of all the circuit configurations discussed. By far the 4-pole T-coil response ***i)*** has the largest bandwidth.

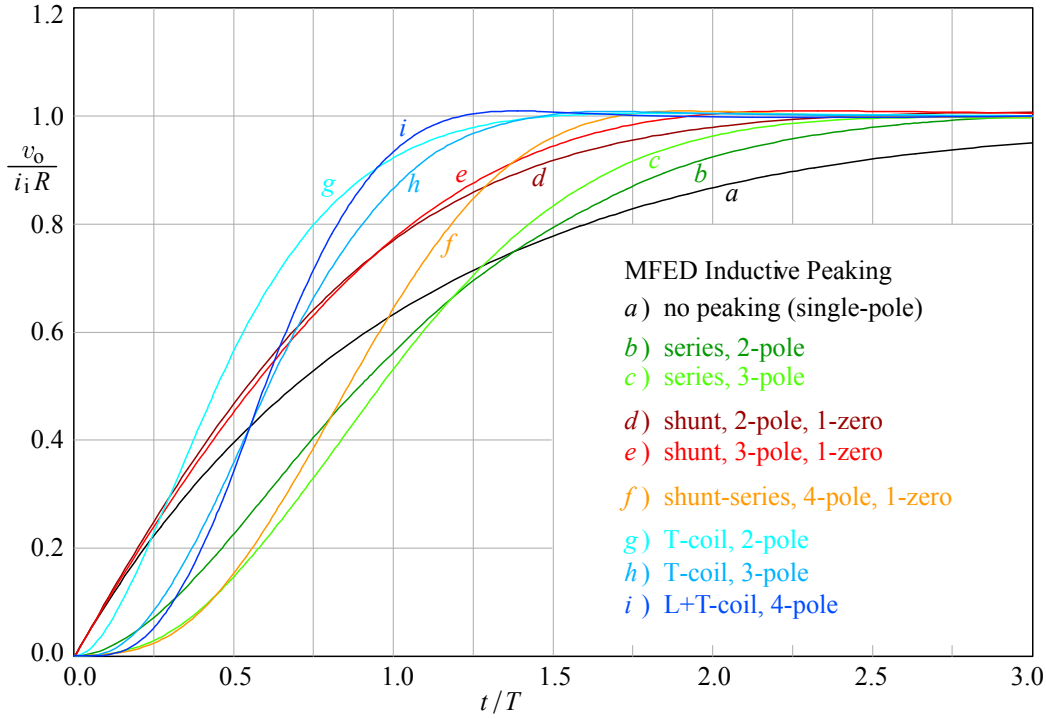

Fig. 2.10.2: MFED step responses of all the circuit configurations discussed. Again, the 4-pole T-coil step response ***i)*** has the steepest slope, but the 3-pole T-coil response ***h)*** is close.

2.11 The Construction of T-coils

Most of the 'know how' concerning the construction of T-coils is a classified matter of different firms, mostly Tektronix, Inc., so we shall discuss only some basic facts about how to make T-coils.

Fig. 2.11.1, made originally by *Carl Battjes* (although with different basic circuit parameters as the reference), shows the performance sensitivity on each component's tolerance of an L+T circuit designed nominally for the MFED response.

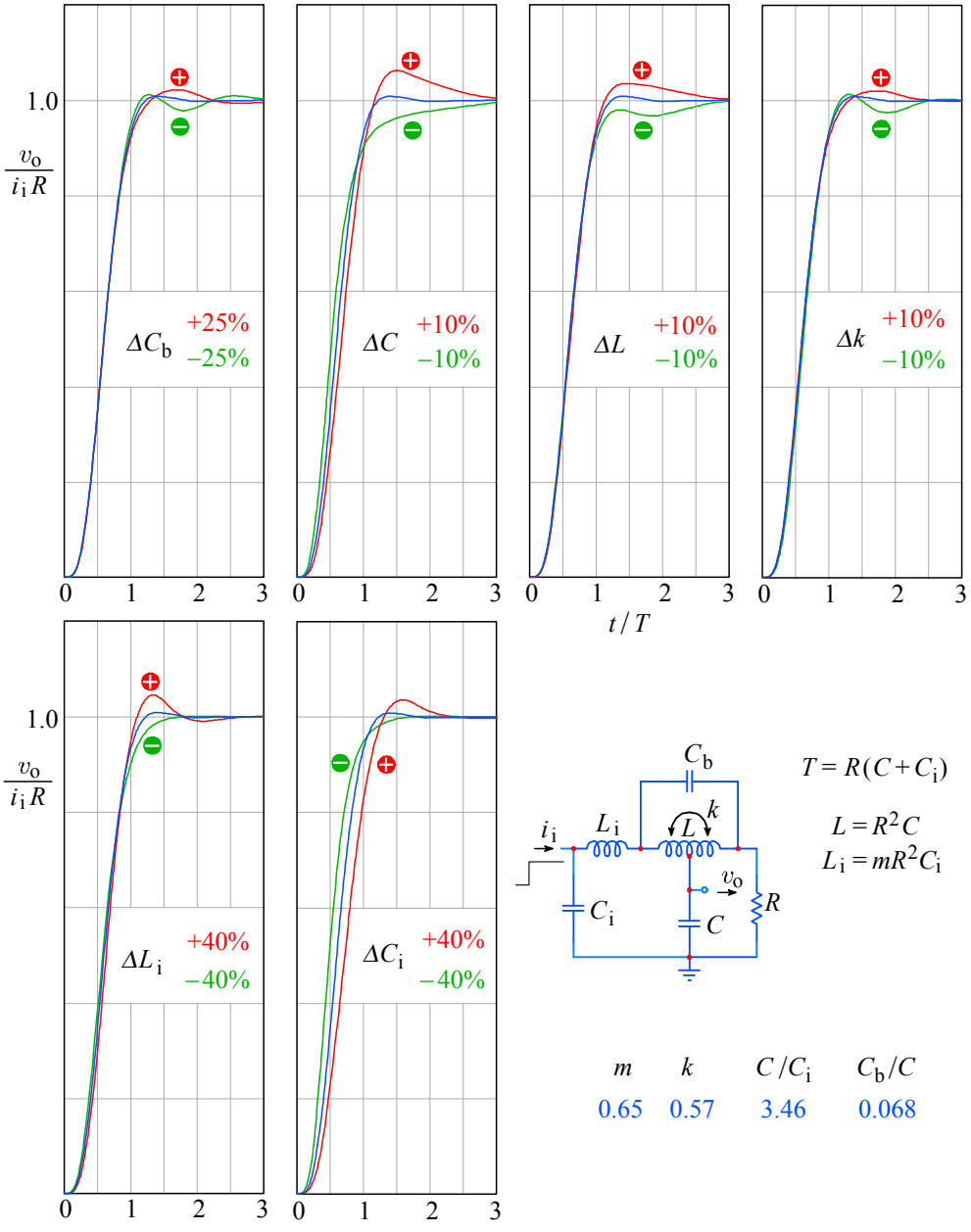

Fig. 2.11.1: Four-pole L+T peaking circuit step response sensitivity on component tolerances. Such graphs were drawn originally by *Carl Battjes* for a class lecture at Tektronix, but with another set of parameters as the reference. The responses presented here were obtained using the MicroCAP–5 circuit analysis program. [Ref.2.36].

These figures prove that the inductance L, the coupling factor k, and the loading capacitance C must be kept within close tolerances in order to achieve the desired performance, whilst the tolerances of the bridging capacitance C_b of the T-coil, the input coil L_i, and input capacitance C_i are less critical. Therefore, the construction of a properly calculated T-coil is not a simple matter. In some respect it resembles a digital AND function: only if all the parameters are set correctly will the result be an efficient peaking circuit. There is not much room for compromise here.

In the serial production of wideband amplifiers there are always some tolerances of stray capacitances, so the T-coils must be made adjustable. Usually the coils are wound on a simple polystyrene cylindrical coil form, with a threaded ferrite core inside. By adjusting the core the required inductance can be set. However, the coupling factor k depends only on the coil *length* to *diameter* ratio (l/D) [Ref. 2.33] **and it is independent of whether the coil has a ferrite core inside or not**. The relation between the coupling factor k and the ratio l/D is shown in the diagram in Fig. 2.11.2, which is valid for the center tapped cylindrical coils.

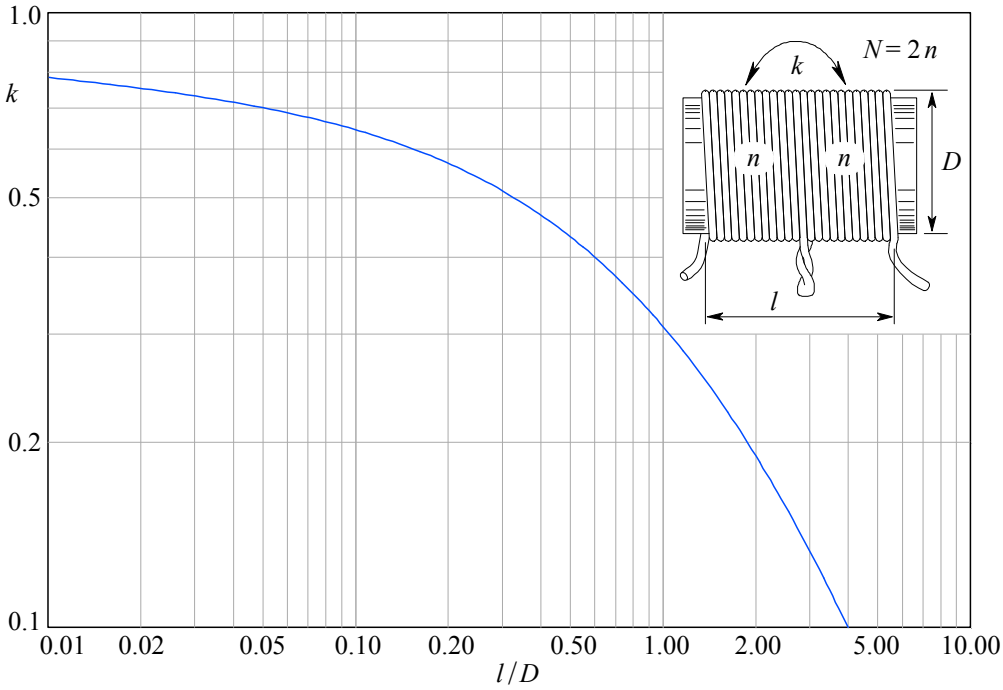

Fig. 2.11.2: T-coil coupling factor k as a function of the coil's length to diameter (l/D) ratio.

The coil inductance L depends on the number of turns, the length to diameter ratio, set by the coil form on which the coil is wound, and on the ferrite core if any is used; both the coil form and the core can be obtained from different manufacturers, together with the formulae for calculating the required number of turns. However, these formulae are often given as some sort of 'cookery book receipts', with the key parameters usually in numerical form for a particular product. As such, they are satisfactory for building general purpose coils, but they do not offer the understanding needed to perform the optimization procedure within a set of possible solutions.

The reader is therefore forced to look for more theoretical explanations in standard physics and electronics text books.

In those text books the following relation can be found:

$$L = \frac{\mu_0 N^2 A}{l} \tag{2.11.1}$$

but this is **valid only for a single layer coreless coil with a homogeneous magnetic field** (such as a tightly wound toroid or a long coil). The parameters represent:

- L inductance in henrys (after *Joseph Henry*, 1791-1878), [$1\,\mathrm{H} = 1\,\mathrm{Vs/A}$]; the inductance of $1\,\mathrm{H}$ produces a self-induced voltage of $1\,\mathrm{V}$ when a current flowing through it changes at a rate of $1\,\mathrm{A/s}$;
- μ_0 the free space magnetic permeability, $\mu_0 = 4\pi \cdot 10^{-7}$ Vs/Am;
- N the total number of turns;
- A the area encircled by one wire turn, measured from the wire central path; for a cylindrical coil, $A = \pi R^2 = \pi D^2/4$, where R is the radius and D is the diameter, both in meters [m];
- l the total coil length in meters [m]; if the turns are wound adjacent to one another with a wire of a diameter d, then $l = Nd$.

The main problem with the Eq. 2.11.1 is the term 'homogeneous'; this implies a uniform magnetic field, entirely contained within the coil, with no appreciable leakage outwards. Toroidal coils are not easy to build and can not be made adjustable, so in practice cylindrical coils are widely used. For a cylindrical coil the magnetic field is of the same form as that of a stick magnet: the field lines close outside the coil and at both ends the field is non-homogeneous. Because of this, the inductance is reduced by a form factor ζ, which is a function of the ratio D/l (Fig. 2.11.3).

An important note for T-coil production: the form factor, and consequently the inductance, increase with D and decrease with l, in contrast to the coupling factor k. This additionally restricts our choice of D and l.

Also, if the coil is going to be adjustable the relative permeability of the core material, μ_r , must be taken into account; however, only a part of the magnetic field will be contained within the core, so we introduce the average permeability, $\overline{\mu_\mathrm{r}}$, reflecting that only a part of the turns will encircle the core. The relative permeability of the air is 1 and that of the ferromagnetic core material can be anything up to several hundred. However, since the field path in air will be much longer than inside the core, the average permeability will be rather low. Note also that the core material is 'slow', i.e., its permeability has an upper frequency limit, often lower than our bandwidth requirement.

Finally, if the bridging capacitance C_b of the T-coil network has to be precisely known, we must take into account the coil's self capacitance, C_s, which appears in parallel with the coil, with a value equivalent to a series connection of capacitances between adjacent turns. Owing to C_s the inductance will appear lower when measured, so C_s should also be measured and the actual inductance value calculated from the two measurements. If the turns are tightly wound the relative permittivity ε_r of the wire isolation lacquer must be considered. Its value is several times larger than for air. The lacquer thickness is also influencing C_s. If C_s is too large it can easily be reduced by increasing the distance between the turns by a small amount, δ, but this will also cause additional field leakage and reduce the inductance slightly. To compensate, the number of turns can be increased; because the inductance increases with N^2, it will outperform the slight decrease resulting from the larger length l.

Multi-layer coils are less suitable for use in wideband amplifiers, because of their high capacitance between the adjacent layers.

Fortunately wideband amplification does not require large inductance values. Also, since the inductances are always in series with relatively large resistive loads (almost never less than 50 Ω), the wire resistance and the skin effect can usually be neglected.

With all these considerations the inductance becomes:

$$L = \zeta \frac{\overline{\mu_r} \mu_0 \pi D^2 l}{4\,(d+\delta)^2} \tag{2.11.2}$$

The Fig. 2.11.3 shows the value of ζ as a function of the ratio D/l. The actual function is found through elliptic integration of the magnetic field flux density, which is too complex to be solved analytically here. But a fair approximation, fitting the experimental data to better than 1%, can be obtained using the following relation:

$$\zeta = \frac{a}{a + \left(\frac{D}{l}\right)^b} \tag{2.11.3}$$

where:

$$a = 2$$

$$b = \sin\frac{\pi}{3}$$

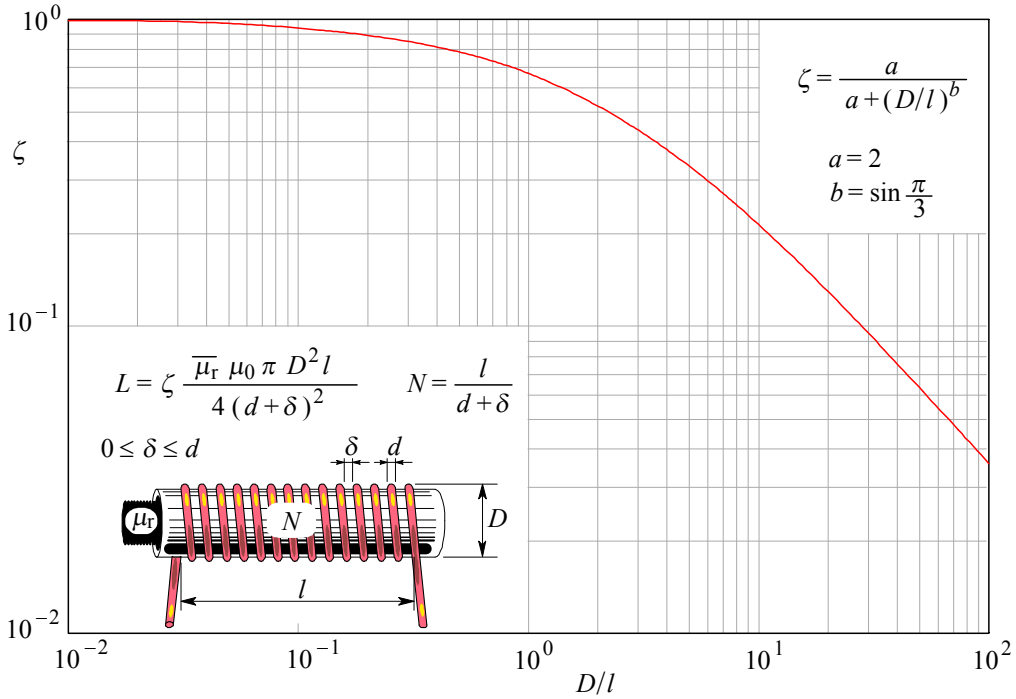

Fig. 2.11.3: The ζ factor as a function of the coil diameter to length ratio, D/l. The equation shown in the upper right corner fits experimental data to better than 1%.

Inductances are susceptible to external fields, mainly from the power supply, or other nearby inductances. The influence of a nearby inductance can be minimized by a perpendicular orientation of coil axes. Otherwise, the circuit should be appropriately

shielded, but the shield will act as a shorted single-turn inductance, lowering the effective coil inductance if it is too close.

In modern miniaturized, bandwidth hungry circuits the coil dimensions become critical, and one possible solution is to construct the coil in a planar spiral form on two sides of a printed circuit board or even within an integrated circuit. This gives the possibility of more tightly controlled parameter tolerances, but there is no free lunch: the price to pay is in many weeks or even months of computer simulation before a satisfactory solution is found by trial and error, since the exact mathematical relations are extremely complicated (a good example of how this is done can be found in the excellent article by *J.Van Hese* of Agilent Technology [Ref. 2.37], where the finite element numerical analysis method is used).

The following figures show a few examples of planar coils made directly on the surface of IC chips, ceramic hybrids, or double-sided conventional PCBs.

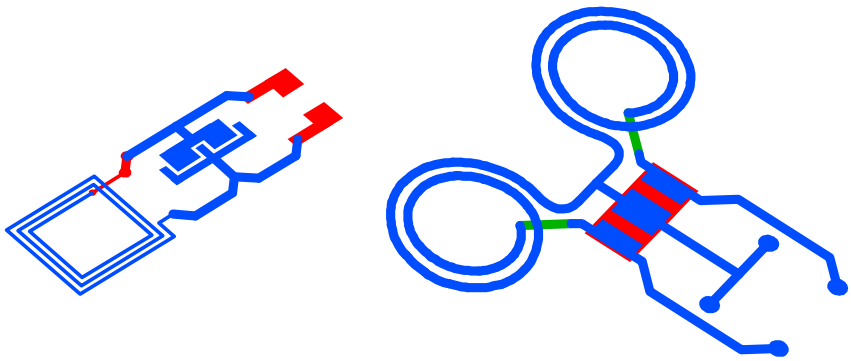

Fig. 2.11.4: Examples of coil structures made directly on an IC chip (left) and on a hybrid circuit (right).

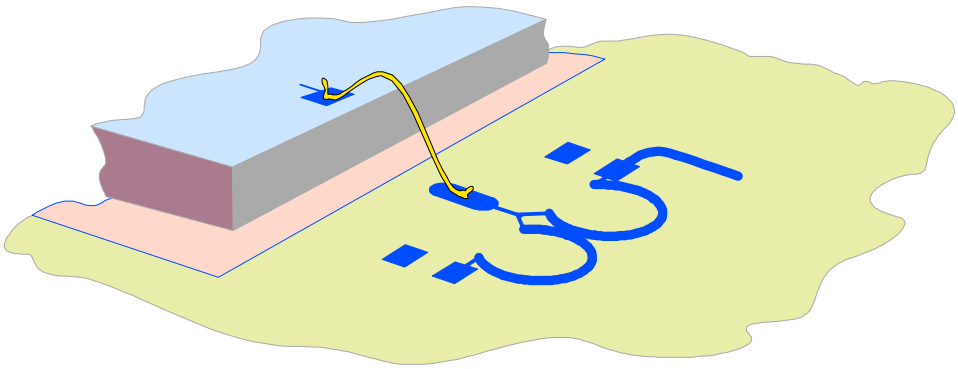

Fig. 2.11.5: A possible compensation of the bonding inductance of an IC chip, mounted on a hybrid circuit, by the negative inductance present at the T-coil center tap.

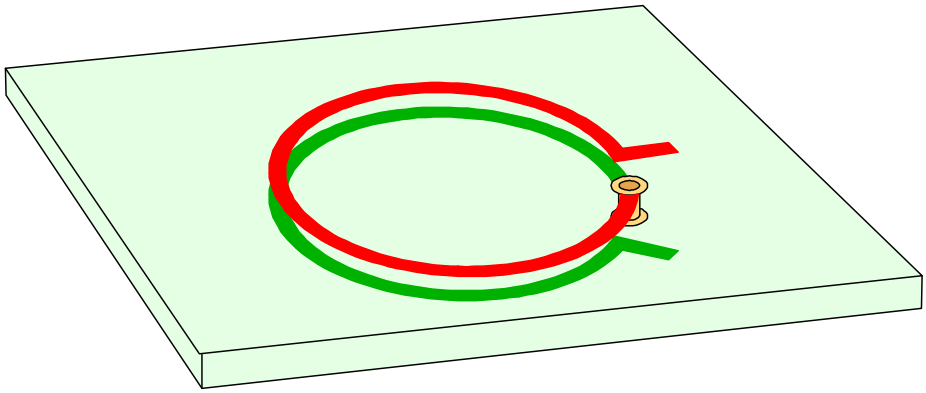

Fig. 2.11.6: A planar T-coil with a high coupling factor, realized on a conventional double-sided PCB. Multi-turn spiral structures are also possible, but need at least a three-layer board for making the inner to outer turn connections.

References:

[2.1] *S. Butterworth*, On the Theory of Filter Amplifiers,
Experimental Wireless & Wireless Engineer, Vol. 7, October, 1930, pp. 536–471.

[2.2] *G.E. Valley & H. Wallman*, Vacuum tube amplifiers,
MIT, Radiation Laboratory Series, Vol. 18, McGraw-Hill, New York, 1948.

[2.3] *J. Bednařík & J. Daněk*, Obrazové zesilovače pro televisi a měřicí techniku
(Video Amplifiers for Television and Measuring Techniques),
Statní nakladatelství technické literatury, Prague, 1957.

[2.4] *E.L. Ginzton, W.R. Hewlett, J.H. Jasberg, J.D. Noe*, Distributed Amplification,
Proc. I.R.E., Vol. 36, August, 1948, pp. 956–969.

[2.5] *P. Starič*, An Analysis of the Tapped-Coil Peaking Circuit for Wideband/Pulse Amplifiers,
Elektrotehniški vestnik, 1982, pp. 66–79.

[2.6] *P. Starič*, Three- and Four-Pole Tapped Coil Circuits for Wideband/Pulse Amplifiers,
Elektrotehniški vestnik, 1983, pp. 129–137.

[2.7] *P. Starič*, Application of T-coil Interstage Coupling in Wideband/Pulse Amplifiers,
Elektrotehniški vestnik, 1990, pp. 143–152.

[2.8] *D.L. Feucht*, Handbook of Analog Circuit Design,
Academic Press, Inc. San Diego, 1990.

[2.9] *J.L. Addis*, Good Engineering and Fast Vertical Amplifiers, Part 4, section 14,
Analog Circuit Design, edited by *J. Williams,*
Butterworth-Heinemann, Boston, 1991.

[2.10] *M.E. Van Valkenburg*, Introduction to Modern Network Synthesis,
John Wiley, New York, 1960.

[2.11] *G. Daryanani*, Principles of Active Network Synthesis and Design,
John Wiley, New York, 1976.

[2.12] *T.R. Cuthbert*, Circuit Design using Personal Computers,
John Wiley, 1983.

[2.13] *G.J.A. Byrd*, Design of Continuous and Digital Electronic Systems,
McGraw-Hill (UK), London, 1980.

[2.14] *P. Starič*, Interpolacija med Butterworthovimi in Thomsonovimi poli
(Interpolation between Butterworth's and Thomson's poles),
Elektrotehniški vestnik, 1987, pp. 133–139.

[2.15] *G.A. Korn & T.M. Korn*, Mathematical Handbook for Scientists and Engineers,
McGraw-Hill, New York, 1961.

[2.16] *F.A. Muller*, High-Frequency Compensation of RC Amplifiers,
Proceedings of the I.R.E., August, 1954, pp. 1271–1276.

[2.17] *C.R. Battjes*, Technical Notes on Bridged T-coil Peaking,
(Internal Publication), Tektronix, Inc., Beaverton, Ore., 1969.

[2.18] *C.R. Battjes*, Who Wakes the Bugler?, Part 2, section 10,
The Art and Science of Analog Circuit Design, edited by *J. Williams,*
Butterworth-Heinemann, Boston, 1995.

[2.19] *N.B. Schrock*, A New Amplifier for Milli-Microsecond Pulses,
Hewlett-Packard Journal, Vol. 1, No. 1., September, 1949.

[2.20] *W.R. Horton, J.H. Jasberg, J.D. Noe*, Distributed Amplifiers: Practical Consideration and
Experimental Results, Proc. I.R.E. Vol. 39, pp. 748–753.

[2.21] *R.I. Ross*, Wang Algebra Speeds Network Computation of Constant Input Impedance Networks,
(Internal Publication), Tektronix, Inc., Beaverton, Ore. 1968.

[2.22] *R.J. Duffin*, An Analysis of the Wang Algebra of the Networks,

Trans. Amer. Math. Soc., 1959, pp. 114–131.

[2.23] *S.P. Chan*, Topology Cuts Circuit Drudgery,
Electronics, November 14, 1966, pp. 112–121.

[2.24] *A.I. Zverev*, Handbook of Filter Synthesis,
John Wiley, New York, 1967.

[2.25] *G.B. Braude, K.V. Epaneshnikov, B.J. Klymushev*, Calculation of a Combined Circuit for the Correction of Television Amplifiers, (in Russian),
Radiotekhnika, T. 4, No. 6. Moscow, 1949, pp. 24–33.

[2.26] *L.J. Giacoletto*, Electronics Designer's Handbook,
Second Edition, McGraw-Hill, New York, 1977.

[2.27] *B. Orwiller*, Vertical Amplifier Circuits,
Tektronix, Inc., Beaverton, Ore., 1969.

[2.28] *D.E. Scott*, An Introduction to Circuit Analysis, A System Approach,
McGraw-Hill, New York, 1987.

[2.29] *J.L. Addis*, Mutual Inductance & T-coils,
(Internal Publication), Tektronix, Inc., Beaverton, Ore. 1977.

[2.30] *A.B. Williams*, Electronic Filter Design Handbook,
McGraw-Hill, New York 1981.

[2.31] *C.R. Battjes*, Amplifier Risetime and Frequency Response,
Class Notes, Tektronix, Inc., Beaverton, Ore. 1969.

[2.32] *W.E. Thomson*, Networks with Maximally Flat Delay,
Wireless Engineer, Vol. 29, 1952, pp 536–541.

[2.33] *F.W. Grover*, Inductance Calculation, (Reprint)
Instrument Society of America, Research Triangle Park, N.C. 27 709, 1973.

[2.34] Mathematica, Wolfram Research, Inc., 100 Trade Center Drive, Champaign, Illinois,
http://www.wolfram.com/

[2.35] Macsyma, Symbolics, Inc., 8 New England Executive Park, East Burlington, Massachusetts, 01803,
http://www.scientek.com/macsyma/main.htm
See also Maxima (free version, GNU Public Licence):
http://www.ma.utexas.edu/users/wfs/maxima.html

[2.36] MicroCAP–5, Spectrum Software, Inc.,
http://www.spectrum-soft.com/

[2.37] *J. Van Hese*, Accurate Modeling of Spiral Inductors on Silicon for Wireless RF-IC Designs,
http://www.techonline.com/ ↦ Feature Articles ↦ Feature Archive ↦ November 20, 2001
See also: http://www.agilent.com/, and:
L. Knockaert, *J. Sercu* and *D. Zutter*, "Generalized Polygonal Basis Functions for the Electromagnetic Simulation of Complex Geometrical Planar Structures," IMS-2001

[2.38] *J.N. Little* and *C.B. Moller,* The MathWorks, Inc.: MATLAB-V For Students
(with the Matlab program on a compact disk), Prentice-Hall, 1998,
http://www.mathworks.com/

[2.39] Derive, http://education.ti.com/product/software/derive/

[2.40] MathCAD, http://www.mathcad.com/

[2.41] *P. Starič*, Inductive peaking circuits,
Electronics & Wireless World, 1988, pp. 471–474.